

1 **The climate and vegetation of Europe, North Africa and the**  
2 **Middle East during the Last Glacial Maximum**  
3 **(21,000 years BP) based on pollen data**

4  
5  
6 Basil A.S. Davis<sup>1</sup>, Marc Fasel<sup>2</sup>, Jed O. Kaplan<sup>3</sup>, Emmanuele Russo<sup>4</sup>, Ariane Burke<sup>5</sup>

7 <sup>1</sup>Institute of Earth Surface Dynamics, University of Lausanne, Lausanne, 1015, Switzerland

8 <sup>2</sup>enviroSPACE lab, Institute for Environmental Sciences, University of Geneva, Geneva,  
9 1211, Switzerland

10 <sup>3</sup>Department of Earth Sciences, The University of Hong Kong, Hong Kong, Peoples Republic  
11 of China

12 <sup>4</sup>Department of Environmental Systems Science, ETH Zurich, Zurich, 8092, Switzerland

13 <sup>5</sup>Laboratoire d'Ecomorphologie et de Paleoanthropologie, Departement d'Anthropologie,  
14 Universite de Montreal, Montreal, Quebec, H3C 3J7, Canada

15  
16 *Correspondence to:* Basil A. S. Davis ([basil.davis@unil.ch](mailto:basil.davis@unil.ch))

17  
18 **Abstract.** Pollen data represents one of the most widely available and spatially-resolved  
19 sources of information about the past land cover and climate of the Last Glacial Maximum  
20 (21,000 years BP). Previous pollen data compilations for Europe, the Mediterranean and the  
21 Middle East however have been limited by small numbers of sites and poor dating control.  
22 Here we present a new compilation of pollen data from the region that improves on both the  
23 number of sites (63) and the quality of the chronological control. Data has been sourced from  
24 both public data archives and published (digitized) diagrams. Analysis is presented based on  
25 a standardized pollen taxonomy and sum, with maps shown for the major pollen taxa, biomes  
26 and total arboreal pollen, as well as quantitative reconstructions of forest cover and winter,  
27 summer and annual temperatures and precipitation. The reconstructions are based on the  
28 modern analogue technique (MAT) with a modern calibration dataset taken from the latest  
29 Eurasian Modern Pollen Database (~8000 samples). A site-by-site comparison of MAT and  
30 Inverse Modelling methods shows little or no significant difference between the methods for  
31 the LGM, indicating that no-modern-analogue and low CO<sub>2</sub> conditions during the LGM do  
32 not appear to have had a major effect on MAT transfer function performance. Previous  
33 pollen-based climate reconstructions using modern pollen calibration datasets show a much  
34 colder and drier climate for the LGM than both Inverse Modelling and climate model  
35 simulations, but our new results suggest much greater agreement. Differences between our  
36 latest MAT reconstruction and those in earlier studies can be largely attributed to bias in the  
37 small modern calibration dataset previously used. We also find that quantitative forest cover  
38 reconstructions show more forest than that previously suggested by biome reconstructions,  
39 but less forest than that suggested by simple percentage arboreal pollen, although  
40 uncertainties remain large. Overall, we find that LGM climatic cooling/drying was  
41 significantly greater in winter than in summer, but with large site to site variance that  
42 emphasizes the importance of topography and other local factors in controlling the climate  
43 and vegetation of the LGM.  
44

## 45 **1 Introduction**

46

47 During the Last Glacial Maximum (LGM) ~21,000 years BP (Mix et al., 2001), the climate,  
48 vegetation and landscape of Europe and its surrounding regions were very different than  
49 today. Scandinavia and a large part of the British Isles were covered by a single ice sheet,  
50 with separate ice sheets covering the Alps and Pyrenees, while many smaller and lower  
51 mountainous areas were also glaciated (Ehlers et al. 2011). As a result of this global build-up  
52 of ice on land, sea levels were around 120 meters lower than today, resulting in the retreat of  
53 Atlantic and Mediterranean coastlines and the emergence on land of the English Channel and  
54 North Sea basin. Falling sea levels also led to the disconnection of the Black Sea from the  
55 Mediterranean, and a subsequent drop in Black Sea water levels as evaporation exceeded  
56 inflow (Arslanov et al. 2007). On land, permafrost and periglacial processes occurred  
57 immediately to the south of the Scandinavian ice sheet, while the massive discharge of glacial  
58 clays and sands provided material to be redeposited by the wind as belts of loess across  
59 northern France, Benelux, Germany and central Europe (Lehmkuhl et al. 2021). Under these  
60 cooler and drier climatic conditions, forests are thought to have retreated to the relative  
61 shelter of Southern Europe and the Mediterranean, while relatively unproductive steppe and  
62 tundra dominated the region north of the Alps (Grichuk 1992).

63

64 This traditional view of the LGM has been established for many years, but many details  
65 concerning the climate and vegetation of the LGM remain debated. Much of this debate  
66 concerns information derived from the pollen record, which represents one of the most  
67 widely available and spatially-resolved sources of information concerning LGM vegetation  
68 and climate, and the primary terrestrial proxy used to evaluate climate models in the  
69 Palaeoclimate Modelling Intercomparison Project (PMIP) (Bartlein et al., 2011; Harrison et  
70 al., 2014).

71

72 For example, climate model simulations continue to indicate a climate that is less cold and  
73 more humid than pollen-based reconstructions (Jost et al., 2005). These results are similar to  
74 reconstructions based on glaciological modelling (Allen et al., 2008b). On the other hand, the  
75 pollen-based reconstructions that show the greatest disagreement with climate models have  
76 themselves been criticized for not considering the possible effect of low atmospheric CO<sub>2</sub> on  
77 the physiological relationship between plants and climate (Ramstein et al., 2007). Methods  
78 that use modern pollen samples for calibration purposes are based on the assumption that the  
79 relationship between vegetation and climate remains the same through time, and that this is  
80 independent of change in CO<sub>2</sub> concentration. Studies have shown however that plant growth  
81 processes and plant resilience are sensitive to CO<sub>2</sub> concentration, and particularly water-use  
82 efficiency which would make plants more drought sensitive in low CO<sub>2</sub> environments  
83 (Cowling & Sykes 1999). Atmospheric CO<sub>2</sub> during the LGM was around 190 ppm, some  
84 100 ppm lower than the pre-industrial period, and 200 ppm lower than the levels experienced  
85 in the last 50 years. Concerns about the effects of lower CO<sub>2</sub> during the LGM has directly led  
86 to the development of pollen-climate reconstruction methods that can take account of CO<sub>2</sub>  
87 effects, either through use of a process-based vegetation model run in inverse mode (Guiot et  
88 al. 2000, Guiot et al. 2009), or through the use of a correction algorithm (Prentice et al.  
89 2017). Pollen-climate reconstructions based on inverse modelling that account for these low  
90 CO<sub>2</sub> effects show less cooling and drying and consequently greater agreement with climate  
91 models (Ramstein et al., 2007; Wu et al., 2007).

92

93 Further data-model discrepancies have also been highlighted concerning LGM vegetation  
94 cover. Earlier pollen synthesis studies, especially those that applied the biomisation method

95 (Elenga et al., 2000) give the impression that non-glaciated areas of LGM Europe were  
96 dominated by treeless steppe, while vegetation models driven by climate model simulations  
97 indicate large areas of forest and woodlands (Binney et al., 2017; Kaplan et al., 2016;  
98 Velasquez et al., 2021). The apparent data-model discrepancy associated with steppe has led  
99 to the suggestion that early humans, which are not included in vegetation models, could have  
100 reduced the forest cover with only a relatively moderate use of fire because of the cold  
101 climate and slow speed of vegetation recovery (Kaplan et al., 2016). This debate is important  
102 because of studies that have shown the sensitivity of the climate system to vegetation  
103 boundary conditions during the LGM (Ludwig et al., 2017; Velasquez et al., 2021). This  
104 suggests that accurate knowledge of the vegetation cover during the LGM is a necessary  
105 prerequisite to understanding the role of other influences on the climate system at this time.  
106

107 More recent pollen and macrofossil studies from eastern Central Europe have shown that at  
108 least in this region there existed areas of open boreal forest and woodland with some  
109 temperate broadleaf species (Kuneš et al., 2008; Willis and Van Andel, 2004). The evidence  
110 of forest, and particularly elements of temperate broadleaf forest, north of the Alps has come  
111 to represent a challenge to the traditional view that forest species only survived the LGM in  
112 sheltered refugia far to the south of the Fenoscandian ice sheet and close to the moderating  
113 influence of the Mediterranean Sea. The presence of micro-refugia north of the Alps is  
114 important because it would represent a very different baseline for understanding the later rate  
115 and route of plant migrations under the rapid warming that occurred during the Late Glacial  
116 to Holocene transition (Douda et al., 2014; Giesecke, 2016; Krebs et al., 2019; Nolan et al.,  
117 2018), as well as understanding patterns of present-day genetic diversity (Normand et al.,  
118 2011; Svenning et al., 2008). Modelling studies have shown difficulty in supporting the very  
119 high rates of postglacial expansion that would be necessary for southern refugia (Feurdean et  
120 al., 2013, Nogués-Bravo et al. 2018).  
121

122 Much of this debate has been informed by an increasing number of LGM pollen studies from  
123 an ever-broader geographical area, and especially from an increasing number of studies from  
124 north of the Alps. Nevertheless, the synthesis of these studies into a single narrative is made  
125 difficult by several factors, for instance: different taxonomic definitions, pollen percentages  
126 calculated from non-standardized pollen sums, and quantitative analyses such as climate  
127 reconstructions that are based on different training sets and methodologies. This has led to  
128 some modelling studies ignoring the pollen record completely, on the basis that data from the  
129 LGM is too scarce (Janská et al., 2017). Where standardized methods have been applied to  
130 multiple LGM pollen records, poor dating control has resulted in the inclusion of many  
131 records that may not actually be from the selected LGM time window. This is particularly  
132 important because the  $21 \pm 2.0$  ka time slice commonly used to represent the LGM period in  
133 PMIP data-model comparisons and other synthesis studies (MARGO members, 2009;  
134 Bartlein et al., 2011) occurs immediately after the glacial maxima in the Alps around 26-23  
135 ka (Heiri et al., 2014; Spötl et al., 2021) and Heinrich stadial HS-2 (24.3-26.5), whilst also  
136 being closely followed by Heinrich stadial HS-1 (15.6-18.0 ka) (Sanchez-Goñi & Harrison,  
137 2010). These closely associated time periods can therefore be expected to represent both a  
138 different vegetation and climate than the LGM itself.  
139

140 For example, of the 18 European pollen records used in the PMIP benchmarking dataset  
141 (Bartlein et al., 2011), 10 fall into the worst class ('poor') in the COHMAP chronological  
142 quality classification scheme if relative dating such as pollen correlation is excluded. More  
143 recent synthesis studies have also relied heavily on records from the European Pollen  
144 Database (EPD) which currently has 116 records with samples of LGM age (as of June

145 2022). Many of these records however are based on chronologies that are considered reliable  
146 for the Holocene (Giesecke et al., 2014), but have large uncertainties for the LGM as a result  
147 of 1) excessive extrapolation back in time from Holocene age dates, 2) the use of pollen  
148 correlation or other relative dating despite poorly defined regional biostratigraphy, or 3) the  
149 inappropriate use of radiocarbon dates contaminated with old carbon. We found that 104 of  
150 these 116 EPD records (Neotoma, 2021) fall into the worst class ('poor') in the COHMAP  
151 chronological quality classification.

152

153 Here we address these problems using a new synthesis of LGM pollen records from  
154 throughout Europe, the Mediterranean and the Middle East (EurMedMidEst) based on  
155 rigorous quality control criteria. Records were compiled from an extensive review of public  
156 databases and archives, and the scientific literature. Pollen records were selected according to  
157 the robustness of their chronological control around the PMIP LGM time-window ( $21 \pm 2$   
158 ka), and combined into a single dataset based on a harmonized taxonomy and standardized  
159 pollen sum. The dataset was then analysed so that standardised maps could be produced to  
160 show the distribution of the major pollen taxa, biomes and total arboreal pollen at the LGM.  
161 In addition, quantitative reconstructions of forest cover as well as winter, summer and annual  
162 temperatures and precipitation were undertaken using the Modern Analogue Technique  
163 (MAT), utilizing the latest Eurasian Modern Pollen Database v2 calibration dataset. These  
164 climate reconstructions are compared and evaluated against previous LGM pollen-climate  
165 reconstructions, as well as reconstructions based on other proxies. The dataset and results are  
166 fully documented and the complete data files are provided in the supplementary information.

167

## 168 **2 Methods**

169

### 170 **2.1 Pollen Data**

171

172 LGM fossil pollen data from Europe and bordering regions including North Africa and the  
173 Middle East were selected and collated into a single standardized project database. This data  
174 was sourced from the EPD/Neotoma database (Williams et al., 2021), the Pangaea data  
175 archive, publications in scientific journals, and from the original authors. We selected LGM  
176 pollen sites/data according to strict quality control criteria. Where possible, primary raw  
177 pollen counts were used where this was available. Where the original electronic data was not  
178 available, the data was digitized from the published diagram. Overall we have included 63  
179 records in our study, of which 35 were digitized and 28 consisted of the original pollen  
180 counts (Table 1).

181

182 The distribution of the 63 sites reflects the distribution of suitable archives, with fewer  
183 records available from climatically or environmentally challenging regions (Fig. 1). High  
184 rates of erosion and a drier and colder climate during the LGM reduced the number of  
185 suitable anoxic sediment sinks for pollen preservation, especially in Central Europe between  
186 the Scandinavian and Alpine ice sheets. Nevertheless, our dataset includes sites from this  
187 region, as well as North Africa and eastern Central Europe through to Iran, although most  
188 sites are located in an arc across eastern Spain, the Alps, and Italy. Lakes sites are the most  
189 numerous archive and tend to be located in the more sheltered and topographically favourable  
190 regions of Southern Europe and the Mediterranean. Peat is the next most important archive,  
191 followed by alluvial and colluvial sediments, as well as cave sites, the later also often being  
192 known for their archaeological significance. Sites located at the ice margins that appear to be  
193 under the ice reflect uncertainties in the location of the ice margin both in time and space  
194 during the LGM, as well as the fact that the selected time window for this study ( $21 \pm 2$  ka) is

195 later than the maximum ice advance in some regions (Hughes and Gibbard, 2015). For  
196 completeness, we also include 7 marine records which have the advantage of more  
197 continuous deposition and often better dating over the LGM period, but which are prone to  
198 taphonomic biases compared to terrestrial records. These biases are discussed later in this  
199 section.

200

201 LGM pollen records were selected according to a number of quality control criteria, but  
202 primary amongst these was the existence of sufficient independent chronological control  
203 points to accurately identify samples that would fall within the  $21 \pm 2$  ka BP time-slice of  
204 interest. We have used all of the samples within this time frame where the samples have been  
205 available in electronic form, else we have used the sample closest to the target time (21 ka  
206 BP). For records taken from the EPD we have used the latest Bayesian age-depth models  
207 where these were available (Giesecke et al., 2014), otherwise we have used the dates and  
208 chronology proposed by the original authors. We classified chronologies according to the  
209 COHMAP chronological quality scheme for the LGM period (Anderson et al., 1988; Yu and  
210 Harrison, 1995), which classifies record quality from 1-6 depending on whether a date falls  
211 within 2000 14C years (or less) of the time being assessed, or whether bracketing dates fall  
212 within 6000 and 8000 14C years (or less) about the time being assessed (Table A1).

213 Chronologies based on dates that fall outside of these limits fall into COHMAP class 7, and  
214 are regarded as ‘poorly dated’ with respect to the LGM. Importantly, we have only included  
215 radiometric and other absolute dates (such as varves) in this assessment, and have excluded  
216 dates based on correlation with regional pollen records. These pollen-based stratigraphic  
217 dates have been widely used in previous LGM studies, but do not include estimates of  
218 uncertainty and are generally regarded as unreliable at this time given the sparsity of well  
219 dated pollen sites and samples on which to base any correlation (Giesecke et al., 2014).

220

221 All records that were classified as poorly dated (COHMAP class 7) were subsequently  
222 excluded from our analysis. This has meant that many of the pollen records used in previous  
223 studies were excluded, including 16 of the 26 LGM records used by PMIP and associated  
224 studies in Europe (Bartlein et al., 2011; Elenga et al., 2000; Tarasov et al. 2000, Jost et al.,  
225 2005; Peyron et al., 1998; Wu et al., 2007; Cleator et al., 2020). We also excluded 104 of the  
226 116 records in the EPD with samples that fall within our LGM time window. Many of these  
227 EPD pollen records have been used in more recent studies, although the exact record (EPD  
228 Entity number) is often not stated. We estimate that we have excluded 16 of the 17 European  
229 sites used by Binney et al. (2017) (this study only included sites above latitude 40N), 5 of the  
230 6 European sites used by Allen et al. (2010), 28 of the 33 sites used by Cao et al. (2019) and  
231 27 of the 71 sites used by Kaplan et al. (2016).

232

233 Other quality control criteria were also used in the selection of LGM pollen records.  
234 Published pollen diagrams that only included a small part of the terrestrial pollen assemblage,  
235 or only presented summary taxa, were excluded. Records were also excluded where the  
236 dating information was incomplete, for instance where radiocarbon dating uncertainties were  
237 not published or where it was not possible to determine if the date shown was in calibrated or  
238 uncalibrated radiocarbon years.

239

240 The modern pollen data for the climate and tree cover reconstructions were sourced from the  
241 latest version 2 of the Eurasian Modern Pollen Database (Davis et al., 2020), which is  
242 managed as part of the EPD. The EMPD2 includes 8133 modern pollen samples from across  
243 the Palearctic biogeographic region from Europe to the far East of Asia. The taxa from both  
244 the fossil and modern pollen data were consolidated into 120 of the most commonly-

245 occurring terrestrial taxa types. This taxa list was designed to be compatible with the  
246 biomisation scheme used in our study (Peyron et al., 1998; Tarasov et al., 2000) and that used  
247 in the Holocene mapping study of Brewer et al. (2017). The count of *Larix* was amplified by  
248 a factor of 10 due to its low pollen representation (Edwards et al. 2000, Bigelow et al. 2003,  
249 Tarasov et al. 1998, 2000, 2013, Binney et al., 2017).

250

## 251 **2.2 Biomisation**

252

253 We converted pollen assemblages to biomes based on the European biomisation scheme of  
254 Peyron et al (1998), which in turn is based on Prentice et al. (1996). The method is described  
255 in detail in Collins et al. (2012). We expanded the number of taxa included in the biomisation  
256 procedure proposed by Peyron et al (1998) to include taxa from the Northern Eurasian  
257 biomisation procedure of Tarasov et al. (1998). The inclusion of additional Northern Eurasian  
258 taxa reflects recent evidence that modern analogues of LGM vegetation occur in parts of  
259 Siberia (Magyari et al., 2014a). The biomisation procedure (Prentice et al. 1996) assigns each  
260 taxa to a plant functional type (PFT) and calculates a score for each of these PFT's based on  
261 the sum of the square root of the percentage of each of the taxa included in that PFT. To  
262 reduce the influence of long-distance transport, taxa below 0.5% are removed at the start of  
263 the procedure. Each biome is then assigned one or more PFT's and a score for each biome is  
264 calculated as the sum of the associated PFT scores. The biome with the highest score is then  
265 viewed as the dominant biome. Where the highest score is the same for more than one biome,  
266 the dominant biome is decided based on a hierarchy of unique PFT's. Peyron et al. (1998)  
267 also included a procedure for distinguishing warm and cold steppe biomes based on re-  
268 assigning certain steppe PFT's according to the presence or otherwise of PFT's indicative of  
269 cold or warm conditions. Following the Biome6000 project (Elenga et al., 2000) and Allen et  
270 al. (2010), we did not apply this additional procedure and present only the merged steppe  
271 biome. In summary, the biomisation procedure categorised 39 arboreal pollen taxa and 39  
272 non-arboreal taxa into 22 plant functional types (PFT's), which were then combined into 12  
273 biomes.

274

## 275 **2.3 Quantitative climate reconstruction**

276

277 We reconstructed climate from pollen data based on a standard Modern Analogue Technique  
278 (MAT) that used PFT scores to match fossil samples with modern calibration pollen samples  
279 (as used by Davis et al., 2003). This is a similar approach to that used by Peyron et al. (1998)  
280 and Jost et al. (2005) who also applied pollen PFT scores to reconstruct LGM climate from  
281 pollen data, but who used an artificial neural network technique (ANN) (Chevalier et al.,  
282 2020). PFT scores have been used in previous large-scale European pollen-based climate  
283 reconstructions for the Holocene (Davis et al., 2003; Mauri et al., 2014, 2015), where  
284 performance was found to be better than the conventional approach based on individual taxa  
285 (eg Marsicek et al., 2018). A particular advantage of the PFT approach for the LGM is that it  
286 can help overcome problems associated with vegetation (pollen) assemblages that may have  
287 no modern analogue (Davis et al. 2003). This can be a problem during the LGM when the  
288 climate and environment could be expected to be very different from today, and when many  
289 taxa formed unusual vegetation assemblages as a result of their forced retreat to sheltered  
290 refugia locations. The problem of modern analogues is also addressed in our reconstruction  
291 by using the latest EMPD2 modern pollen dataset for calibration purposes. The EMPD2  
292 provides a large number of potential modern analogues for many different LGM vegetation  
293 types and climates found today across the Palearctic region. PFT scores were calculated

294 according to the methods outlined already in the Biomisation section, then normalized so that  
295 each sample was proportional to every other sample (Juggins and Birks, 2012).

296  
297 The MAT method was applied using the Rioja program for R (Juggins, 2020). The modern  
298 calibration data was taken from the latest version 2 of the EMPD (as detailed earlier). The  
299 EMPD2 includes 8133 samples, which is considerably larger than the modern datasets used  
300 in previous LGM pollen-based reconstructions. For instance, Peyron et al. (1998) used a  
301 calibration dataset of 683 samples, which was updated by Jost et al (2005) to include an  
302 additional 185 samples. These datasets were also mainly taken from the steppes of Kazakstan  
303 and Mongolia, while the EMPD2 covers a much wider area, spanning most of the Eurasian  
304 Palearctic region (Davis et al., 2020). The size and distribution of the modern training set in  
305 climate and vegetation space is important because in order for the method to work  
306 effectively, it is necessary to have samples representative of the likely vegetation and climate  
307 space that could be occupied by the fossil assemblage (Turner et al. 2021, Chevalier et al.,  
308 2020; Salonen et al. 2012, Juggins, 2013).

309  
310 A known problem with MAT is the role of spatial auto-correlation in providing  
311 unrealistically low estimates of uncertainty (Chevalier et al., 2020; Telford and Birks, 2009).  
312 This results from the fact that closely analogous modern pollen samples can also be located  
313 closely in physical space, and therefore in climate space. To reduce this problem it is possible  
314 to exclude closely located samples from the analogue matching process using a filter based  
315 on a set distance (h-block filter) (Telford and Birks, 2009). While this approach can help,  
316 there are also three main problems associated with it. The first is error substitution, since  
317 removing samples also reduces the number of potential analogues, creating a different source  
318 of error that is not easy to categorise. Secondly, multiple samples taken from the same  
319 location are actually a strength of pollen training sets, since they are more likely to capture  
320 the full range of the assemblage diversity associated with a given climate. Thirdly, current  
321 methods that limit spatial range such as the h-block filter only do so on the horizontal axis,  
322 and do not consider the fact that samples can also be found at different elevations. In hilly or  
323 mountainous regions samples can therefore be excluded because they are closely located in  
324 horizontal space, but in fact they actually occupy very different climates and vegetation  
325 associations, contradicting the logical premise of the h-block filter. It was therefore decided  
326 not to apply this filter.

327  
328 Uncertainties for the pollen-climate reconstructions were calculated using a standard method  
329 for MAT (Juggins 2020) based on the spread of the climates associated with the best modern  
330 pollen analogues used for each fossil sample. The closer the climates of the best modern  
331 pollen analogues (6 in the case of this study) then the smaller are the calculated uncertainties  
332 assigned to the reconstructed climate of the fossil pollen sample.

333  
334 Climate reconstructions are presented as anomalies. These have been calculated with respect  
335 to modern climate (1970-2000 average) at each core site location using WorldClim 2 (Fick  
336 and Hijmans, 2017) (Table A2), which was also used to assign the modern climate for the  
337 modern pollen samples in the transfer function (Davis et al., 2020).

## 338 339 **2.4 Quantitative tree cover reconstruction**

340  
341 It has long been recognized that the proportional representation of individual pollen taxa in a  
342 pollen assemblage does not necessarily reflect the proportion of land area covered by that  
343 taxa in the pollen source area surrounding the sample site (Davis 1963, Gaillard et al. 2010,

344 Zanon et al. 2018). These differences can be caused by variations in pollen productivity,  
345 differential transport, deposition and preservation of pollen grains, and even the ease or  
346 otherwise of the identification of pollen grains themselves. This can make the interpretation  
347 of pollen taxa percentages difficult, even for relatively simple questions such as the  
348 proportion of forest to non-forest in the landscape.

349  
350 There have been two main methods developed to account for this quantification problem, one  
351 using a physical modelling technique (PMT) based on estimates of pollen production for  
352 individual taxa (Gaillard et al., 2010), and the other using a MAT very similar to that used in  
353 pollen-climate reconstructions (Williams and Jackson, 2003). Both approaches have been  
354 widely applied during the Holocene in Europe (Zanon et al., 2018), but we know of no  
355 previous study that has applied either of these approaches to the LGM. The LGM presents a  
356 number of challenges, not least the problem of potential missing vegetation analogues, as  
357 well as low atmospheric CO<sub>2</sub>, which has been shown to influence pollen productivity (Leroy  
358 and Arpe, 2007).

359  
360 Here we use the MAT to provide quantitative estimates of forest cover, following the  
361 approach of Zanon et al. (2018) who applied this method to the Holocene pollen record of  
362 Europe. We apply MAT in exactly the same way as for the climate reconstructions described  
363 earlier, including the use of PFT scores to match fossil and modern pollen samples. Instead of  
364 modern climate values, we assigned an estimate of modern forest cover to each of our  
365 modern pollen sites. To do this we use a high resolution (~100m) remote sensing dataset  
366 derived from satellite observations (Hansen et al., 2013). Zanon et al. (2018) have shown that  
367 the MAT calibrated in this way gives comparable results to the PMT approach in Europe, at  
368 least for the Holocene. One of the main differences however is that the PMT is designed to  
369 provide estimates of the proportions of different taxa, whereas the MAT (as applied here) is  
370 designed to provide estimates of the proportion of forest cover. Where the PMT can only  
371 reconstruct the proportion of forest forming trees, irrespective of their size, the MAT  
372 (following Zanon et al. 2018) is calibrated specifically to reconstruct forest composed of trees  
373 over 5m tall. This follows the FAO definition of forest as “land spanning more than 0.5  
374 hectares with trees higher than 5 meters and a canopy cover of more than 10 percent, or trees  
375 able to reach these thresholds in situ” (FAO Terms and definitions 2020  
376 <http://www.fao.org/3/I8661EN/i8661en.pdf>).

377

## 378 **2.5 Maps**

379

380 We present our results in the form of maps that include the main physiographic features of  
381 the LGM in the study area. The maps are based on the WGS84 projection. Coastlines reflect  
382 LGM sea level at 120m below present, while ice sheets are based on Ehlers et al. (2011).  
383 Modern national country boundaries are also included for reference.

384

## 385 **2.6 Marine pollen records**

386

387 We have included marine pollen records in our analysis for reasons explained below, but it is  
388 important that these records should be viewed with caution, particularly when used for biome  
389 and quantitative MAT reconstructions, and when compared with terrestrial records from  
390 different archives. Biomisation methods have been applied to individual marine pollen  
391 records (Combourieu Nebout et al., 2009), as well as multi-site synthesis studies such as the  
392 ACER project (ACER project members et al., 2017). However, marine records were  
393 specifically excluded from the Biome6000 project (Elenga et al., 2000). Similarly,



394 quantitative climate methods have been applied to individual marine pollen records  
395 (Combourieu Nebout et al., 2009; Fletcher et al., 2010), as well as multi-site synthesis studies  
396 (Sánchez Goñi et al., 2005; Brewer et al., 2008; Salonen et al., 2021). However, marine  
397 records have also been specifically excluded from other major pollen-climate studies  
398 (Cheddadi et al., 1996; Davis et al., 2003; Marsicek et al., 2018), as well as quantitative forest  
399 cover reconstructions (Zanon et al. 2018).

400

401 Discussion on the advantages and problems associated with marine records can be found  
402 elsewhere (Chevalier et al., 2020; Daniau et al., 2019), but are reviewed briefly here where  
403 relevant to the methodologies applied in this study. Marine sedimentary records provide  
404 continuous and well dated pollen records for the LGM that are often lacking from many  
405 terrestrial regions, especially in arid areas with few alternative anaerobic sediment sinks.  
406 Conversely however, pollen source areas for marine sites may be many hundreds of  
407 kilometers from the coring site and may be liable to change through time in response to  
408 changes in distance to the coastline, rates of river discharge and ocean and atmospheric  
409 dynamics. This can theoretically give rise to changes in the vegetation shown in the pollen  
410 assemblage recorded at the marine site without any actual change in climate or other  
411 environmental pressure. The large and indeterminable source area of marine records also  
412 mean that it is difficult to apply quantitative MAT reconstruction methods, not least because  
413 the mean climate or forest cover of the source area is almost impossible to determine. In  
414 addition, the pollen record and the calibration dataset to which it is being compared are  
415 composed largely of terrestrial lakes and bog sites with much smaller and more homogeneous  
416 source areas. This creates a series of problems, the more obvious of which is the calculation  
417 of anomalies, since we cannot assume that the modern climate at the (marine) coring site  
418 location is representative of the (terrestrial) source area. In this study we have taken the  
419 closest point on land as the modern climate for the calculation of anomalies, but provide the  
420 absolute values for all sites so that these can be recalculated if necessary (Table A2). The  
421 next problem is that the large source area may capture a combination of different vegetation  
422 types that is not going to be represented in a calibration dataset based on samples from  
423 terrestrial sites with much smaller source areas, for instance a mixture of coastal and  
424 mountain vegetation, or even vegetation from different continents (Magri and Parra, 2002).  
425 However, in our analysis we did not find any sample from a marine record (or terrestrial  
426 record) that did not have a reasonable modern analogue in our training set (chord distance  
427 <0.3)(Huntley, 1990), even though we did not adjust the pollen assemblage for the over-  
428 representation of *Pinus* in the marine pollen samples.

429

430 Typically, the Pine component is excluded from the terrestrial pollen sum when calculating  
431 percentages for marine pollen samples, and in some cases Pine has been excluded entirely  
432 from the samples used in marine pollen-climate reconstructions (Combourieu Nebout et al.,  
433 2009). The problem with excluding *Pinus* is two-fold, the first is that *Pinus* often represents  
434 the main forest forming tree in the Koeppen Csb climate zone on the Atlantic coast where  
435 many marine sites are located (García-Amorena et al., 2007), as well as representing the most  
436 abundant tree taxa in Europe during the LGM (Figure A3c). Removing *Pinus* from the  
437 assemblage would almost certainly create an artificially arid assemblage in these  
438 circumstances, undermining the ability of the transfer function to reconstruct precipitation,  
439 although temperature would likely be less affected since *Pinus* is a generalist found in both  
440 hot and cold temperature regions. The second problem is that the remaining terrestrial taxa  
441 often constitute a very small number of pollen grains in a typical marine pollen sample (<100  
442 grains), which can result in pollen assemblages that are not based on a statistically stable  
443 count of the pollen sample (Chevalier et al., 2020).

444

### 445 3. Results

446

#### 447 3.1 Vegetation & Biomes

448

449 Results of the biomisation analysis shows that steppe (STEP) was the most common biome at  
450 the LGM across the study area, occurring at 36 out of 63 sites, indicating that the landscape  
451 was largely dominated by cool temperate grasslands across much of western Central Europe,  
452 central and eastern Mediterranean, as well as North Africa and the Middle East (Fig. 2).

453 However, at the same time we also find that there were a significant number of sites where  
454 we find that woody and forest biomes occur, more particularly in southern and eastern Iberia,  
455 northern Italy and central eastern Europe. The most dominant of these forest and woody  
456 biomes are taiga (TAIG) in the north, and cool-mixed forest (COMX) and xerophytic  
457 woodlands (XERO) in the south.

458

459 As would be expected, the dominance of STEP biomes is generally reflected in low arboreal  
460 pollen percentages across the same areas/sites (Fig. 3 & 4). Exceptions to this rule can be  
461 found at marine sites such as [MD99-2331 site #3] and [MD01-2430 site #58] where STEP is  
462 reconstructed despite arboreal pollen percentages of 71 and 80 percent respectively. This  
463 apparent contradiction illustrates some of the idiosyncrasies of the biomisation method,  
464 especially when applying the method to marine pollen samples. In this case it is important to  
465 remember that the AP% is calculated from the sum of the percentages of each relevant taxa,  
466 but the score for each biome is the sum of the square root of the percentages of each of its  
467 constituent taxa. This results in biomes with taxa with large percentage values scoring  
468 proportionally smaller, and biomes with taxa with small percentage values scoring  
469 proportionally larger. For example, a single taxa at 50% has a square root of 7.07, but the  
470 sum of the square roots of 10 taxa each at 5% is 22.36 even though the sum of the  
471 percentages is the same 50%. This effect can be particularly pronounced in marine pollen  
472 samples because they are usually dominated by a single taxa (*Pinus*) that forms a high  
473 percentage of the total assemblage. Since there are often more non-arboreal taxa than  
474 arboreal taxa in a pollen assemblage, the non-arboreal taxa can dominate in the biomisation  
475 process even if collectively their percentage of the assemblage is a lot less than the arboreal  
476 taxa, resulting in a non-arboreal biome such as STEP having the highest biome score.

477

478 Of the main arboreal biomes, Taiga (TAIG) is the dominant biome at 3 sites at the eastern  
479 end of the Alpine ice sheet, as well as at a site just to the north in northern Germany and a  
480 site in Slovakia, while Cool Conifer Forest (COCO) is found at 1 site close to the  
481 Scandinavian ice sheet in Lithuania. Cool Mixed Forest (COMX) is found much more widely  
482 at 8 sites south of the Alps from south-west Iberia to Romania, with Xerophytic Scrub  
483 (XERO) occurring at 8 sites with a similar distribution but not as far east or west. Cold  
484 Mixed Forest (CLMX) occurs at just two sites in Georgia and the Alboran Sea at the far east  
485 and west of the study area, while Warm Mixed Forest (WAMX) is the dominant biome at just  
486 1 site in Southern Spain. We do not record Temperate Deciduous Forest (TEDE), Tundra  
487 (TUND) or Desert (DESE) as the dominant biome at any site at the LGM, although they do  
488 occur as sub-dominant biomes.

489

490 An alternative picture of LGM tree-cover is provided by the MAT reconstructions (Fig. 4).  
491 MAT performance statistics for tree cover are shown in table 2, based on an evaluation using  
492 the modern training set. This shows a relatively large root mean square error (RMSE) of  
493 21.03. and an R2 of 0.52 that is not as good as for the MAT climate analysis, but overall the

494 results are comparable with previous MAT tree cover studies (Zanon et al., 2018). In general,  
495 the MAT values (site average 34%) show forest-cover around 16% less than that suggested  
496 from AP% (site average 50%) (Fig. A1), although sites with very low AP% also show higher  
497 values based on MAT. These differences are consistent with comparisons between MAT and  
498 AP% in Zanon et al (2018), although it should be noted that uncertainties related to the MAT  
499 reconstructions are large ( $\pm 23\%$ ). Zanon et al (2018) found that the differences between  
500 MAT and AP% were greatest over Northern Europe and in Arctic and sub-Arctic climate  
501 regions that are likely to be comparable to many areas of Europe during the LGM. These  
502 regions today are associated with tree-forming taxa such as Birch that fail to grow to a height  
503 of 5m or more, developing only as shrubs or krummholz forms.

504  
505 Pollen taxa percentages are shown in supplementary figure A2, and distribution maps of the  
506 33 most common taxa are shown in the supplementary figures A3a-f. Of the 21 arboreal taxa,  
507 *Pinus* generally has the highest values and is the most widespread, being present at all 63  
508 sites. Other acicular arboreal taxa include *Juniperus*, which also has a wide distribution  
509 across EurMedMidEst although at lower values. The rest of the acicular arboreal taxa have  
510 more regional distributions. *Picea* is found mainly to the north of the study region, away from  
511 the Mediterranean, whilst *Abies* is generally found more to the south. *Larix* occurs only in the  
512 central European area including the northern edge of the Po plain just south of the Alps,  
513 whilst *Cedrus* is found mainly across south and west Europe in locations much further north  
514 than its Holocene and modern distribution which is confined mainly to Morocco and Lebanon  
515 (Collins et al., 2012). Temperate broadleaf arboreal taxa which also include cold-tolerant  
516 species such as *Betula* and *Salix* are relatively widely spread across the EurMedMidEst  
517 during the LGM, while less drought tolerant taxa such as *Alnus*, *Carpinus* and *Corylus* are  
518 found more to the south-west through to the north-east. Other temperate broadleaf arboreal  
519 taxa such as *Quercus* (deciduous) and *Ulmus* have a much more southern distribution, with  
520 *Fraxinus*, *Olea*, and *Quercus* (evergreen) being more prevalent in the south-west. In contrast,  
521 *Fagus* occurs more to centre and the east, while *Tilia* is found even in more northern  
522 locations of central Europe. The remaining arboreal taxa are more shrubby and drought  
523 adapted, with *Ephedra* and particularly *Ephedra fragilis* having a southern distribution,  
524 whilst the more cold adapted *Hippophae* being found even in the north of central Europe  
525 (similar to *Tilia*).

526  
527 The main non-arboreal taxa generally indicate cool, dry and environmentally disturbed  
528 conditions across much of the EurMedMidEst. The most widely distributed taxon is Poaceae,  
529 which like *Pinus*, is found in all records. Other non-arboreal taxa with a widespread  
530 distribution include Rubiaceae, Apiaceae and Asteraceae (Asteroideae), while *Plantago*,  
531 Cayophyllaceae, Brassicaceae and Asteraceae (Cichorioideae) have a more southern and  
532 western distribution. *Thalictrum* can be found mostly at sites in the centre of the  
533 EurMedMidEst, along with *Helianthemum* which also extends to sites in the south-west.  
534 Other taxa such as *Chenopodiaceae* and *Artemisia* have a more southern distribution,  
535 reflecting their preference for drier and less cold climates.

### 536 537 **3.2 Climate reconstruction evaluation**

538  
539 Evaluation of transfer function performance based on the modern training set is presented in  
540 table 2. This shows that root mean square error predicted (RMSEP) values were smallest for  
541 summer temperatures (2.21C), and largest for winter temperature (3.35C), with mean annual  
542 temperatures in between (2.28C). The weaker performance for winter temperatures largely  
543 reflects the much greater range of winter temperatures in the training set. In turn, this

544 contributes to a better R2 performance for winter temperatures (0.91) than annual  
545 temperatures (0.9) and summer temperatures (0.81). Overall R2 performance for precipitation  
546 is weaker than for temperature, which is typical because of the higher spatial variability of  
547 precipitation compared to temperature. Summer precipitation has the strongest R2  
548 performance (0.75) compared to winter and annual precipitation (both 0.69), as well as  
549 smaller RMSE values (52mm) than winter (78mm).

550  
551 Given the widespread occurrence of steppe during the LGM, we also undertook a separate  
552 evaluation of transfer function performance in this type of environment. For this we used a  
553 subset of 1588 pollen samples from the EMPD2 that are classified with the steppe pollen-  
554 biome (Davis et al. 2020). The results indicate (Table A3) little difference in performance  
555 compared to the full dataset, with a small decrease in performance in annual and summer  
556 seasons in both precipitation and temperature, and a slight increase in performance in winter.

557  
558 The results overall indicate good transfer function performance especially for temperature,  
559 and are comparable with those found in other continental scale pollen-climate studies  
560 (Bartlein et al., 2011). It is important to remember though that comparisons between studies  
561 can only be made with caution because results are often heavily dependent on the nature of  
562 the modern pollen dataset used as the training set, which is not the same in all studies  
563 (Juggins, 2013).

564  
565

### 566 **3.3 Climate reconstruction**

567  
568 Reconstructed LGM temperatures indicate an overall mean annual cooling of  $-7.2 \pm 3.3\text{C}$ ,  
569 with a greater cooling of around  $-9.3 \pm 4.5\text{C}$  in winter and  $-5.0 \pm 3.2\text{C}$  in summer (Fig. 5). All  
570 sites apart from Lake Van [site #62] in eastern Turkey show cooler temperatures at the LGM  
571 compared to modern (Fig. 6), and even at this site cooler conditions fall within the  
572 uncertainties. With greater cooling in winter compared to summer, the difference in  
573 temperature between winter and summer also increased (shown by positive anomalies) at  
574 most (but not all) sites (Fig. 6). This increase in continentality was around  $+4.2\text{C}$  on average  
575 across all sites (Fig. 5).

576  
577 We reconstruct an overall decline in mean annual precipitation of around  $-91 \pm 270\text{mm}$  (-  
578 13%) at the LGM. Most of this decline is in winter ( $-38 \pm 90\text{mm}$ ) (-21%), while in summer a  
579 small increase is shown ( $10 \pm 57\text{mm}$ ) (6%), although uncertainties are large (Fig. 7).  
580 Compared to temperature there is significant seasonal and spatial variability in positive and  
581 negative precipitation anomalies (Fig. 8). Positive anomalies appear more predominant in  
582 eastern and southern Spain and in central eastern Europe in both summer and winter, while  
583 positive anomalies are found more generally in summer across sites in Southern Europe and  
584 the Mediterranean. These more positive summer anomalies also reflect a relative shift from  
585 winter to summer in the seasonality of precipitation in this region.

586  
587

### 587 **4.0 Discussion**

588  
589 Before we consider the results of our analysis it is important to provide some context in terms  
590 of European LGM geography and environment, which was very different from today (Fig. 1).  
591 Major ice sheets covered Scandinavia and much of the UK, the Alps, and the Pyrenees. Sea  
592 level was 120m lower, resulting in much of the North Sea and English Channel becoming dry  
593 land, and the European coastline extending over 100 km out into the Atlantic and

594 Mediterranean, especially around the Bay of Biscay and Adriatic. The Black Sea was no  
595 longer connected to the Mediterranean, and was smaller with a water level around 100m  
596 lower than today (Genov, 2016). These changes in sea or water level had two main  
597 consequences, the first being that the marine sites were closer to land, and therefore closer to  
598 (low lying) terrestrial vegetation and (pollen carrying) river discharge points than they are  
599 today. The second consequence of lower seas levels is that terrestrial pollen sites were  
600 located further from the moderating effect of the ocean than they are today, resulting in a  
601 localised modification of the climate experienced by the site irrespective of regional or global  
602 changes (Geiger, 1960).

603  
604 The maps used in our analysis shows the maximum ice sheet at  $21k \pm 2k$  (Ehlers et al., 2011).  
605 The precise geographical location of the ice sheet is difficult to resolve at a fine spatial scale,  
606 however, which explains why some sites close to the ice margin appear to be actually located  
607 under the ice (for example sites Kersdorf-Briesen site #46 & Mickunai site #54). The  
608 resolution of the map also shows the occurrence of permanent ice not only to the north and  
609 over the Alps, but also on many subsidiary areas of high ground across central and southern  
610 Europe, including areas such as the Pyrenees, Massif Central, Vosges and Carpathian  
611 Mountains. While global ice volume may have peaked  $\sim 21$  ka individual ice sheets in Europe  
612 and other areas are known to have reached their maximum extent at different times (Hughes  
613 et al., 2016). The larger ice sheets are likely to have had a significant influence on regional  
614 climate and environmental conditions across Europe, but the smaller ice sheets had similar if  
615 more localized impacts as well. Surrounding each ice sheet would have been an unglaciated  
616 area of active peri-glacial processes and newly created and unstable ground. This would  
617 include outwash plains, impounded lakes and recently drained lake beds, seasonally and  
618 sporadically flooded areas, moraines, kettle holes and other glaciological and peri-glacial  
619 features. Soils in these areas would be non-existent or skeletal, and vegetation would find it  
620 difficult to obtain nutrients and water for survival, irrespective of the prevailing climatic  
621 conditions. Outside of these areas, permafrost is also likely to have been present, particularly  
622 north of the Alps (Vandenbergh et al., 2014), which would also act as an impediment to  
623 vegetation growth.

624  
625 In terms of regional climate, the major ice sheets would have provided significant barriers to  
626 westerly atmospheric circulation, or even north-south circulation in the case of the Alps and  
627 Pyrenees. As well as representing a physical obstruction, the thermodynamic response of the  
628 atmosphere to these high, cold obstructions would have been to encourage the formation of  
629 areas of semi-permanent high pressure, similar to those found today for instance over the  
630 Greenland ice sheet. In addition, the Laurentide ice sheet located over North America would  
631 have generated downstream effects over Europe (COHMAP, 1988). These physical and  
632 thermodynamic effects would have affected the direction of storm tracks, as well as more  
633 local climatic effects commonly associated with ice sheets such as strong katabatic winds  
634 (Kageyama, et al. 2021, Velasquez et al. 2021, Luetscher et al. 2015, Lefort et al. 2019)

#### 635 636 **4.1 Vegetation Cover**

637  
638 The nature and extent of forest cover during the LGM remains a matter of considerable  
639 debate. Vegetation models driven by LGM climate model simulations generally indicate  
640 extensive areas of boreal forest north of the Alps, and a mix of temperate and warm-  
641 temperate woodland to the south across southern Europe and much of the Mediterranean.  
642 Treeless areas such as steppe are mainly confined to those areas where it is also found today,  
643 namely inland Iberia, Ukraine, southern Russia and Turkey, while Tundra is found to the

644 north close to the Scandinavian Ice Sheet (Allen et al., 2010; Cao et al., 2019; Prentice et al.,  
645 2011; Velasquez et al., 2021).

646  
647 Evaluation of these vegetation-model simulations against data has been largely based on  
648 comparison with compilations of pollen-biome reconstructions (Prentice et al., 2011; Allen et  
649 al., 2010; Cao et al., 2019; Velasquez et al., 2021). Early studies were based on only a limited  
650 number of sites from southern Europe, and showed steppe at all sites in contradiction with  
651 model simulations (Elenga et al. 2000). More recent pollen compilations have included more  
652 sites especially to the north that have revealed a more mixed picture of vegetation cover, with  
653 forest biomes at some sites both south and north of the Alps that appear more consistent with  
654 model simulations (Binney et al., 2017; Cao et al., 2019). However, many of these pollen  
655 sites used in these studies were assigned an LGM age based on poor or incorrect dating  
656 control, and likely date to MIS3, the Late-Glacial or even the Holocene. Nevertheless, based  
657 on our compilation of more securely dated LGM pollen sites, we also show a wider  
658 distribution of forest biomes particularly in Iberia, northern Italy and Central Europe,  
659 although with greater areas of steppe than suggested by the models over the remaining  
660 regions.

661  
662 However, the interpretation of biome reconstructions requires care since the forest cover and  
663 vegetation composition may not be as clear as the dominant biome suggests. For instance, we  
664 find that steppe is still reconstructed as the dominant biome at some sites despite arboreal  
665 pollen forming 70-80% of the pollen assemblage. In addition, it is important to remember  
666 that pollen-biomes are based only on the proportion of taxa that can form forest and  
667 woodland, while these taxa may in fact exist only as shrubs or stunted krummholz forms in  
668 the challenging climate and environment of the LGM. Alternatively, similar conditions may  
669 favour low-lying non-arboreal taxa forms with poor pollen dispersion or even insect  
670 pollinated taxa forms that may be poorly represented in the pollen assemblage, giving greater  
671 prominence to arboreal taxa whose pollen may be the result of long-distance transport  
672 particularly *Pinus*. However there also appear to be plenty of samples with low or even very  
673 low (<20%) arboreal percentages, so not all sites in open areas may be affected by long-  
674 distance transport of *Pinus* in the same way.

675  
676 Quantitative MAT based reconstructions of forest cover can overcome some of these  
677 problems, where they can be detected, based on the composition of the pollen assemblage  
678 when compared with the modern land-cover. Chord-distance measurements of the match  
679 between fossil and modern pollen assemblages indicate good LGM analogues exist in our  
680 large Eurasian modern pollen dataset. The results of the MAT forest cover reconstruction  
681 indicates that forest cover was low but not entirely devoid of woodland in most areas, similar  
682 to the modern boreal forests of Siberia and consistent with a steppe-tundra-woodland mosaic  
683 proposed by many authors (e.g. Birks and Willis, 2008; Willis and Van Andel, 2004). This is  
684 confirmed in an analysis of the most commonly found modern analogue ecoregions for LGM  
685 pollen samples at each site (Table A4). Uncertainties are large, but for comparison the MAT  
686 site-average of 33% forest cover is slightly less than the average today over the Boreal region  
687 of Europe (43%) and slightly more than the average today over Mediterranean region (27%)  
688 (Zanon et al. 2018).

689  
690 By calculating the percentage of each of the taxa in each LGM pollen sample using a  
691 standardized pollen sum, we are able to make direct comparisons between different LGM  
692 pollen records and their taxa percentages (Figure A2, A3). The results show a preponderance  
693 of boreal forest taxa to the north of the Alps, consistent with biome results mentioned earlier.

694 *Pinus* is the most common forest forming taxa in this boreal zone, together with *Picea*, and  
695 including *Larix* to the east and *Abies* to the west. The occurrence of *Betula* and *Juniperus*  
696 also suggests shrubby elements consistent with arctic shrub-tundra, although high Poaceae  
697 and other herbaceous taxa such as *Artemisia* and *Chenopodiaceae* indicate more steppe than  
698 tundra. Other deciduous taxa found north of the Alps include cold tolerant generalists such as  
699 *Corylus* and *Alnus*, as well as low percentages of relatively thermophilous taxa in the east,  
700 such as *Carpinus* and *Tilia*.

701  
702 These results are consistent with charcoal (Magyari et al., 2014a; Willis and Van Andel,  
703 2004), malacological (Juříčková et al., 2014), biomarkers (Zech et al., 2010) and genetic  
704 evidence (Stivrints et al., 2016; Willis and Van Andel, 2004) that the main forest region north  
705 of the Alps was in the eastern region of Central Europe around the Carpathian basin. This  
706 was also an area where cold and moisture sensitive deciduous taxa were also able to survive  
707 (Magyari et al., 2014), although evidence of temperate taxa found in the pollen record has yet  
708 to be supported by charcoal and macrofossil records (Feurdean et al., 2014). Our pollen  
709 evidence indicates an open taiga or cool mixed forest that extended in central and eastern  
710 Europe to areas close to the Scandinavian and Alpine ice caps, as proposed by Willis and Van  
711 Andel (2004) and Huntley and Allen (2003), although whether this represents isolated  
712 pockets of forest or an extended open steppe-forest is difficult to determine (Kuneš et al.,  
713 2008). Even steppe or tundra areas in western Europe show a low but significant presence of  
714 the pollen of tree taxa at sites close to the ice sheets that are unlikely to be solely the result of  
715 long distance transport or reworking (Kelly et al., 2010). The presence of woodland in these  
716 areas is also supported by mammalian remains, for instance at Kents Cavern in SW England  
717 (Stewart and Lister, 2001).

718  
719 Overall however, our results clearly show a much greater predominance of thermophilous  
720 and moisture sensitive deciduous taxa south of the Alps, particularly in Iberia and Northern  
721 Italy, where temperate broadleaf forests survived in sheltered refugia (Kaltenrieder et al.,  
722 2009). Most of these appear to be in hilly areas with the ability to generate orographic rainfall  
723 (Monegato et al., 2015), on south facing slopes to make the most of the sun's radiant energy  
724 and located above the valley floor to escape frost and flooding. We might also expect these  
725 areas to be sheltered from cold northerly winds, and benefit from relatively mild and moisture  
726 laden winds coming from the Mediterranean Sea. For instance, the presence of woodland and  
727 low glacier altitudes along the southern slopes of the Alps around the Po Valley and Trentino  
728 region is consistent with strong orographic rains generated by southerly and easterly winds  
729 that today can be generated by low pressure located south of the Alps in the Gulf of Genoa,  
730 and consistent with a southerly storm track around the Alps (Kehrwald et al., 2010; Luetscher  
731 et al., 2015). Generally, as might be expected, areas of forest reconstruct similar or increased  
732 precipitation compared to today, and areas of steppe indicate decreased precipitation (see next  
733 section).

734  
735 Independent evidence of LGM vegetation is provided by archaeozoological data. This data  
736 supports the palynological evidence for the existence of forest and woodland refugia across  
737 the ice-free areas of Europe at latitudes north of the Alps. For instance, large vertebrates in  
738 these areas show patterns of extirpation and extinction in response to shifts in climate and  
739 vegetation cover that is different for different species, indicating a variety of environments  
740 and niches (Lister and Stuart, 2008; Stewart and Lister, 2001). As with the pollen record, the  
741 presence of temperate adapted large vertebrate taxa within the glacial landscape of Western  
742 Europe also suggests the existence of temperate "micro-refugia" (Stewart and Lister, 2001),  
743 consistent with suggestions that temperate arboreal taxa were not entirely extirpated from the

744 region during the LGM (Magri, 2010). Further east, mammal assemblages indicate  
745 generalized loss of forest components in the East European Plain (Demay et al. 2021,  
746 Puzachenko et al., 2021) which is consistent with our data indicating low forest cover in this  
747 region. In other areas, evidence of the prevailing land cover at the LGM comes from studies  
748 of small vertebrate communities, which have a closer affinity to the prevailing environment  
749 than large vertebrates (López-García and Blain, 2020) that have the propensity to migrate  
750 large distances, often on a seasonal basis. These studies of small vertebrate assemblages also  
751 support the existence of temperate “micro-refugia” in France (Royer et al., 2016) and the  
752 existence of woodland components in many regions across Southern Europe including parts  
753 of Iberia (Bañuls-Cardona et al., 2014) Italy (Berto et al., 2019) and the Balkan Peninsula  
754 (Mauch Lenardić et al., 2018).

755  
756 Other paleobotanical evidence also supports our land cover reconstruction. Schafer et al.  
757 (2016) suggest leaf wax patterns from palaeosols in Spain may indicate the presence of  
758 drought intolerant deciduous trees and more humid conditions during the LGM. Significantly,  
759 none of the pollen sites indicate that temperate broadleaf forests were dominant, and  
760 broadleaf temperate taxa always appear part of a mixed woodland together with cold or  
761 aridity adapted evergreen and needleleaf taxa, including typical Mediterranean taxa. This type  
762 of mixed vegetation probably extended to the Balkans where the hilly terrain and proximity  
763 to the Mediterranean would appear to have provided favourable climatic conditions, although  
764 we still lack LGM sites from this region. At sites in central and southern Italy and east  
765 through Greece and Turkey to the Middle East (and including North Africa), the vegetation  
766 appears drier with a greater prevalence of steppe. Only a site in Georgia at the edge of the  
767 Caucasian mountains indicates the presence of significant amounts of forest (mainly *Pinus*), a  
768 result that was also found by Tarasov et al. (2000), and probably linked to favourable  
769 orographic precipitation and proximity to the Black Sea.

770  
771 Comparison with LGM land cover from vegetation modelling studies driven by climate  
772 model simulations indicate a much wider presence of forest than that shown by the pollen  
773 data (Kaplan et al., 2016). Data-model agreement appears to be closest over eastern-central  
774 Europe where pollen indicates the presence of open Boreal forest, and over south-west  
775 Europe with the presence of cool mixed temperate forest, including broadleaf deciduous and  
776 thermophilous elements (Prentice et al., 2011; Allen et al., 2010; Cao et al., 2019; Velasquez  
777 et al., 2021). Nevertheless, agreement still appears to be weak over western-central Europe  
778 and Southern and Eastern Europe through to the Middle East, where pollen data continues to  
779 indicate widespread steppe. One proposed explanation for this data-model discrepancy has  
780 been the role of fire (including man-made fire) in maintaining forest openness, a factor  
781 influencing forest cover that is not included in most vegetation models (Kaplan et al., 2016).  
782 In the Carpathian basin Magyari et al. (2014a) noted that charcoal increased as forest cover  
783 declined, suggesting that wildfires played a role in decreasing forest cover during the LGM.  
784 Other studies have noted low levels of charcoal and therefore fires during the LGM, although  
785 these tend to be from steppe areas with low biomass and fuel availability (Connor et al.,  
786 2013; Kaltenrieder et al., 2009). Recent LGM vegetation simulations that include fire indicate  
787 much lower values of forest cover than those without fire over western central Europe, while  
788 forest remains in central eastern Europe (see figure 6 in Velasquez et al., 2021). This appears  
789 closer to the data, but the values are perhaps too low compared with our MAT  
790 reconstructions here (Figure 4).

## 791 792 **4.2 Climate** 793



#### 794 **4.2.1 Comparison with previous pollen-based reconstructions**

795

796 The climate of the LGM is generally considered to have been cooler and drier than today, but  
797 data-model comparisons continue to highlight important discrepancies, not only in the degree  
798 of cooling and drying but also in their seasonal and spatial distribution. Data-model  
799 comparisons over Europe have mainly used pollen-based climate reconstructions, especially  
800 the Paleoclimate Modelling Intercomparison Project (PMIP/CMIP) (Kageyama et al., 2021,  
801 Bartlein et al., 2011; Harrison et al., 2015; Kageyama et al., 2006). The most commonly used  
802 reconstructions have been based on two main methods, a neural-network methodology  
803 (ANN) of Peyron et al. (1998) and Jost et al. (2005), and an Inverse Modelling approach  
804 (INV) applied by Wu et al. (2007). The ANN method uses modern pollen samples for  
805 calibration and does not include any correction for CO<sub>2</sub> effects, being similar in these  
806 respects with the MAT method used in this study. In contrast the INV method does not use  
807 modern pollen samples for calibration, but instead uses a process-based vegetation model run  
808 in inverse mode. Ordinarily, a vegetation model will use climate as an input to generate a  
809 vegetation as an output, but in inverse mode the model is reconfigured to generate climate as  
810 an output given a particular vegetation (pollen) assemblage as an input. One of the  
811 advantages of the INV method is that CO<sub>2</sub> can also be varied as an input, and therefore the  
812 effect of changes in CO<sub>2</sub> on the vegetation, and therefore reconstructed climate, can be  
813 investigated. Comparison of these ANN and INV reconstructions have shown important  
814 differences, with the INV reconstruction generally not as cold and somewhat drier than ANN  
815 (Wu et al. 2007). These differences between pollen-climate methods have often been  
816 attributed to CO<sub>2</sub> effects (Wu et al. 2007) but this is not clear since there may be other  
817 factors, such as the size and location of the training set used in the ANN reconstruction.

818

819 We make a comparison with these earlier reconstructions based on 10 sites/records in our  
820 dataset which we identified as also being included in these earlier studies (Fig. 9). While we  
821 were able to identify the site and data source, as well as the time window, we were unable to  
822 establish if the the data represented a single sample or the mean of multiple samples within a  
823 time-window or the exact depth of those samples, or the actual sediment core in the case of  
824 multiple cores from the same site. While these aspects are unknown, it seems likely that the  
825 pollen data we used in our analysis was very similar if not identical in most cases, and  
826 reconstructed biomes for these sites from our pollen dataset are identical to the biomes  
827 reconstructed using the earlier pollen dataset (Elena et al., 2000).

828

829 We compare our MAT with the ANN and INV reconstructions in figure 9. On average across  
830 all 10 records, the MAT and INV methods give almost identical results for both anomalies of  
831 mean annual temperature (MAT -6.6C, INV -7.2C) and precipitation (MAT 158mm, INV  
832 165mm). Uncertainties are also similar for both methods. In contrast, the ANN method gives  
833 much cooler mean annual temperature anomalies (ANN -13.9C) and drier precipitation  
834 anomalies (ANN -474mm). On a site by site basis the MAT and INV methods show closer  
835 agreement for temperatures than precipitation, although precipitation has proportionally  
836 larger uncertainties. The reconstructions based on these two methods are close enough that  
837 the uncertainties overlap at all sites for both temperature and precipitation, except the  
838 precipitation reconstruction at Lac de Bouchet (site #25). The reason for this is not clear, but  
839 there could easily be minor differences with the pollen data analysed by Wu et al. (2007) in  
840 their INV reconstruction since the pollen record (Reille and de Beaulieu, 1988) includes  
841 multiple cores each with many different samples covering the LGM period.

842

843 This comparison shows that our MAT reconstructions are very similar to the INV method,  
844 but not as cold or dry as the ANN method. This has two main implications. The first is that  
845 our reconstructions indicate greater agreement with the results of climate model simulations  
846 since climate models indicate temperatures closer to the INV reconstructions (Latombe et al.,  
847 2018) than the ANN reconstructions (Jost et al., 2005; Kageyama et al., 2006). The difference  
848 between our MAT and earlier ANN reconstructions is likely the result of the modern  
849 calibration datasets used, since the ANN reconstruction was based on a considerably smaller  
850 number of samples taken mainly from the cold dry steppes of Kazakstan and Mongolia.

851  
852 The second implication is that the MAT method may not be significantly impacted by the  
853 effects of lower CO<sub>2</sub> (Cowling and Sykes, 1999; Prentice and Harrison, 2009; Williams et  
854 al., 2000) or indeed insolation changes during the LGM, since the MAT results are similar to  
855 those based on the INV method which specifically takes account of these non-climatic factors  
856 (Wu et al., 2007). This would suggest that MAT could also work well for pollen-based  
857 climate reconstructions on longer glacial-interglacial timescales where insolation and CO<sub>2</sub>  
858 vary significantly from their modern values. This is consistent with the findings of Pini et al.  
859 (2021) who applied a correction algorithm developed by Prentice et al. (2017) and Cleator et  
860 al. (2020) to a MAT reconstruction of mean annual precipitation at Lake Fimon in Northern  
861 Italy. This shows a very small correction of 0mm to 30mm for samples across the LGM time-  
862 window, which indicates that CO<sub>2</sub> is not a very significant factor in influencing this type of  
863 reconstruction, at least compared to the overall uncertainties (+/- 200mm) of the  
864 reconstruction itself. The uncertainties associated with the correction algorithm are not  
865 discussed, but given that inputs include estimates of both LGM temperature and cloud cover,  
866 it seems likely that these could be significant. Importantly, both Pini et al (2021) and Cleator  
867 et al (2020) specifically exclude the necessity of applying a correction algorithm to  
868 temperature reconstructions, since they consider only hydrological variables to be affected by  
869 changes in atmospheric CO<sub>2</sub>.

870

871

## 872 **4.2.2 Comparison with climate reconstructions based on other proxies**

873

### 874 **4.2.2.1 Temperature**

875

876 Proxies that are not based on plants should remain unaffected by the CO<sub>2</sub> problem during the  
877 LGM, and provide an alternative basis for evaluating pollen-based reconstructions. Samartin  
878 et al. (2016) reconstructed LGM summer temperatures based on chironomid remains from  
879 Lago della Costa (site #34) in Northern Italy. They also undertook pollen analysis on the  
880 same samples down the core, allowing us to make a sample-by-sample comparison between  
881 the chironomid temperature record and our MAT reconstruction (Fig. 10). Our pollen-climate  
882 reconstruction is for JJA mean temperature, while the chironomid reconstruction is for July  
883 mean temperature, with the anomalies based on the modern equivalent JJA and July mean  
884 temperatures respectively. The average anomaly values for all 8 samples reconstructed by the  
885 pollen-climate MAT are  $-10.2 \pm 3.5^{\circ}\text{C}$ , and for the chironomids  $-9.5 \pm 3.0^{\circ}\text{C}$ . This indicates  
886 that pollen and chironomid average summer temperature reconstructions are very similar on  
887 average, taking into account the overlapping uncertainties, while also showing a strong  
888 similarity on a sample-by-sample basis throughout the time-series.

889

890 Other reconstructions based on other proxies provide a basis for more general regional  
891 comparisons (Figure A4, A5). We reconstruct both summer and winter temperatures and  
892 show that cooling in winter was greater than in summer at most sites, associated with an

893 increase in continentality (increased temperature difference between summer and winter). A  
894 similar seasonal pattern of temperature change has also been shown in other studies that  
895 reconstruct both summer and winter LGM temperatures, including Prud'homme et al. (2016)  
896 using  $\delta^{18}\text{O}$  analysis of earthworm calcite granules at Nussloch near the French-German  
897 border, Bañuls-Cardona et al. (2014) using faunal remains of small mammals at 4 locations in  
898 western Spain, and Ferguson et al. (2011) who examined seasonal temperature change using  
899  $\delta^{18}\text{O}$  and Mg/Ca analysis of limpet shells at Gibraltar in southern Spain. The increase in  
900 continentality at Nussloch (Prud'homme et al., 2016) was reconstructed at between 11.6 to  
901 15.6 °C, comparable at the lower end with nearby pollen sites [La Grotte Walou site #28]  
902  $10.4 \pm 5.8$  °C and [Bergsee site #29]  $7.9 \pm 5.7$  °C. The faunal sites in western Spain studied  
903 by Bañuls-Cardona et al. (2014) gave much reduced increases in continentality, but  
904 nevertheless similar to nearby pollen sites. For instance at Valdavara 5.1 °C [MD99-2331 site  
905 #3]  $5.2 \pm 3.1$  °C, El Miron 1.2 °C [Tourbiere de l'Estarres site #19]  $5.1 \pm 6.2$  °C, El Portalon  
906 0.9C [Torrecilla de Valmadrid site #16]  $2.8 \pm 1.8$  °C and Cueva de Maltrvieso 6.1C [SU81-18  
907 site #2]  $4.8 \pm 3.4$  °C. Further south at Gibraltar the limpet-based study of Ferguson et al.  
908 (2011) also shows a relatively small increase of 2 °C. The nearest pollen site [Gorham Cave  
909 site #5] however shows a larger increase of  $4.7 \pm 2.3$  °C, although differences could be  
910 expected given the different temporal resolution of annual laminae on mollusk shells  
911 compared to pollen assemblages that reflecting much slower changes in trees and other long-  
912 lived flora.

913

914 Summer temperatures were warm enough during the LGM over the Alpine areas that Swiss  
915 lakes were largely ice free in summer, while glacier ELA's around the time of the LGM  
916 suggest summers were -6.5 to -7.7 °C cooler compared to the LIA (Heiri et al., 2014). This  
917 cooling was similar to that found at Nussloch some 200km north of the Swiss border by  
918 Prud'homme et al. (2016), who reconstructed anomalies of -6 to  $-8 \pm 4$  °C from  $\delta^{18}\text{O}$   
919 analysis of earthworm calcite granules (representing warm season May-September  
920 temperatures). Slightly less cooling was found close by at the nearby site of Achenheim  
921 where analysis of Mollusc assemblages gave summer (August) cooling estimates of -3.5 to -  
922 6.5 °C based on MAT (Rousseau, 1991), and -5.5 to -9.5 °C based on the Mutual Climatic  
923 Range method (Moine et al., 2002). These reconstructions appear somewhat cooler than  
924 nearby pollen sites [La Grotte Walou site #28]  $-1.4 \pm 3.6$  °C and [Bergsee site #29]  $-2.7 \pm 5.1$   
925 °C, although comparable with the pollen site [Pilsensee site #32]  $-7.3 \pm 5.0$  °C 200 km further  
926 east. Similar differences also occur at the site of Les Echets on the western edge of the Alps  
927 where a diatom based reconstruction of summer (July) temperatures (Ampel et al., 2010)  
928 indicated a greater cooling (-10.5 to -11.5 °C) than our pollen reconstruction [Les Echets G  
929 site #27] ( $-4 \pm 2.7$  °C). However, the authors caution that the results were based on poor  
930 analogues and rare taxa, as well as a small training set of only 90 lakes in Switzerland.

931

932 South of the Alps, other proxies show the opposite relationship with the pollen  
933 reconstructions. For instance, at Lago della Costa in the Po valley, a summer (July)  
934 temperature chironomid reconstruction by Samartin et al. (2016) is around 1-2 °C less cool  
935 than the pollen reconstruction (JJA) for the same site [Lago della Costa site #34]  $-11.4 \pm$   
936  $2.7$  °C, although both reconstructions fall within their respective uncertainty ranges (Figure 8).  
937 In the Pindus Mountains in Greece, Hughes et al. (2006) estimated LGM summer  
938 temperature anomalies of - 7 °C based on glacier modelling, which is comparable with that  
939 reconstructed at the nearest pollen site [Ioannina site #51]  $-7.7 \pm 2.8$  °C. In Spain the analysis  
940 of small mammal remains by Bañuls-Cardona et al. (2014) shows similarly less cooling in  
941 summer or even warmer than present positive anomalies compared to the nearest pollen sites,  
942 such as Valdavara 1.4 °C [MD99-2331 site #3]  $-2.3 \pm 2.8$  °C, El Miron -2.3 °C [Tourbiere de

943 l'Estarres site #19]  $-5.7 \pm 5.4$  °C, El Portalon  $0.8$  °C [Torrecilla de Valmadrid site #16]  $-2.6 \pm$   
944  $1.1$  °C and Cueva de Maltrvieso  $-1.1$ C [SU81-18 site #2]  $-10.4 \pm 2.8$  °C. Further south at  
945 Gibraltar, the limpet-based study of Ferguson et al. (2012) suggests an anomaly of around  $-7$   
946 °C, which is a greater cooling than the pollen reconstruction from this location [Gorham Cave  
947 site #5]  $-1.3 \pm 2.2$  °C, although comparable with other pollen sites slightly further east.  
948

949 Winter temperature reconstructions from non-pollen proxies show a similar pattern in relation  
950 to pollen reconstructions as for summer temperatures. North of the Alps at Achenheim,  
951 Prud'homme et al. (2016) use d18O on earthworm remains to reconstruct particularly cold  
952 winter anomalies of  $-17.6$  to  $-23.6$  °C compared to nearby pollen sites [La Grotte Walou site  
953 #28]  $-11.8 \pm 8.0$  °C and [Bergsee site #29]  $-10.6 \pm 6.3$  °C. South of the Alps in Spain, the  
954 analysis by Bañuls-Cardona et al (2014) based on the remains of small mammals shows less  
955 cooling in winter compared to the nearest pollen sites, in particular Valdavara  $-3.7$  °C  
956 [MD99-2331 site #3]  $-7.5 \pm 3.4$  °C, El Miron  $-3.5$  °C [Tourbiere de l'Estarres site #19]  $-10.8$   
957  $\pm 7.0$  °C, El Portalon  $-0.1$  °C [Torrecilla de Valmadrid #16]  $-5.4 \pm 2.5$  °C and Cueva de  
958 Maltrvieso  $-7.2$ C [SU81-18 site #2]  $-15.2 \pm 4.0$  °C. And again, in southern Spain at Gibraltar,  
959 analysis of limpet shells by Ferguson et al (2011) suggests winter cooling of around  $-9$  °C  
960 while the pollen reconstruction suggests [Gorham Cave site #5]  $-6.0 \pm 2.5$  °C, although sites  
961 further east indicate cooler conditions.  
962

963 A number of additional proxies have also been used to reconstruct LGM mean annual  
964 temperature. Heyman et al. (2013) applied glacier mass balance modelling at sites located in  
965 the smaller mountain regions north of the Alps. These are generally slightly cooler than our  
966 pollen-based reconstructions at sites close to the Vosge Mountains  $-12.7 \pm 2.0$  °C and Black  
967 Forest  $-11.4 \pm 2.3$  °C [Bergsee site #29]  $-8.2 \pm 3.3$  °C, Bavarian Forest  $-10.7 \pm 2.2$  [Pilsensee  
968 site #32]  $-9.2 \pm 1.2$  °C and Giant Mountains  $-8.5 \pm 1.8$  [Kersdorf-Briesen site #46]  $-7.3 \pm 0.3$   
969 °C. These values obtained by Heyman et al. (2013) are warmer than Pud'homme et al. (2016)  
970 who estimated annual mean temperature anomalies of  $-15.1$  to  $-19.1$  °C based on d18O of  
971 earthworm calcite at the Nussloch site just north of the Vosge and Black Forest. The annual  
972 temperatures reconstructed by Heyman et al. (2013) are also around 2C warmer than Allen et  
973 al. (2008) who applied a similar, although simpler method to over 29 different mountainous  
974 regions across Europe that had been glaciated during the LGM. Since glacier mass balance is  
975 a function of both snowfall and temperature, these estimated temperatures vary according to  
976 estimated changes in precipitation. For instance, mean annual temperature estimates by Allen  
977 et al. (2008a) are much cooler than reconstructed by pollen, with an average anomaly of  $-13.2$   
978 °C for the 29 sites assuming a 40% reduction in precipitation, but this is reduced to  $-11.8$  °C  
979 assuming the same precipitation as modern. This compares with  $-7.2$  °C for our 63 pollen  
980 sites. The glacier mass balance modelling by Allen et al. (2008a) assumes a seasonal  
981 distribution of precipitation that is similar to the present day, and does not consider increases  
982 in winter precipitation or mean annual precipitation above present day levels. Both of these  
983 are suggested by the pollen data in some regions, and both could explain glacier extent found  
984 during the LGM based on less extreme temperature anomalies more comparable with the  
985 pollen data.  
986

987 To the east of the Alps in the Panonian basin, mean annual temperature anomaly estimates  
988 have been made from noble gas measurements on groundwater ranging from  $-2$  to  $-4$  °C  
989 (Stute and Deak, 1990) up to  $-9$  °C (Varsányi et al., 2011). These are similar to estimates  
990 ranging from  $-2$  to  $-9$  °C from oxygen isotope ratios from mammoth tooth enamel (Kovács et  
991 al., 2012) and are comparable with nearby pollen sites [Feher Lake site #50]  $-8.2 \pm 3.3$  °C and  
992 [Kokad site #52]  $-4.5 \pm 2.3$  °C. On a broader scale, Sanchi et al (2014) estimated LGM

993 cooling in the Danube and Dneiper basins based on Lipid biomarkers in a core from the  
994 Black Sea and came up with similar mean annual temperature anomalies between -6 to -10  
995 °C, which again are comparable with pollen sites from the region that range from  
996 [Nagymohos site #48]  $-10.5 \pm 4.1$  °C to [Straldzha site #57]  $-4.3 \pm 5.8$  °C.

997  
998 Further south and west, García-Amorena et al. (2007) reported mean annual temperature  
999 anomalies of -2.0 to -11.3 °C at LGM sites along the Portuguese coast, based on an indicator  
1000 species method using plant macrofossils. This is similar to the closest marine pollen sites off  
1001 the coast, which recorded values of [MD95-2039 site #1]  $-10.5 \pm 4.6$  °C and [MD99-2331 site  
1002 #3]  $-5.3 \pm 2.9$  °C. Meanwhile, in the far east of the study area, Zaarur et al. (2016) estimated a  
1003 mean annual temperature anomaly of around -3 °C based on clumped isotope analysis of  
1004 *Melanopsis* shells from LGM sediments in the Sea of Galilee. This limited cooling appears  
1005 similar to the nearest pollen site [Lake Zeribar site #63] where we reconstruct a cooling of -  
1006  $2.2 \pm 4.6$  °C.

1007  
1008 Reconstructions of LGM sea surface temperatures (SST's) provide yet another source of  
1009 comparison with our terrestrial pollen-based reconstructions, although many of the physical  
1010 processes controlling surface sea temperatures such as upwelling, surface mixing, surface  
1011 currents, stratification and thermal inertia through the seasonal cycle, represent quite different  
1012 processes to those controlling surface temperatures over land, particularly at the sub-regional  
1013 scale. Nevertheless, the Atlantic coastal waters of Iberia and the waters throughout the  
1014 Mediterranean Sea include many SST sites that lie in relative proximity to our terrestrial  
1015 pollen-sites, allowing us to make a comparison at the largest scale. Within this area the  
1016 MARGO database (MARGO Members, 2009) includes 13 Alkenone, 2 Mg/Ca and 41  
1017 Foraminifera based SST records of mean annual temperature, with the Foraminifera records  
1018 also providing an additional 41 winter (JFM) and summer (JAS) SST estimates. We compare  
1019 the SST records with the 36 closest terrestrial pollen records which fall within a box of -11 to  
1020 35 degrees longitude and 32 to 43 degrees latitude containing all of the SST records. A  
1021 simple site average indicates a mean annual SST anomaly of  $-5.5 \pm 1.0$  °C which is relatively  
1022 close to the value of  $-7.2 \pm 3.4$  °C obtained from the terrestrial pollen sites [sites #1-4, 5, 7-  
1023 24, 25, 26, 30, 35-38, 41, 47, 51, 53, 56-59]. Interestingly the inter-site variance (standard  
1024 deviation of the reconstructed temperatures across all sites) is almost identical for the two  
1025 datasets, 2.57 °C for the SST sites and 2.63 °C for the pollen sites, despite representing very  
1026 different environments, proxies and uncertainties. However, when we look at the seasonal  
1027 temperature anomalies, we find very different results. Site averaged winter SST anomalies  
1028 are  $-3.7 \pm 1.1$  °C compared to  $-9.3 \pm 4.2$  °C for winter temperatures from terrestrial pollen  
1029 sites, while in summer the values are reversed,  $-7.0 \pm 0.8$  °C compared to  $-5.38 \pm 3.3$  °C  
1030 respectively. This suggests that SST's experienced greater cooling in summer compared to  
1031 winter, which is the opposite to that generally found in terrestrial seasonal temperature  
1032 reconstructions throughout the region, although this is consistent with model simulations  
1033 (Mikolajewicz, 2011).

#### 1034 1035 **4.2.2.2 Precipitation**

1036  
1037 Few proxies apart from pollen provide quantitative reconstructions of precipitation during the  
1038 LGM. Glacier mass balance modelling includes assumptions about precipitation in order to  
1039 derive temperatures (Allen et al., 2008a), but neither is independent of the other. Hughes et  
1040 al. (2006) estimate from glacier modelling that mean annual precipitation during the LGM at  
1041 sites in the Pindus mountains in Greece was around  $2300 \pm 200$ mm, which they consider to  
1042 be similar to the present day ( $>2000$ mm). A small change in precipitation compared to

1043 modern values is also indicated by the nearest pollen site, which is around 47 km to the south  
1044 [Ioannina #51], and indicates a mean annual precipitation anomaly of  $-152 \pm 294$ mm,  
1045 representing just 15% of the modern value. A larger reduction in mean annual precipitation of  
1046 -45% (maximum) is reconstructed by García-Amorena et al. (2007) based on plant  
1047 macrofossil remains from sites on the Portuguese coast. In comparison, the closest pollen  
1048 sites record values which are a little lower, ranging from [MD95-2039 site #1] -22% to  
1049 [MD99-2331 site #3] -34%. Further north in south-west Germany, Prud'homme et al. (2018)  
1050 reconstructed mean annual precipitation from the delta  $^{13}\text{C}$  of earthworm calcite granules at  
1051 Fussloch. They estimate a field site average of 333 (159-574) mm/yr at the LGM, which  
1052 represents an anomaly of -503 mm/yr (-60%) relative to the modern precipitation of 836  
1053 mm/yr. This is comparable with the closest pollen site [Bergsee #29] with an anomaly of -  
1054 540 mm/yr.

1055  
1056 As with glaciers, lake levels reflect changes in moisture balance that includes the effects of  
1057 both temperature (via evapotranspiration) and precipitation, rather than just precipitation.  
1058 They also represent semi-quantitative data at best, with changes often described relative to  
1059 the modern or other baseline. There are few lake level records available north of the Alps, but  
1060 to the south, many records indicate high lake levels in areas such as Spain (Lacey et al., 2016;  
1061 Moreno et al., 2012; Vegas et al., 2010), Italy (Belis et al., 1999; Giraudi, 2017), Greece and  
1062 Turkey (Harrison et al., 1996; Reimer et al., 2009) and the Middle East (Kolodny et al., 2005;  
1063 Lev et al., 2019). These lake records are also supported by evidence of higher river levels in  
1064 Morocco (El Amrani et al., 2008). The cause of the higher lake levels has been the subject of  
1065 some debate, since many pollen records (and especially early biome reconstructions) show  
1066 steppe vegetation that would suggest aridity that appears incompatible with higher lake  
1067 levels. Prentice et al. (1992) proposed that the co-existence of steppe vegetation and high lake  
1068 levels could be possible if precipitation increased outside of the summer growing season,  
1069 while summers themselves were drier and cooler with decreased evaporation. However, the  
1070 results of our analysis tend to indicate the opposite in regions with higher lake levels, with  
1071 increased summer rainfall and decreased winter rainfall. In addition, the increase in summer  
1072 precipitation was enough to compensate for the decrease in winter rainfall, leading to an  
1073 overall increase in mean annual precipitation at many pollen sites in Spain and Greece for  
1074 instance. This together with depressed temperatures and consequently decreased evaporation  
1075 could explain the higher lake levels, whilst also limiting the growth of trees as a result of  
1076 cooler temperatures and prolonged aridity outside of the summer season. Davis & Stevenson  
1077 (2007) also note a differential hydrological response between summer and winter rainfall in  
1078 the Mediterranean during the Holocene that may also provide an explanation. In this case  
1079 sporadic summer storms may result in high rates of runoff that may fill run-off fed lakes, but  
1080 low rates of soil moisture recharge that fails to benefit vegetation in the same way winter  
1081 rainfall does.

1082  
1083 Overall, we reconstruct only a small reduction in precipitation during the LGM of around  
1084 91mm (13%) averaged over all sites, which is less than the ~200mm reduction based on the  
1085 sites in the pollen-climate compilation used by PMIP (Bartlein et al., 2011). Since our  
1086 precipitation reconstruction on average matches that of the INV reconstruction by Wu et al  
1087 (2007), we can attribute much of the difference to the greater aridity shown in the ANN  
1088 reconstruction by Peyron et al and Jost et al (2005) (see figure 9). As with temperature, this is  
1089 probably a reflection of the modern training set used in the ANN reconstruction which is  
1090 much smaller than our training set and is largely taken from the arid steppes of Kazakhstan  
1091 and Mongolia. However, it is also important to recognize the significant spatial variability in  
1092 precipitation, which means that a simple average of different sets of sites from different

1093 regions may not accurately reflect the change in LGM precipitation at the European scale.  
1094 Nevertheless, one of the most consistent signals in our dataset is for an increase in summer  
1095 precipitation over many areas of Southern Europe and the Mediterranean. This is also found  
1096 in climate models, where it has been attributed to an increase in convection-driven  
1097 precipitation, although the amount of precipitation generated by this mechanism varies  
1098 significantly between models (Beghin et al., 2016). It may seem counter-intuitive to see an  
1099 increase in reconstructed precipitation in the same regions where we also find a  
1100 preponderance of steppe or xerophytic biomes and taxa, including *Artemisia* and  
1101 *Chenopodiaceae*. This is attributable to the fact that climate can change quite markedly with  
1102 necessarily invoking a major change in vegetation, and especially the pollen biome. For  
1103 instance, a semi-arid climate ranges from 250-500mm rainfall a year, so we could expect a  
1104 semi-arid vegetation to be dominant even if the rainfall increases 250mm (100%).  
1105

1106 A more consistent response in models is for an increase in winter precipitation across  
1107 Southern Europe and the Mediterranean related to a stronger and more southerly displaced jet  
1108 stream, with winter precipitation also accounting for much of the change in mean annual  
1109 precipitation (Beghin et al., 2016). Our reconstruction of winter precipitation however shows  
1110 less support for this scenario with a more general decrease in winter precipitation apart from  
1111 southern and eastern Iberia, and with summer precipitation generally more important in those  
1112 sites that show an overall increase in mean annual precipitation. This may not necessarily  
1113 contradict the models in terms of the strength and position of the winter jet stream, but may  
1114 instead indicate that models over-estimate the amount of moisture being carried westward  
1115 from the cold North Atlantic along the storm track, especially across the far northern  
1116 Mediterranean. The increase in winter precipitation across southern and eastern Iberia is  
1117 however entirely consistent with a strengthened and more southerly jet stream, which also  
1118 brings increased winter precipitation to the region today as a result of blocking over northern  
1119 Europe/Atlantic and a negative NAO (Vicente-Serrano et al., 2011).  
1120

1121 Other areas that show an increase in winter precipitation include pollen sites around the  
1122 eastern end of the Alps. This is consistent with a recent study by Spötl et al (2021) who  
1123 argued, on the basis of cryogenic carbonates preserved in a cave in Austria, that heavy winter  
1124 (and autumn) precipitation was a significant factor in driving LGM glaciation in the region.  
1125 The seasonally specific nature of this precipitation is also supported by the same pollen sites,  
1126 which do not show any increase in summer precipitation at this time.  
1127

## 1128 **5.0 Conclusions**

1129

1130 We have reconstructed the climate and vegetation cover across Europe, North Africa and the  
1131 Middle East at the time of the LGM based on 63 pollen records. These records were selected  
1132 using strict quality control criteria, with particular attention paid to dating control, which led  
1133 to the exclusion of many records that have been used in previous studies. This fully  
1134 documented dataset represents the most chronologically precise and spatially resolved view  
1135 of LGM climate and vegetation during the PMIP benchmarking time window at  $21 \pm 2$  ka.  
1136 Nevertheless, it is important to recognize that there are still significant spatial gaps in pollen  
1137 sites especially north of the Alps, the Balkans, Turkey and the Middle East, and we continue  
1138 to have only a partial understanding of the LGM over these areas.  
1139

1140 One of the key questions concerning the vegetation landscape of the LGM in Europe has  
1141 been the extent to which forest rather than steppe covered the continent, and to what extent  
1142 temperate elements could be found north of the classical refugia areas of Southern Europe

1143 and the Mediterranean. Our results show that although steppe and tundra was extensive at the  
1144 time of the LGM, areas of open forest also occurred in many regions, particularly (but not  
1145 exclusively) in Iberia, northern Italy and Central Europe. These forest or woodland stands are  
1146 likely to have been located in environmentally favourable areas, with good soils, elevated  
1147 rainfall and shelter from cold, desiccating winds. In those areas where woodland existed,  
1148 Boreal taxa generally dominated north and east of the Alps, while temperate and  
1149 thermophilous (mainly drought adapted) taxa were generally confined to areas south of the  
1150 Alps and around the Mediterranean. The temperate deciduous forests that compose the  
1151 climax community in many areas of Europe today were displaced to the south and reduced to  
1152 a partnership role with Boreal elements. Overall our new reconstruction indicates greater  
1153 agreement with model land cover simulations, but models still appear to over-estimate the  
1154 amount of forest and woodland over areas such as France and the Benelux, Greece, Turkey  
1155 and the Far East.

1156  
1157 Another key question about the LGM concerns the ability of climate models to simulate the  
1158 climate of this period and whether pollen-based climate reconstructions which show  
1159 disagreement with models have been biased by the effects of low CO<sub>2</sub> on plant physiology.  
1160 We find that our new pollen-climate reconstruction shows much closer agreement with  
1161 climate models than previous reconstructions that did not take account of low CO<sub>2</sub> effects.  
1162 We also find close agreement with previous reconstructions that did take account of CO<sub>2</sub>  
1163 effects. Since our MAT method itself does not specifically take account of low CO<sub>2</sub> effects,  
1164 this would suggest that this problem is not a significant hindrance to MAT performance at the  
1165 time of the LGM, at least not compared to other uncertainties. Instead, we suggest that the  
1166 main factor in the performance of pollen-climate transfer functions that use modern analogue  
1167 methods is the provision of a large enough modern pollen dataset with suitable LGM  
1168 analogues.

1169  
1170 This conclusion is supported by comparison with climate reconstructions based on other  
1171 proxies. We found little difference between our MAT reconstruction and a Chironomid-based  
1172 summer temperature record based on a downcore sample by sample comparison, as well as  
1173 comparisons with records from a variety of other proxies at a regional scale. However, it is  
1174 notable that some studies using glacier mass balance modelling methods indicate LGM  
1175 temperatures that are much cooler than our pollen-based reconstruction. The reasons behind  
1176 this are not clear, but our pollen-based results indicate higher than present precipitation in  
1177 some areas that could potentially explain low elevation glacier ELA's without the need for  
1178 such cold temperatures.

1179  
1180 We also find that although our pollen-based reconstruction and those of SST's generally  
1181 agree in terms of mean annual temperatures, SST's indicate greater cooling in summer  
1182 compared to winter, while terrestrial records indicate greater cooling in winter compared to  
1183 summer. These seasonal differences are also reproduced in climate models, and probably  
1184 reflect the different processes driving seasonal temperature change in the terrestrial and  
1185 marine domain.

1186  
1187 Our reconstructions of precipitation show large spatial and seasonal variability, but generally  
1188 indicate less overall aridity than previously suggested from smaller scale studies which  
1189 sampled less of the spatial domain. We find that in some regions of Southern Europe  
1190 precipitation may actually have been greater than present, especially in summer, but also in  
1191 winter in southern and eastern Iberia and around the southern slopes of the Alps. This may  
1192 have important implications in understanding the development of LGM glaciation, which



1193 may be less a function of temperature than previously supposed. This could also help better  
1194 explain the observed asynchronous nature of glaciation even within relatively small regions  
1195 such as Europe, as a result of more localized controls on ice sheet development such as  
1196 precipitation.

1197  
1198 We hope that this new continental-scale dataset of climate and vegetation reconstructions will  
1199 provide an improved baseline for data-model comparisons and other studies that will allow us  
1200 to better understand the complex LGM environment.

1201

1202

### 1203 **Code/Data availability**

1204

1205 All of the data shown in the figures together with the fossil and modern pollen datasets will  
1206 be made available on pangaea.de once the review process has been completed and these  
1207 datasets are therefore no longer subject to change.

1208

### 1209 **Author contribution**

1210

1211 BASD designed the study, undertook the analysis and wrote the manuscript. MF and ER  
1212 designed and prepared the maps. JOK and AB reviewed the manuscript and provided  
1213 additional input.

1214

### 1215 **Competing interests**

1216

1217 The authors declare that they have no conflict of interest.

1218

### 1219 **Acknowledgements**

1220

1221 This work was supported by a grant from the Fonds de Recherche du Québec Société et  
1222 Culture (2019-SE3-254686) to AB. Data were obtained from the European Pollen Database  
1223 (EPD), based within the Neotoma Paleoecology Database (<http://www.neotomadb.org>). The  
1224 work of data contributors, data stewards, and the Neotoma and EPD community is gratefully  
1225 acknowledged. We dedicate this paper in memory of Eric Grimm, whose tireless work for the  
1226 EPD and Neotoma helped make this study possible.

1227

1228

1229

1230 **References**

1231

1232 ACER project members, Goñi, M. F. S., Desprat, S., Daniau, A. L., Bassinot, F. C., Polanco-  
1233 Martínez, J. M., Harrison, S. P., Allen, J. R. M., Scott Anderson, R., Behling, H., Bonnefille,  
1234 R., Burjachs, F., Carrión, J. S., Cheddadi, R., Clark, J. S., Combourieu-Nebout, N., Mustaphi,  
1235 C. J. C., Debusk, G. H., Dupont, L. M., Finch, J. M., Fletcher, W. J., Giardini, M., González,  
1236 C., Gosling, W. D., Grigg, L. D., Grimm, E. C., Hayashi, R., Helmens, K., Heusser, L. E.,  
1237 Hill, T., Hope, G., Huntley, B., Igarashi, Y., Irino, T., Jacobs, B., Jiménez-Moreno, G.,  
1238 Kawai, S., Peter Kershaw, A., Kumon, F., Lawson, I. T., Ledru, M. P., Lézine, A. M., Mei  
1239 Liew, P., Magri, D., Marchant, R., Margari, V., Mayle, F. E., Merna Mckenzie, G., Moss, P.,  
1240 Müller, S., Müller, U. C., Naughton, F., Newnham, R. M., Oba, T., Pérez-Obiol, R., Pini, R.,  
1241 Ravazzi, C., Roucoux, K. H., Rucina, S. M., Scott, L., Takahara, H., Tzedakis, P. C., Urrego,  
1242 D. H., Van Geel, B., Guido Valencia, B., Vandergoes, M. J., Vincens, A., Whitlock, C. L.,  
1243 Willard, D. A. and Yamamoto, M.: The ACER pollen and charcoal database: A global  
1244 resource to document vegetation and fire response to abrupt climate changes during the last  
1245 glacial period, *Earth Syst. Sci. Data*, 9(2), 679–695, doi:10.5194/essd-9-679-2017, 2017.

1246

1247 Allen, J. R. M., Hickler, T., Singarayer, J. S., Sykes, M. T., Valdes, P. J. and Huntley, B.:  
1248 Last glacial vegetation of northern Eurasia, *Quat. Sci. Rev.*, 29(19–20), 2604–2618,  
1249 doi:10.1016/j.quascirev.2010.05.031, 2010.

1250

1251 Allen, R., Siegert, M. J. and Payne, A. J.: Reconstructing glacier-based climates of LGM  
1252 Europe and Russia – Part 2 : A dataset of LGM precipitation / temperature relations derived  
1253 from degree-day modelling of palaeo glaciers, , 249–263, 2008a.

1254

1255 Allen, R., Siegert, M. J. and Payne, A. J.: Reconstructing glacier-based climates of LGM  
1256 Europe and Russia – Part 3 : Comparison with previous climate reconstructions, , (1999),  
1257 265–280, 2008b.

1258

1259 Ampel, L., Bigler, C., Wohlfarth, B., Risberg, J., Lotter, A. F. and Veres, D.: Modest summer  
1260 temperature variability during DO cycles in western Europe, *Quat. Sci. Rev.*, 29(11–12),  
1261 1322–1327, doi:10.1016/j.quascirev.2010.03.002, 2010.

1262

1263 El Amrani, M., Macaire, J. J., Zarki, H., Bréhéret, J. G. and Fontugne, M.: Contrasted  
1264 morphosedimentary activity of the lower Kert River (northeastern Morocco) during the Late  
1265 Pleistocene and the Holocene. Possible impact of bioclimatic variations and human action,  
1266 *Comptes Rendus - Geosci.*, 340(8), 533–542, doi:10.1016/j.crte.2008.05.004, 2008.

1267

1268 Anderson, P. M., Barnosky, C. W., Bartlein, P. J., Behling, P. J., Brubaker, L., Cushing, E. J.,  
1269 Dodson, J., Dworetsky, B., Guetter, P. J., Harrison, S. P., Huntley, B., Kutzbach, J. E.,  
1270 Markgraf, V., Marvel, R., McGlone, M. S., Mix, A., Moar, N. T., Morley, J., Perrott, R. A.,  
1271 Peterson, G. M., Prell, W. L., Prentice, I. C., Ritchie, J. C., Roberts, N., Ruddiman, W. F.,  
1272 Salinger, M. J., Spaulding, W. G., Street-Perrott, F. A., Thompson, R. S., Wang, P. K., Webb,  
1273 T., Winkler, M. G. and Wright, H. E.: Climatic changes of the last 18,000 years:  
1274 Observations and model simulations, *Science* (80-. ), 241(4869), 1043–1052,  
1275 doi:10.1126/science.241.4869.1043, 1988.

1276

1277 Arpe, K., Leroy, S. A. G. and Mikolajewicz, U.: A comparison of climate simulations for the  
1278 last glacial maximum with three different versions of the ECHAM model and implications  
1279 for summer-green tree refugia, *Clim. Past*, 91–114, doi:10.5194/cp-7-91-2011, 2011.  
1280

1281 Arslanov, K. A., Dolukhanov, P. M. and Gei, N. A.: Climate, Black Sea levels and human  
1282 settlements in Caucasus Littoral 50,000-9000 BP, *Quat. Int.*, 167–168, 121–127,  
1283 doi:10.1016/j.quaint.2007.02.013, 2007.  
1284

1285 Bañuls-Cardona, S., López-García, J. M., Blain, H. A., Lozano-Fernández, I. and Cuenca-  
1286 Bescós, G.: The end of the Last Glacial Maximum in the Iberian Peninsula characterized by  
1287 the small-mammal assemblages, *J. Iber. Geol.*, 40(1), 19–27,  
1288 doi:10.5209/rev\_JIGE.2014.v40.n1.44085, 2014.  
1289

1290 Bartlein, P. J., Harrison, S. P., Brewer, S., Connor, S., Davis, B. A. S., Gajewski, K., Guiot,  
1291 J., Harrison-Prentice, T. I., Henderson, A., Peyron, O., Prentice, I. C., Scholze, M., Seppä, H.,  
1292 Shuman, B., Sugita, S., Thompson, R. S., Vial, A. E., Williams, J. and Wu, H.: Pollen-based  
1293 continental climate reconstructions at 6 and 21 ka: A global synthesis, *Clim. Dyn.*, 37(3),  
1294 775–802, doi:10.1007/s00382-010-0904-1, 2011.  
1295

1296 de Beaulieu, J.-L. and Reille, M.: Pollen analysis of a long upper Pleistocene continental  
1297 sequence in a Velay maar (Massif Central, France), *Palaeogeogr. Palaeoclimatol. Palaeoecol.*,  
1298 80(1), 35–48, 1990.  
1299

1300 Beghin, P., Charbit, S., Kageyama, M., Combourieu-Nebout, N., Hatté, C., Dumas, C. and  
1301 Peterschmitt, J. Y.: What drives LGM precipitation over the western Mediterranean? A study  
1302 focused on the Iberian Peninsula and northern Morocco, *Clim. Dyn.*, 46(7–8), 2611–2631,  
1303 doi:10.1007/s00382-015-2720-0, 2016.  
1304

1305 Belis, C. A., Lami, A., Guilizzoni, P., Ariztegui, D. and Geiger, W.: The late Pleistocene  
1306 ostracod record of the crater lake sediments from Lago di Albano (Central Italy): Changes in  
1307 trophic status, water level and climate, *J. Paleolimnol.*, 21(2), 151–169,  
1308 doi:10.1023/A:1008095805748, 1999.  
1309

1310 Berto, C., López-García, J. M. and Luzi, E.: Changes in the Late Pleistocene small-mammal  
1311 distribution in the Italian Peninsula, *Quat. Sci. Rev.*, 225,  
1312 doi:10.1016/j.quascirev.2019.106019, 2019.  
1313

1314 Bigelow, N.H., Brubaker, L.B., Edwards, M.E., Harrison, S.P., Prentice, I.C., Anderson,  
1315 P.M., Andreev, A.A., Bartlein, P.J., Christiansen, T.R., Cramer, W., Kaplan, J.O., Lozhkin,  
1316 A.V., Matveyeva, N.V., Murray, D.F., McGuire, A.D., Razzhivin, V.Y., Ritchie, J.C., Smith,  
1317 B., Walker, D.A., Gajewski, K., Wolf, V., Holmqvist, B.H., Igarashi, Y., Kremenetskii, K.,  
1318 Paus, A., Pisaric, M.F.J., Volkova, V.S.: Climate change and arctic ecosystems: 1. Vegetation  
1319 changes north of 55 N between the last glacial maximum, mid-Holocene, and present. *J.*  
1320 *Geophys. Res.* 108 (D19), 8170. [doi.org/10.1029/2002JD002558](https://doi.org/10.1029/2002JD002558), 2013.  
1321

1322 Binney, H., Edwards, M., Macias-Fauria, M., Lozhkin, A., Anderson, P., Kaplan, J. O.,  
1323 Andreev, A., Bezrukova, E., Blyakharchuk, T., Jankovska, V., Khazina, I., Krivonogov, S.,  
1324 Kremenetski, K., Nield, J., Novenko, E., Ryabogina, N., Solovieva, N., Willis, K. and  
1325 Zernitskaya, V.: Vegetation of Eurasia from the last glacial maximum to present: Key  
1326 biogeographic patterns, *Quat. Sci. Rev.*, 157, 80–97, doi:10.1016/j.quascirev.2016.11.022,  
2017.

1327  
1328 Birks, H. J. B. and Willis, K. J.: Alpines, trees, and refugia in Europe, *Plant Ecol. Divers.*,  
1329 1(2), 147–160, doi:10.1080/17550870802349146, 2008.  
1330  
1331 Bonatti, E.: Pollen sequence in the lake sediments. In: *Ianula: an account of the history and*  
1332 *development of the Lago di Monterosi, Latium, Italy*, in *Trans. Am. phil. Soc.*, vol. 60, edited  
1333 by G. E. Hutchinson, pp. 26–31., 1970.  
1334  
1335 Brewer, S., Guiot, J., Sánchez-Goñi, M. F. and Klotz, S.: The climate in Europe during the  
1336 Eemian: a multi-method approach using pollen data, *Quat. Sci. Rev.*, 27(25–26), 2303–2315,  
1337 doi:10.1016/j.quascirev.2008.08.029, 2008.  
1338  
1339 Brewer, S., Giesecke, T., Davis, B. A. S., Finsinger, W., Wolters, S., Binney, H., de  
1340 Beaulieu, J. L., Fyfe, R., Gil-Romera, G., Köhl, N., Kuneš, P., Leydet, M. and Bradshaw, R.  
1341 H.: Mapping Lateglacial and Holocene European pollen data: The maps, *J. Maps*, 13(2), 921–  
1342 928, doi:10.1080/17445647.2016.1197613, 2017.  
1343  
1344 Camuera, J., Jiménez-Moreno, G., Ramos-Román, M. J., García-Alix, A., Toney, J. L.,  
1345 Anderson, R. S., Jiménez-Espejo, F., Bright, J., Webster, C., Yanes, Y. and Carrión, J. S.:  
1346 Vegetation and climate changes during the last two glacial-interglacial cycles in the western  
1347 Mediterranean: A new long pollen record from Padul (southern Iberian Peninsula), *Quat. Sci.*  
1348 *Rev.*, 205, 86–105, doi:10.1016/j.quascirev.2018.12.013, 2019.  
1349  
1350 Cao, X., Tian, F., Dallmeyer, A. and Herzschuh, U.: Northern Hemisphere biome changes  
1351 (>30°N) since 40 cal ka BP and their driving factors inferred from model-data comparisons,  
1352 *Quat. Sci. Rev.*, 220, 291–309, doi:10.1016/j.quascirev.2019.07.034, 2019.  
1353  
1354 Carrión, J. S.: Late quaternary pollen sequence from Carihuela Cave, southern Spain, *Rev.*  
1355 *Palaeobot. Palynol.*, 71(1–4), doi:10.1016/0034-6667(92)90157-C, 1992.  
1356  
1357 Carrión, J. S.: Patterns and processes of Late Quaternary environmental change in a montane  
1358 region of southwestern Europe, *Quat. Sci. Rev.*, 21, 2047–2066, 2002.  
1359  
1360 Carrión, J. S., Finlayson, C., Fernández, S., Finlayson, G., Allué, E., López-Sáez, J. A.,  
1361 López-García, P., Gil-Romera, G., Bailey, G. and González-Sampériz, P.: A coastal reservoir  
1362 of biodiversity for Upper Pleistocene human populations: palaeoecological investigations in  
1363 Gorham’s Cave (Gibraltar) in the context of the Iberian Peninsula, *Quat. Sci. Rev.*, 27(23–  
1364 24), 2118–2135, doi:10.1016/j.quascirev.2008.08.016, 2008.  
1365  
1366 Cheddadi, R., Yu, G., Guiot, J., Harrison, S. P. and Colin Prentice, I.: The climate of Europe  
1367 6000 years ago, *Clim. Dyn.*, 13(1), 1–9, 1996.  
1368  
1369 Chevalier, M., Davis, B. A. S., Heiri, O., Seppä, H., Chase, B. M., Gajewski, K., Lacourse,  
1370 T., Telford, R. J., Finsinger, W., Guiot, J., Köhl, N., Maezumi, S. Y., Tipton, J. R., Carter, V.  
1371 A., Brussel, T., Phelps, L. N., Dawson, A., Zanon, M., Vallé, F., Nolan, C., Mauri, A., de  
1372 Vernal, A., Izumi, K., Holmström, L., Marsicek, J., Goring, S., Sommer, P. S., Chaput, M.  
1373 and Kupriyanov, D.: Pollen-based climate reconstruction techniques for late Quaternary  
1374 studies, *Earth-Science Rev.*, 210, doi:10.1016/j.earscirev.2020.103384, 2020.  
1375

1376 Cleator, S. F., Harrison, S. P., Nichols, N. K., Colin Prentice, I. and Roulstone, I.: A new  
1377 multivariable benchmark for Last Glacial Maximum climate simulations, *Clim. Past*, 16(2),  
1378 699–712, doi:10.5194/cp-16-699-2020, 2020.

1379  
1380 COHMAP,: Climatic changes of the last 18,000 years: observations and model  
1381 simulations. *Science*, 241, 1043-1052, 1988.

1382  
1383 Collins, P. M., Davis, B. A. S. and Kaplan, J. O.: The mid-Holocene vegetation of the  
1384 Mediterranean region and southern Europe, and comparison with the present day, *J.*  
1385 *Biogeogr.*, 39(10), doi:10.1111/j.1365-2699.2012.02738.x, 2012.

1386  
1387 Combourieu Nebout, N., Peyron, O., Dormoy, I., Desprat, S., Beaudouin, C., Kotthoff, U.  
1388 and Marret, F.: Rapid climatic variability in the west Mediterranean during the last 25 000  
1389 years from high resolution pollen data, *Clim. Past*, 5(3), 503–521, doi:10.5194/cp-5-503-  
1390 2009, 2009.

1391  
1392 Connor, S. E., Ross, S. A., Sobotkova, A., Herries, A. I. R., Mooney, S. D., Longford, C. and  
1393 Iliev, I.: Environmental conditions in the SE Balkans since the Last Glacial Maximum and  
1394 their influence on the spread of agriculture into Europe, *Quat. Sci. Rev.*, 68, 200–215,  
1395 doi:10.1016/j.quascirev.2013.02.011, 2013.

1396  
1397 Cowling, S. A. and Sykes, M. T.: Physiological significance of low atmospheric CO<sub>2</sub> for  
1398 plant-climate interactions, *Quat. Res.*, 52(2), 237–242, doi:10.1006/qres.1999.2065, 1999.

1399  
1400 Damblon, F.: L'enregistrement palynologique de la sequence pléistocène et holocène de la  
1401 grotte Walou, in *La grotte Walou à Trooz (Belgique)*, edited by C. Draily, S. Pirson, and M.  
1402 Toussaint, pp. 84–129, Service public de Wallonie (Etudes et Documents, Archéologie, 21).,  
1403 2011.

1404  
1405 Daniau, A.-L., Desprat, S., Aleman, J. C., Bremond, L., Davis, B., Fletcher, W., Marlon, J.  
1406 R., Marquer, L., Montade, V., Morales-Molino, C., Naughton, F., Rius, D. and Urrego, D. H.:  
1407 Terrestrial plant microfossils in palaeoenvironmental studies, pollen, microcharcoal and  
1408 phytolith. Towards a comprehensive understanding of vegetation, fire and climate changes  
1409 over the past one million years, *Rev. Micropaleontol.*, 63, doi:10.1016/j.revmic.2019.02.001,  
1410 2019.

1411  
1412 Davis, B. A. S. and Stevenson, A. C.: The 8.2 ka event and Early-Mid Holocene forests, fires  
1413 and flooding in the Central Ebro Desert, NE Spain, *Quat. Sci. Rev.*, 26(13–14),  
1414 doi:10.1016/j.quascirev.2007.04.007, 2007.

1415  
1416 Davis, B. A. S., Brewer, S., Stevenson, A. C., Guiot, J., Allen, J., Almqvist-Jacobson, H.,  
1417 Ammann, B., Andreev, A. A., Argant, J., Atanassova, J., Balwierz, Z., Barnosky, C. D.,  
1418 Bartley, D. D., De Beaulieu, J. L., Beckett, S. C., Behre, K. E., Bennett, K. D., Berglund, B.  
1419 E. B., Beug, H.-J., Bezusko, L., Binka, K., Birks, H. H., Birks, H. J. B., Björck, S.,  
1420 Bliakhartchouk, T., Bogdel, I., Bonatti, E., Bottema, S., Bozilova, E. D. B., Bradshaw, R.,  
1421 Brown, A. P., Brugiapaglia, E., Carrion, J., Chernavskaya, M., Clerc, J., Clet, M., Coûteaux,  
1422 M., Craig, A. J., Cserny, T., Cwynar, L. C., Dambach, K., De Valk, E. J., Digerfeldt, G.,  
1423 Diot, M. F., Eastwood, W., Elina, G., Filimonova, L., Filipovitch, L., Gaillard-Lemdhal, M.  
1424 J., Gauthier, A., Göransson, H., Guenet, P., Gunova, V., Hall, V. A. H., Harmata, K., Hicks,  
1425 S., Huckerby, E., Huntley, B., Huttunen, A., Hyvärinen, H., Ilves, E., Jacobson, G. L., Jahns,

1426 S., Jankovská, V., Jóhansen, J., Kabailiene, M., Kelly, M. G., Khomutova, V. I., Königsson,  
 1427 L. K., Kremenetski, C., Kremenetskii, K. V., Krisai, I., Krisai, R., Kvavadze, E., Lamb, H.,  
 1428 Lazarova, M. A., Litt, T., Lotter, A. F., Lowe, J. J., Magyari, E., Makohonienko, M.,  
 1429 Mamakowa, K., Mangerud, J., Mariscal, B., Markgraf, V., McKeever, Mitchell, F. J. G.,  
 1430 Munuera, M., Nicol-Pichard, S., Noryskiewicz, B., Odgaard, B. V., Panova, N. K.,  
 1431 Pantaleon-Cano, J., Paus, A. A., Pavel, T., Peglar, S. M., Penalba, M. C., Pennington, W.,  
 1432 Perez-Obiol, R., et al.: The temperature of Europe during the Holocene reconstructed from  
 1433 pollen data, *Quat. Sci. Rev.*, 22(15–17), doi:10.1016/S0277-3791(03)00173-2, 2003.  
 1434  
 1435 Davis, B. A. S., Chevalier, M., Sommer, P., Carter, V. A., Finsinger, W., Mauri, A., Phelps,  
 1436 L. N., Zanon, M., Abegglen, R., Åkesson, C. M., Alba-Sánchez, F., Scott Anderson, R.,  
 1437 Antipina, T. G., Atanassova, J. R., Beer, R., Belyanina, N. I., Blyakharchuk, T. A., Borisova,  
 1438 O. K., Bozilova, E., Bukreeva, G., Jane Bunting, M., Clò, E., Colombaroli, D., Combourieu-  
 1439 Nebout, N., Desprat, S., Di Rita, F., Djamali, M., Edwards, K. J., Fall, P. L., Feurdean, A.,  
 1440 Fletcher, W., Florenzano, A., Furlanetto, G., Gaceur, E., Galimov, A. T., Gałka, M., García-  
 1441 Moreiras, I., Giesecke, T., Grindean, R., Guido, M. A., Gvozdeva, I. G., Herzsuh, U.,  
 1442 Hjelle, K. L., Ivanov, S., Jahns, S., Jankovska, V., Jiménez-Moreno, G., Karpińska-Kołaczek,  
 1443 M., Kitaba, I., Kołaczek, P., Lapteva, E. G., Latałowa, M., Lebreton, V., Leroy, S., Leydet,  
 1444 M., Lopatina, D. A., López-Sáez, J. A., Lotter, A. F., Magri, D., Marinova, E., Matthias, I.,  
 1445 Mavridou, A., Mercuri, A. M., Mesa-Fernández, J. M., Mikishin, Y. A., Milecka, K.,  
 1446 Montanari, C., Morales-Molino, C., Mrotzek, A., Sobrino, C. M., Naidina, O. D., Nakagawa,  
 1447 T., Nielsen, A. B., Novenko, E. Y., Panajiotidis, S., Panova, N. K., Papadopoulou, M.,  
 1448 Pardoe, H. S., Pędziszewska, A., Petrenko, T. I., Ramos-Román, M. J., Ravazzi, C., Rösch,  
 1449 M., Ryabogina, N., Ruiz, S. S., Sakari Salonen, J., Sapelko, T. V., Schofield, J. E., Seppä, H.,  
 1450 Shumilovskikh, L., Stivrins, N., Stojakowits, P., Svitavska, H. S., Święta-Musznicka, J.,  
 1451 Tantau, I., Tinner, W., Tobolski, K., Tonkov, S., Tsakiridou, M., et al.: The Eurasian Modern  
 1452 Pollen Database (EMPD), version 2, *Earth Syst. Sci. Data*, 12(4), 2423–2445,  
 1453 doi:10.5194/essd-12-2423-2020, 2020.  
 1454  
 1455 Davis M.B.: On the theory of pollen analysis. *American Journal of Sciences*, 26, 897–912,  
 1456 1963.  
 1457  
 1458 Demay, L., Julien, M.A., Anghelinu, M., Shydlovskiy, P.S., Koulakovska, L.V., P'ean, S.,  
 1459 Stupak, D.V., Vasyliiev, P.M., Obřada, T., Wojtal, P., Belyaeva, V.I.: Study of human  
 1460 behaviors during the Late Pleniglacial in the East European Plain through their relation to the  
 1461 animal world. *Quat. Int.* <https://doi.org/10.1016/j.quaint.2020.10.047>, 2021.  
 1462  
 1463 Douda, J., Doudová, J., Drařnarová, A., Kuneř, P., Hadincová, V., Krak, K., Zákřavský, P.  
 1464 and Mandák, B.: Migration patterns of subgenus *Alnus* in Europe since the last glacial  
 1465 maximum: A systematic review, *PLoS One*, 9(2), doi:10.1371/journal.pone.0088709, 2014.  
 1466  
 1467 Duprat-Oualid, F., Rius, D., Bégeot, C., Magny, M., Millet, L., Wulf, S. and Appelt, O.:  
 1468 Vegetation response to abrupt climate changes in Western Europe from 45 to 14.7k cal a BP:  
 1469 the Bergsee lacustrine record (Black Forest, Germany), *J. Quat. Sci.*, 32(7), 1008–1021,  
 1470 doi:10.1002/jqs.2972, 2017.  
 1471  
 1472 Dupre Ollivier, M.: *Palinología y paleoambiente- nuevos datos españoles referencias*,  
 1473 Universidad de Valencia., 1988.  
 1474

1475 Edwards, M. E., Anderson, P. M., Brubaker, L. B., Ager, T., Andreev, A. A., Bigelow, N. H.,  
1476 Cwynar, L. C., Eisner, W. R., Harrison, S. P., Hu, F.-S., Jolly, D., Lozhkin, A. V.,  
1477 MacDonald, G. M., Mock, C. J., Ritchie, J. C., Sher, A. V., Spear, R. W., Williams, J. & Yu,  
1478 G.: Pollen-based biomes for Beringia 18,000, 6000 and 0 14C yr bp. *Journal of*  
1479 *Biogeography*, **27**, 521– 554, doi: [10.1046/j.1365-2699.2000.00426.x](https://doi.org/10.1046/j.1365-2699.2000.00426.x), 2000.  
1480  
1481 Ehlers, J., Gibbard, P. L. and Hughes, P. D.: Quaternary Glaciations - Extent and Chronology  
1482 A Closer Look, edited by J. Ehlers, P. L. Gibbard, and P. D. Hughes, Elsevier., 2011.  
1483  
1484 Elenga, H., Peyron, O., Bonnefille, R., Jolly, D., Cheddadi, R., Guiot, J., Andrieu, V.,  
1485 Bottema, S., Buchet, G., De Beaulieu, J. L., Hamilton, A. C., Maley, J., Marchant, R., Perez-  
1486 Obiol, R., Reille, M., Riollet, G., Scott, L., Straka, H., Taylor, D., Van Campo, E., Vincens,  
1487 A., Laarif, F. and Jonson, H.: Pollen-based biome reconstruction for southern Europe and  
1488 Africa 18,000 yr BP, *J. Biogeogr.*, **27**(3), 621–634, doi:10.1046/j.1365-2699.2000.00430.x,  
1489 2000.  
1490  
1491 Ferguson, J. E., Henderson, G. M., Fa, D. A., Finlayson, J. C. and Charnley, N. R.: Increased  
1492 seasonality in the Western Mediterranean during the last glacial from limpet shell  
1493 geochemistry, *Earth Planet. Sci. Lett.*, **308**(3–4), 325–333, doi:10.1016/j.epsl.2011.05.054,  
1494 2011.  
1495  
1496 Feurdean A, Bhagwat SA, Willis KJ, Birks HJB, Lischke H, Hickler T.: Tree migration-rates:  
1497 narrowing the gap between inferred post-glacial rates and projected rates. *PLoS ONE* **8**:  
1498 e71797, 2013.  
1499  
1500 Feurdean, A., Perşoiu, A., Tanţău, I., Stevens, T., Magyari, E. K., Onac, B. P., Marković, S.,  
1501 Andrić, M., Connor, S., Fărcaş, S., Gałka, M., Gaudeny, T., Hoek, W., Kolaczek, P., Kuneš,  
1502 P., Lamentowicz, M., Marinova, E., Michezyńska, D. J., Perşoiu, I., Płóciennik, M.,  
1503 Słowiński, M., Stancikaite, M., Sumegi, P., Svensson, A., Tămaş, T., Timar, A., Tonkov, S.,  
1504 Toth, M., Veski, S., Willis, K. J. and Zernitskaya, V.: Climate variability and associated  
1505 vegetation response throughout Central and Eastern Europe (CEE) between 60 and 8ka, *Quat.*  
1506 *Sci. Rev.*, **106**, 206–224, doi:10.1016/j.quascirev.2014.06.003, 2014.  
1507  
1508 Fick, S. E. and Hijmans, R. J.: WorldClim 2: new 1-km spatial resolution climate surfaces for  
1509 global land areas, *Int. J. Climatol.*, **37**(12), 4302–4315, doi:10.1002/joc.5086, 2017.  
1510  
1511 Fletcher, W. J., Goni, M. F. S., Peyron, O. and Dormoy, I.: Abrupt climate changes of the last  
1512 deglaciation detected in a Western Mediterranean forest record, *Clim. Past*, **6**(2), 245–264,  
1513 doi:10.5194/cp-6-245-2010, 2010.  
1514  
1515 Gaillard, M. J., Sugita, S., Mazier, F., Trondman, A. K., Broström, A., Hickler, T., Kaplan, J.  
1516 O., Kjellström, E., Kokfelt, U., Kuneš, P., Lemmen, C., Miller, P., Olofsson, J., Poska, A.,  
1517 Rundgren, M., Smith, B., Strandberg, G., Fyfe, R., Nielsen, A. B., Alenius, T., Balakauskas,  
1518 L., Barnekow, L., Birks, H. J. B., Bjune, A., Björkman, L., Giesecke, T., Hjelle, K., Kalnina,  
1519 L., Kangur, M., Van Der Knaap, W. O., Koff, T., Lageras, P., Latałowa, M., Leydet, M.,  
1520 Lechterbeck, J., Lindbladh, M., Odgaard, B., Peglar, S., Segerström, U., Von Stedingk, H.  
1521 and Seppä, H.: Holocene land-cover reconstructions for studies on land cover-climate  
1522 feedbacks, *Clim. Past*, **6**(4), 483–499, doi:10.5194/cp-6-483-2010, 2010.  
1523

1524 García-Amorena, I., Gómez Manzaneque, F., Rubiales, J. M., Granja, H. M., Soares de  
1525 Carvalho, G. and Morla, C.: The Late Quaternary coastal forests of western Iberia: A study of  
1526 their macroremains, *Palaeogeogr. Palaeoclimatol. Palaeoecol.*, 254(3–4), 448–461,  
1527 doi:10.1016/j.palaeo.2007.07.003, 2007.

1528  
1529 Genov, I.: The Black Sea level from the Last Glacial Maximum to the present time, *Geol.*  
1530 *Balc.*, 45(1–3), 3–19, 2016.

1531  
1532 Giesecke, T.: Did thermophilous trees spread into central Europe during the Late Glacial?,  
1533 *New Phytol.*, 212(1), 15–18, doi:10.1111/nph.14149, 2016.

1534  
1535 Giesecke, T., Davis, B., Brewer, S., Finsinger, W., Wolters, S., Blaauw, M., de Beaulieu, J.-  
1536 L., Binney, H., Fyfe, R. M., Gaillard, M.-J., Gil-Romera, G., van der Knaap, W. O., Kuneš,  
1537 P., Köhl, N., van Leeuwen, J. F. N., Leydet, M., Lotter, A. F., Ortu, E., Semmler, M. and  
1538 Bradshaw, R. H. W.: Towards mapping the late Quaternary vegetation change of Europe,  
1539 *Veg. Hist. Archaeobot.*, 23(1), doi:10.1007/s00334-012-0390-y, 2014.

1540  
1541 Geiger, R.: *The climate near the ground*. Cambridge: Blue Hill Met. Observ. Harvard  
1542 University 1960

1543  
1544 Giraudi, C.: Lake levels and climate for the last 30,000 years in the fucino area (Abruzzo-  
1545 Central Italy) - A review, *Palaeogeogr. Palaeoclimatol. Palaeoecol.*, 70(1–3), 249–260,  
1546 doi:10.1016/0031-0182(89)90094-1, 1989.

1547  
1548 Giraudi, C.: Climate evolution and forcing during the last 40 ka from the oscillations in  
1549 Apennine glaciers and high mountain lakes, Italy, *J. Quat. Sci.*, 32(8), 1085–1098,  
1550 doi:10.1002/jqs.2985, 2017.

1551  
1552 Guido, M. A., Molinari, C., Moneta, V., Branch, N., Black, S., Simmonds, M., Stastney, P.  
1553 and Montanari, C.: Climate and vegetation dynamics of the Northern Apennines (Italy)  
1554 during the Late Pleistocene and Holocene, *Quat. Sci. Rev.*, 231,  
1555 doi:10.1016/j.quascirev.2020.106206, 2020.

1556 Hansen, M. C., Potapov, P. V., Moore, R., Hancher, M., Turubanova, S. A., Tyukavina, A.,  
1557 Thau, D., Stehman, S. V., Goetz, S. J., Loveland, T. R., Kommareddy, A., Egorov, A., Chini,  
1558 L., Justice, C. O. and Townshend, J. R. G.: High-resolution global maps of 21st-century  
1559 forest cover change, *Science (80-. )*, 342(6160), 850–853, doi:10.1126/science.1244693,  
1560 2013.

1561  
1562 Grichuk, V. P.: Main types of vegetation (ecosystems) for the maximum cooling of the last  
1563 glaciation. B. Frenzel, B. Pecs, A.A. Velichko (Eds.), *Atlas of Palaeoclimates and*  
1564 *Palaeoenvironments of the Northern Hemisphere*, NQUA/Hungarian Academy of  
1565 Sciences, Budapest, pp. 123-124, doi: [10.2307/1551555](https://doi.org/10.2307/1551555), 1992.

1566  
1567 Guiot, J., Torre, F., Jolly, D., Peyron, O., Boreux, J.J., Cheddadi, R.: Inverse vegetation  
1568 modeling by Monte Carlo sampling to reconstruct palaeoclimates under changed precipitation



1569 seasonality and CO2 conditions: application to glacial climate in Mediterranean region. *Ecol.*  
1570 *Model.* 127, 119–140. doi: 10.1016/  
1571 S0304-3800(99)00219-7, 2000.  
1572  
1573 Harrison, S. P., Yu, G. E. and Tarasov, P. E.: Late Quaternary Lake-Level Record from  
1574 Northern Eurasia, *Quat. Res.*, 45(2), 138–159, doi:10.1006/qres.1996.0016, 1996.  
1575  
1576 Harrison, S. P., Bartlein, P. J., Brewer, S., Prentice, I. C., Boyd, M., Hessler, I., Holmgren,  
1577 K., Izumi, K. and Willis, K.: Climate model benchmarking with glacial and mid-Holocene  
1578 climates, *Clim. Dyn.*, 43(3–4), 671–688, doi:10.1007/s00382-013-1922-6, 2014.  
1579  
1580 Harrison, S. P., Bartlein, P. J., Izumi, K., Li, G., Annan, J., Hargreaves, J., Braconnot, P. and  
1581 Kageyama, M.: Evaluation of CMIP5 palaeo-simulations to improve climate projections, *Nat.*  
1582 *Clim. Chang.*, 5(8), 735–743, doi:10.1038/nclimate2649, 2015.  
1583  
1584 Heiri, O., Koinig, K. A., Spötl, C., Barrett, S., Brauer, A., Drescher-Schneider, R., Gaar, D.,  
1585 Ivy-Ochs, S., Kerschner, H., Luetscher, M., Moran, A., Nicolussi, K., Preusser, F., Schmidt,  
1586 R., Schoeneich, P., Schwörer, C., Sprafke, T., Terhorst, B. and Tinner, W.: Palaeoclimate  
1587 records 60–8 ka in the Austrian and Swiss Alps and their forelands, *Quat. Sci. Rev.*, 106,  
1588 186–205, doi:10.1016/j.quascirev.2014.05.021, 2014.  
1589  
1590 Heyman, B. M., Heyman, J., Fickert, T., Harbor, J. M. and Forest, B.: Paleo-climate of the  
1591 central European uplands during the last glacial maximum based on glacier mass-balance  
1592 modeling Bavarian Forest Republic, *Quat. Res.*, 79(1), 49–54,  
1593 doi:10.1016/j.yqres.2012.09.005, 2013.  
1594  
1595 Hughes, A. L. C., Gyllencreutz, R., Lohne, Ø. S., Mangerud, J. and Svendsen, J. I.: The last  
1596 Eurasian ice sheets - a chronological database and time-slice reconstruction, *DATED-1,*  
1597 *Boreas*, 45(1), 1–45, doi:10.1111/bor.12142, 2016.  
1598  
1599 Hughes, P. D. and Gibbard, P. L.: A stratigraphical basis for the Last Glacial Maximum  
1600 (LGM), *Quat. Int.*, 383(June 2014), 174–185, doi:10.1016/j.quaint.2014.06.006, 2015.  
1601  
1602 Hughes, P. D., Woodward, J. C. and Gibbard, P. L.: Late Pleistocene glaciers and climate in  
1603 the Mediterranean, *Glob. Planet. Change*, 50(1–2), 83–98,  
1604 doi:10.1016/j.gloplacha.2005.07.005, 2006.  
1605 Huntley, B.: Dissimilarity mapping between fossil and contemporary pollen spectra in  
1606 Europe for the past 13,000 years, *Quat. Res.*, 33(3), 360–376, doi:10.1016/0033-  
1607 5894(90)90062-P, 1990.  
1608  
1609 Huntley B.: Dissimilarity mapping between fossil and contemporary pollen spectra in Europe  
1610 for the past 13,000 years. *Quaternary Research* 33:360–376, 1990.  
1611  
1612 Huntley, B. and Allen, J. R. M.: Glacial environments III. Palaeovegetation patterns in late  
1613 glacial Europe, in *Neanderthals and modern humans in the European landscape during the*  
1614 *last glaciation*, edited by T. H. Van Andel and H. C. Davies, pp. 79–102, McDonald Institute  
1615 for Archaeological Research, Cambridge., 2003.  
1616

- 1617 Huntley, B. and Birks, H. J. B.: An Atlas of Past and Present Pollen Maps for Europe: 0–  
1618 13,000 B.P. years ago, Cambridge University Press, Cambridge., 1983.  
1619
- 1620 Jalut, G., Andrieu, V., Delibrias, G., Fontaugne, M. and Pages, P.: Palaeoenvironment of the  
1621 valley of Ossau (Western French Pyrenees) during the last 27 000 year, *Pollen et Spores*,  
1622 30(3–4), 357–393, 1988.  
1623
- 1624 Jalut, G., Marti, J. M., Fontugne, M., Delibrias, G., Vilaplana, J. M. and Julia, R.: Glacial to  
1625 interglacial vegetation changes in the northern and southern Pyrénées: Deglaciation,  
1626 vegetation cover and chronology, *Quat. Sci. Rev.*, 11(4), 449–480, doi:10.1016/0277-  
1627 3791(92)90027-6, 1992.  
1628
- 1629 Jankovska, V.: Vegetation cover in West Carpathians during the Last Glacial period -  
1630 analogy of present day siberian forest-tundra nad taiga, *Palynol. Stratigr. geoecology*,  
1631 (SEPTEMBER 2008), 282–289, 2008.  
1632
- 1633 Janská, V., Jiménez-Alfaro, B., Chytrý, M., Divíšek, J., Anenkhonov, O., Korolyuk, A.,  
1634 Lashchinskyi, N. and Culek, M.: Palaeodistribution modelling of European vegetation types  
1635 at the Last Glacial Maximum using modern analogues from Siberia: Prospects and  
1636 limitations, *Quat. Sci. Rev.*, 159, 103–115, doi:10.1016/j.quascirev.2017.01.011, 2017.  
1637
- 1638 Jost, A., Lunt, D., Abe-Ouchi, A., Abe-Ouchi, A., Peyron, O., Valdes, P. J. and Ramstein, G.:  
1639 High-resolution simulations of the last glacial maximum climate over Europe: A solution to  
1640 discrepancies with continental palaeoclimatic reconstructions?, *Clim. Dyn.*, 24(6), 577–590,  
1641 doi:10.1007/s00382-005-0009-4, 2005.  
1642
- 1643 Juggins, S.: Quantitative reconstructions in palaeolimnology : new paradigm or sick  
1644 science ?, *Quat. Sci. Rev.*, 64, 20–32, doi:10.1016/j.quascirev.2012.12.014, 2013.  
1645
- 1646 Juggins, S.: Rioja: Analysis of Quaternary Science Data, [online] Available from:  
1647 <https://cran.r-project.org/package=rioja>, 2020.  
1648
- 1649 Juggins, S. and Birks, H. J. B.: Quantitative Environmental Reconstructions from Biological  
1650 Data, in *Developments in Paleoenvironmental Research 5*, edited by H. J. B. Birks, pp. 431–  
1651 494, Springer ScienceCBusiness Media B.V., 2012.  
1652
- 1653 Juříčková, L., Horáčková, J. and Ložek, V.: Direct evidence of central European forest  
1654 refugia during the last glacial period based on mollusc fossils, *Quat. Res. (United States)*,  
1655 82(1), 222–228, doi:10.1016/j.yqres.2014.01.015, 2014.  
1656
- 1657 Kageyama, M., Laine, A., Abe-Ouchi, A., Braconnot, P., Cortijo, E., Crucifix, M., de Vernal,  
1658 A., Guiot, J., Hewitt, C. D., Kitoh, A., Kucera, M., Marti, O., Ohgaito, R., Otto-Bliesner, B.,  
1659 Peltier, W. R., Rosell-Melé, A., Vettoretti, G., Weber, S. L. and Yu, Y.: Last Glacial  
1660 Maximum temperatures over the North Atlantic, Europe and western Siberia: a comparison  
1661 between PMIP models, MARGO sea-surface temperatures and pollen-based reconstructions,  
1662 *Quat. Sci. Rev.*, 25(17–18), 2082–2102, doi:10.1016/j.quascirev.2006.02.010, 2006.  
1663
- 1664 Kageyama, M., Harrison, S. P., Kapsch, M. L., Lofverstrom, M., Lora, J. M., Mikolajewicz,  
1665 U., ... & Zhu, J. The PMIP4 Last Glacial Maximum experiments: preliminary results and  
1666 comparison with the PMIP3 simulations. *Climate of the Past*, 17(3), 1065–1089, 2021.

1667  
1668 Kaltenrieder, P., Belis, C. A., Hofstetter, S., Ammann, B., Ravazzi, C. and Tinner, W.:  
1669 Environmental and climatic conditions at a potential Glacial refugial site of tree species near  
1670 the Southern Alpine glaciers. New insights from multiproxy sedimentary studies at Lago  
1671 della Costa (Euganean Hills, Northeastern Italy), *Quat. Sci. Rev.*, 28(25–26), 2647–2662,  
1672 doi:10.1016/j.quascirev.2009.05.025, 2009.  
1673  
1674 Kaplan, J. O., Pfeiffer, M., Kolen, J. C. A. and Davis, B. A. S.: Large scale anthropogenic  
1675 reduction of forest cover in last glacial maximum Europe, *PLoS One*, 11(11),  
1676 doi:10.1371/journal.pone.0166726, 2016.  
1677  
1678 Kehrwald, N. M., McCoy, W. D., Thibeault, J., Burns, S. J. and Oches, E. A.: Paleoclimatic  
1679 implications of the spatial patterns of modern and LGM European land-snail shell  $\delta^{18}\text{O}$ ,  
1680 *Quat. Res.*, 74(1), 166–176, doi:10.1016/j.yqres.2010.03.001, 2010.  
1681  
1682 Kelly, A., Charman, D. J. and Newnham, R. M.: A last glacial maximum pollen record from  
1683 bodmin moor showing a possible cryptic Northern refugium in Southwest England, *J. Quat.*  
1684 *Sci.*, 25(3), 296–308, doi:10.1002/jqs.1309, 2010.  
1685  
1686 Kolodny, Y., Stein, M. and Machlus, M.: Sea-rain-lake relation in the Last Glacial East  
1687 Mediterranean revealed by  $\delta^{18}\text{O}$ - $\delta^{13}\text{C}$  in Lake Lisan aragonites, *Geochim. Cosmochim.*  
1688 *Acta*, 69(16), 4045–4060, doi:10.1016/j.gca.2004.11.022, 2005.  
1689  
1690 Kovács, J., Moravcová, M., Újvári, G. and Pintér, A. G.: Reconstructing the  
1691 paleoenvironment of East Central Europe in the Late Pleistocene using the oxygen and  
1692 carbon isotopic signal of tooth in large mammal remains, *Quat. Int.*, 276–277, 145–154,  
1693 doi:10.1016/j.quaint.2012.04.009, 2012.  
1694  
1695 Krebs, P., Pezzatti, G. B., Beffa, G., Tinner, W. and Conedera, M.: Revising the sweet  
1696 chestnut (*Castanea sativa* Mill.) refugia history of the last glacial period with extended pollen  
1697 and macrofossil evidence, *Quat. Sci. Rev.*, 206, 111–128,  
1698 doi:10.1016/j.quascirev.2019.01.002, 2019.  
1699  
1700 Kuneš, P., Pelánková, B., Chytrý, M., Jankovská, V., Pokorný, P. and Petr, L.: Interpretation  
1701 of the last-glacial vegetation of eastern-central Europe using modern analogues from southern  
1702 Siberia, *J. Biogeogr.*, 35(12), 2223–2236, doi:10.1111/j.1365-2699.2008.01974.x, 2008.  
1703  
1704 Küster, H.: Postglaziale Vegetationsgeschichte Südbayerns. Geobotanische Studien zur  
1705 Prähistorischen Landschaftskunde, Akademie Verlag, Berlin., 1995.  
1706  
1707 Lacey, J. H., Leng, M. J., Höbig, N., Reed, J. M., Valero-Garcés, B. and Reicherter, K.:  
1708 Western Mediterranean climate and environment since Marine Isotope Stage 3: a 50,000-year  
1709 record from Lake Banyoles, Spain, *J. Paleolimnol.*, 55(2), 113–128, doi:10.1007/s10933-015-  
1710 9868-9, 2016.  
1711  
1712 Latombe, G., Burke, A., Vrac, M., Levavasseur, G. and Dumas, C.: Comparison of spatial  
1713 downscaling methods of general circulation model results to study climate variability during  
1714 the Last Glacial Maximum, , 2563–2579, 2018.  
1715

- 1716 Lefort J.P., Monnier J.L., Danukalova G.: Transport of Late Pleistocene loess particles by  
 1717 katabatic winds during the lowstands of the English Channel. *Journal of the Geological*  
 1718 *Society* 176: 1169–1181, doi: [10.1144/jgs2019-07](https://doi.org/10.1144/jgs2019-07), 2019.
- 1719  
 1720 Lehmkuhl, F., Nett, J.J., Pöfner, S., Schulte, P., Sprafke, T., Jary, Z., Antoine, P., Wacha, L.,  
 1721 Wolf, D., Zerboni, A., Hoesek, J., Marković, S.B., Obrecht, I., Sümege, P., Veres, D.,  
 1722 Zeeden, C., Boemke, B., Schaubert, V., Viehweger, J., Hambach, U.: Loess landscapes of  
 1723 Europe re-mapping, geomorphology, and zonal differentiation. *Earth Sci. Rev.* 215, 103496.  
 1724 <https://doi.org/10.1016/j.earscirev.2020.103496>, 2021.
- 1725  
 1726 Leroy, S. A. G. and Arpe, K.: Glacial refugia for summer-green trees in Europe and south-  
 1727 west Asia as proposed by ECHAM3 time-slice atmospheric model simulations, *J. Biogeogr.*,  
 1728 34(12), 2115–2128, doi:10.1111/j.1365-2699.2007.01754.x, 2007.
- 1729  
 1730 Lev, L., Stein, M., Ito, E., Fruchter, N., Ben-Avraham, Z. and Almogi-Labin, A.:  
 1731 Sedimentary, geochemical and hydrological history of Lake Kinneret during the past 28,000  
 1732 years, *Quat. Sci. Rev.*, 209, 114–128, doi:10.1016/j.quascirev.2019.02.015, 2019.
- 1733  
 1734 Lister, A. M. and Stuart, A. J.: The impact of climate change on large mammal distribution  
 1735 and extinction: Evidence from the last glacial/interglacial transition, *Comptes Rendus -*  
 1736 *Geosci.*, 340(9–10), 615–620, doi:10.1016/j.crte.2008.04.001, 2008.
- 1737  
 1738 López-García, J. M. and Blain, H. A.: Quaternary small vertebrates: State of the art and new  
 1739 insights, *Quat. Sci. Rev.*, 233, doi:10.1016/j.quascirev.2020.106242, 2020.
- 1740  
 1741 Ludwig, P., Pinto, J. G., Raible, C. C. and Shao, Y.: Impacts of surface boundary conditions  
 1742 on regional climate model simulations of European climate during the Last Glacial  
 1743 Maximum, *Geophys. Res. Lett.*, 44(10), 5086–5095, doi:10.1002/2017GL073622, 2017.
- 1744  
 1745  
 1746 Luetscher, M., Boch, R., Sodemann, H., Spötl, C., Cheng, H., Edwards, R. L., Frisia, S., Hof,  
 1747 F. and Müller, W.: North Atlantic storm track changes during the Last Glacial Maximum  
 1748 recorded by Alpine speleothems, *Nat. Commun.*, 6, 27–32, doi:10.1038/ncomms7344, 2015.
- 1749  
 1750 Magri, D.: Persistence of tree taxa in Europe and Quaternary climate changes, *Quat. Int.*,  
 1751 219(1–2), 145–151, doi:10.1016/j.quaint.2009.10.032, 2010.
- 1752  
 1753 Magri, D. and Parra, I.: Late Quaternary western Mediterranean pollen records and African  
 1754 winds, *Earth Planet. Sci. Lett.*, 200(3–4), 401–408, doi:10.1016/S0012-821X(02)00619-2,  
 1755 2002.
- 1756  
 1757 Magri, D. and Sadori, L.: Late Pleistocene and Holocene pollen stratigraphy at Lago di Vico,  
 1758 central Italy, *Veg. Hist. Archaeobot.*, 8(4), 247–260, doi:10.1007/BF01291777, 1999.
- 1759  
 1760 Magyari, E., Jakab, G., Rudner, E. and Sümege, P.: Palynological and plant macrofossil data  
 1761 on Late Pleistocene short-term climatic oscillations in NE-Hungary, *Acta Palaeobot. Suppl.*,  
 1762 2(January), 491–502, 1999.
- 1763  
 1764 Magyari, E. K., Kuneš, P., Jakab, G., Sümege, P., Pelánková, B., Schäbitz, F., Braun, M. and  
 1765 Chytrý, M.: Late Pleniglacial vegetation in eastern-central Europe: Are there modern

1766 analogues in Siberia?, *Quat. Sci. Rev.*, 95, 60–79, doi:10.1016/j.quascirev.2014.04.020,  
1767 2014a.

1768

1769 Magyari, E. K., Veres, D., Wennrich, V., Wagner, B., Braun, M., Jakab, G., Karátson, D.,  
1770 Pál, Z., Ferenczy, G., St-Onge, G., Rethemeyer, J., Francois, J. P., von Reumont, F. and  
1771 Schäbitz, F.: Vegetation and environmental responses to climate forcing during the Last  
1772 Glacial Maximum and deglaciation in the East Carpathians: Attenuated response to  
1773 maximum cooling and increased biomass burning, *Quat. Sci. Rev.*, 106, 278–298,  
1774 doi:10.1016/j.quascirev.2014.09.015, 2014b.

1775

1776 Magyari, E. K., Pál, I., Vincze, I., Veres, D., Jakab, G., Braun, M., Szalai, Z., Szabó, Z. and  
1777 Korponai, J.: Warm Younger Dryas summers and early late glacial spread of temperate  
1778 deciduous trees in the Pannonian Basin during the last glacial termination (20-9 kyr cal BP),  
1779 *Quat. Sci. Rev.*, 225, doi:10.1016/j.quascirev.2019.105980, 2019.

1780

1781 Margari, V., Gibbard, P. L., Bryant, C. L. and Tzedakis, P. C.: Character of vegetational and  
1782 environmental changes in southern Europe during the last glacial period; evidence from  
1783 Lesvos Island, Greece, *Quat. Sci. Rev.*, 28(13–14), 1317–1339,  
1784 doi:10.1016/j.quascirev.2009.01.008, 2009.

1785

1786 Marsicek, J., Shuman, B. N., Bartlein, P. J., Shafer, S. L. and Brewer, S.: Reconciling  
1787 divergent trends and millennial variations in Holocene temperatures, *Nature*, 554(7690), 92–  
1788 96, doi:10.1038/nature25464, 2018.

1789

1790 Mauch Lenardić, J., Oros Sršen, A. and Radović, S.: Quaternary fauna of the Eastern Adriatic  
1791 (Croatia) with the special review on the Late Pleistocene sites, *Quat. Int.*, 494, 130–151,  
1792 doi:10.1016/j.quaint.2017.11.028, 2018.

1793

1794 Mauri, A., Davis, B. A. S., Collins, P. M. and Kaplan, J. O.: The influence of atmospheric  
1795 circulation on the mid-Holocene climate of Europe: A data-model comparison, *Clim. Past*,  
1796 10(5), 1925–1938, doi:10.5194/cp-10-1925-2014, 2014.

1797

1798 Mauri, A., Davis, B. A. S., Collins, P. M. and Kaplan, J. O.: The climate of Europe during the  
1799 Holocene: A gridded pollen-based reconstruction and its multi-proxy evaluation, *Quat. Sci.*  
1800 *Rev.*, 112, doi:10.1016/j.quascirev.2015.01.013, 2015.

1801

1802 MARGE Project Members.: Constraints on the magnitude and patterns of ocean cooling at  
1803 the Last Glacial Maximum, , (January), 1–6, doi:10.1038/ngeo411, 2009.

1804

1805 Mikolajewicz, U.: Modeling mediterranean ocean climate of the last glacial maximum, *Clim.*  
1806 *Past*, 7(1), 161–180, doi:10.5194/cp-7-161-2011, 2011.

1807

1808 Miola, A., Bondesan, A., Corain, L., Favaretto, S., Mozzi, P., Piovan, S. and Sostizzo, I.:  
1809 Wetlands in the Venetian Po Plain (northeastern Italy) during the Last Glacial Maximum:  
1810 Interplay between vegetation, hydrology and sedimentary environment, *Rev. Palaeobot.*  
1811 *Palynol.*, 141(1–2), 53–81, doi:10.1016/j.revpalbo.2006.03.016, 2006.

1812

1813 Mix, A. C., Bard, E. and Schneider, R.: Environmental processes of the ice age: Land,  
1814 oceans, glaciers (EPILOG), *Quat. Sci. Rev.*, 20(4), 627–657, doi:10.1016/S0277-  
1815 3791(00)00145-1, 2001.

- 1816 Moine, O., Rousseau, D. D., Jolly, D. and Vianey-Liaud, M.: Paleoclimatic reconstruction  
 1817 using mutual climatic range on terrestrial mollusks, *Quat. Res.*, 57(1), 162–172,  
 1818 doi:10.1006/qres.2001.2286, 2002.
- 1819
- 1820 Monegato, G., Ravazzi, C., Donegana, M., Pini, R., Calderoni, G. and Wick, L.: Evidence of  
 1821 a two-fold glacial advance during the last glacial maximum in the Tagliamento end moraine  
 1822 system (eastern Alps), *Quat. Res.*, 68(2), 284–302, doi:10.1016/j.yqres.2007.07.002, 2007.
- 1823
- 1824 Monegato, G., Ravazzi, C., Culiberg, M., Pini, R., Bavec, M., Calderoni, G., Jež, J. and  
 1825 Perego, R.: Sedimentary evolution and persistence of open forests between the south-eastern  
 1826 Alpine fringe and the Northern Dinarides during the Last Glacial Maximum, *Palaeogeogr.*  
 1827 *Palaeoclimatol. Palaeoecol.*, 436, 23–40, doi:10.1016/j.palaeo.2015.06.025, 2015.
- 1828
- 1829 Moreno, A., González-Sampériz, P., Morellón, M., Valero-Garcés, B. L. and Fletcher, W. J.:  
 1830 Northern Iberian abrupt climate change dynamics during the last glacial cycle: A view from  
 1831 lacustrine sediments, *Quat. Sci. Rev.*, 36, 139–153, doi:10.1016/j.quascirev.2010.06.031,  
 1832 2012.
- 1833
- 1834 Nogues-Bravo D, Rodríguez-Sánchez F, Orsini L, de Boer E, Jansson R, Morlon, H.,  
 1835 Fordham, D.A., Jackson, S.T.: Cracking the code of biodiversity responses to past climate  
 1836 change. *Trends Ecol. Evol.* 33:765–76, 2018.
- 1837
- 1838
- 1839 Nolan, C., Overpeck, J. T., Allen, J. R. M., Anderson, P. M., Betancourt, J. L., Binney, H. A.,  
 1840 Brewer, S., Bush, M. B., Chase, B. M., Cheddadi, R., Djamali, M., Dodson, J., Edwards, M.  
 1841 E., Gosling, W. D., Haberle, S., Hotchkiss, S. C., Huntley, B., Ivory, S. J., Kershaw, A. P.,  
 1842 Kim, S. H., Latorre, C., Leydet, M., Lézine, A. M., Liu, K. B., Liu, Y., Lozhkin, A. V.,  
 1843 McGlone, M. S., Marchant, R. A., Momohara, A., Moreno, P. I., Müller, S., Otto-Bliesner, B.  
 1844 L., Shen, C., Stevenson, J., Takahara, H., Tarasov, P. E., Tipton, J., Vincens, A., Weng, C.,  
 1845 Xu, Q., Zheng, Z. and Jackson, S. T.: Past and future global transformation of terrestrial  
 1846 ecosystems under climate change, *Science* (80-. ), 361(6405), 920–923,  
 1847 doi:10.1126/science.aan5360, 2018.
- 1848
- 1849 Normand, S., Treier, U. A. and Odgaard, B. V.: Tree refugia and slow forest development in  
 1850 response to post - LGM warming in North - Eastern European Russia, , 2(4), 2–5, 2011.
- 1851
- 1852 Paganelli, A.: Evolution of vegetation and climate in the Veneto-Po Plain during the Late-  
 1853 Glacial and Early Holocene using pollen-stratigraphical data, *Alp. Mediterr. Quat.*, 9(2),  
 1854 581–589, 1996.
- 1855
- 1856 Peyron, O., Guiot, J., Cheddadi, R., Tarasov, P., Reille, M., De Beaulieu, J. L., Bottema, S.  
 1857 and Andrieu, V.: Climatic Reconstruction in Europe for 18,000 YR B.P. from Pollen Data,  
 1858 *Quat. Res.*, 49(2), 183–196, doi:10.1006/qres.1997.1961, 1998a.
- 1859
- 1860 Pons, A. and Reille, M.: The Holocene- and upper Pleistocene pollen record from Padul  
 1861 (Granada, Spain): A new study, *Palaeogeogr. Palaeoclimatol. Palaeoecol.*, 66(3–4),  
 1862 doi:10.1016/0031-0182(88)90202-7, 1988.
- 1863
- 1864 Potì, A., Kehl, M., Broich, M., Carrión Marco, Y., Hutterer, R., Jentke, T., Linstädter, J.,  
 1865 López-Sáez, J. A., Mikdad, A., Morales, J., Pérez-Díaz, S., Portillo, M., Schmid, C., Vidal-

1866 Matutano, P. and Weniger, G. C.: Human occupation and environmental change in the  
1867 western Maghreb during the Last Glacial Maximum (LGM) and the Late Glacial. New  
1868 evidence from the Iberomaurusian site Ifri El Baroud (northeast Morocco), *Quat. Sci. Rev.*,  
1869 220, 87–110, doi:10.1016/j.quascirev.2019.07.013, 2019.

1870  
1871 Prentice, I. C., Cleator, S. F., Huang, Y. H., Harrison, S. P., and Roulstone, I.: Reconstructing  
1872 ice-age palaeoclimates: Quantifying low-CO<sub>2</sub> effects on plants, *Global Planet. Change*, 149,  
1873 166–176, <https://doi.org/10.1016/j.gloplacha.2016.12.012>, 2017.

1874  
1875 Prentice, I. C. and Harrison, S. P.: Ecosystem effects of CO<sub>2</sub> concentration: Evidence from  
1876 past climates, *Clim. Past*, 5(3), 297–307, doi:10.5194/cp-5-297-2009, 2009.

1877  
1878 Prentice, I. C., Guiot, J. and Harrison, S. P.: Mediterranean vegetation, lake levels and  
1879 palaeoclimate at the Last Glacial Maximum, *Nature*, 360(6405), 658–660,  
1880 doi:10.1038/360658a0, 1992.

1881  
1882 Prentice, I. C., Guiot, J., Huntley, B., Jolly, D. and Cheddadi, R.: Reconstructing biomes  
1883 from palaeoecological data: A general method and its application to European pollen data at  
1884 0 and 6 ka, *Clim. Dyn.*, 12(3), 185–194, doi:10.1007/BF00211617, 1996.

1885  
1886 Prentice, I. C., Harrison, S. P. and Bartlein, P. J.: Global vegetation and terrestrial carbon  
1887 cycle changes after the last ice age, *New Phytol.*, 189(4), 988–998, doi:10.1111/j.1469-  
1888 8137.2010.03620.x, 2011.

1889  
1890 Prud'homme, C., Lécuyer, C., Antoine, P., Moine, O., Hatté, C., Fourel, F., Martineau, F. and  
1891 Rousseau, D. D.: Palaeotemperature reconstruction during the Last Glacial from  $\delta^{18}\text{O}$  of  
1892 earthworm calcite granules from Nussloch loess sequence, Germany, *Earth Planet. Sci. Lett.*,  
1893 442, 13–20, doi:10.1016/j.epsl.2016.02.045, 2016.

1894  
1895 Prud'homme, C., Lécuyer, C., Antoine, P., Hatté, C., Moine, O., Fourel, F., Amiot, R.,  
1896 Martineau, F. and Rousseau, D. D.:  $\delta^{13}\text{C}$  signal of earthworm calcite granules: A new proxy  
1897 for palaeoprecipitation reconstructions during the Last Glacial in western Europe, *Quat. Sci.*  
1898 *Rev.*, 179, 158–166, doi:10.1016/j.quascirev.2017.11.017, 2018.

1899  
1900 Puzachenko, A. Y., Markova, A. K. and Pawłowska, K.: Evolution of Central European  
1901 regional mammal assemblages between the late Middle Pleistocene and the Holocene (MIS7–  
1902 MIS1), *Quat. Int.*, (November), doi:10.1016/j.quaint.2021.11.009, 2021.

1903  
1904 Ramstein, G., Kageyama, M., Guiot, J. and Wu, H.: How cold was Europe at the Last Glacial  
1905 Maximum? A synthesis of the progress achieved since the first PMIP model-data  
1906 comparison, , 331–339, 2007.

1907  
1908 Reille, M. and Andrieu, V.: The late Pleistocene and Holocene in the Lourdes Basin, Western  
1909 Pyrénées, France: new pollen analytical and chronological data, *Veg. Hist. Archaeobot.*, 4(1),  
1910 1–21, doi:10.1007/BF00198611, 1995.

1911  
1912 Reille, M. and de Beaulieu, J. L.: History of the Würm and Holocene vegetation in western  
1913 velay (Massif Central, France): A comparison of pollen analysis from three corings at Lac du  
1914 Bouchet, *Rev. Palaeobot. Palynol.*, 54(3–4), 233–248, doi:10.1016/0034-6667(88)90016-4,  
1915 1988.

1916

1917 Reimer, A., Landmann, G. and Kempe, S.: Lake Van, Eastern Anatolia, hydrochemistry and

1918 history, *Aquat. Geochemistry*, 15(1–2), 195–222, doi:10.1007/s10498-008-9049-9, 2009.

1919

1920 Rousseau, D. D.: Climatic transfer function from quaternary molluscs in European loess

1921 deposits, *Quat. Res.*, 36(2), 195–209, doi:10.1016/0033-5894(91)90025-Z, 1991.

1922

1923 Royer, A., Montuire, S., Legendre, S., Discamps, E., Jeannet, M. and Lécuyer, C.:

1924 Investigating the influence of climate changes on rodent communities at a regional-scale

1925 (MIS 1-3, Southwestern France), *PLoS One*, 11(1), 1–25, doi:10.1371/journal.pone.0145600,

1926 2016.

1927

1928 Ruiz-Zapata, M. B., Vegas, J., Garcia-Cortes, A., Gil Garcia, M. J., Torres, T., Ortiz, J. E.

1929 and Perez-Gonzalez, A.: Vegetation evolution during the Last Maximum Glacial Period in

1930 FU-1 sequence (Fuentillejo Lacustrin Maar, Campo de Calatrava, Ciudad Real), *Polen*, 18,

1931 37–49, 2008.

1932

1933 Salonen, J., Sanchez Goñi, M.F., Renssen, H. and Plikk, A.: Contrasting northern and

1934 southern European winter climate trends during the Last Interglacial. *Geology* 49.

1935 [10.1130/G49007.1](https://doi.org/10.1130/G49007.1). 2021

1936

1937 Salonen, J.S., Ilvonen, L., Seppä, H., Holmström, L., Telford, R.J., Gaidamavicius, A.,

1938 Stancikaite, M., Subetto, D. Comparing different calibration methods (WA/WA-PLS

1939 regression and Bayesian modelling) and different-sized calibration sets in pollen-based

1940 quantitative climate reconstruction. *The Holocene* 22, 413–424, 2012.

1941

1942 Samartin, S., Heiri, O., Kaltenrieder, P., Köhl, N. and Tinner, W.: Reconstruction of full

1943 glacial environments and summer temperatures from Lago della Costa, a refugial site in

1944 Northern Italy, *Quat. Sci. Rev.*, 143, 107–119, doi:10.1016/j.quascirev.2016.04.005, 2016.

1945

1946 Sánchez Goñi, M.F., Loutre, M.F., Crucifix, M., Peyron, O., Santos, L., Duprat, J., Malaizé,

1947 B., Turon, J.-L., and Peypouquet, J.-P.: Increasing vegetation and climate gradient in western

1948 Europe over the Last Glacial inception (122–110 ka): Data–model comparison. *Earth and*

1949 *Planetary Science Letters*, 231, 111–130, doi: 10.1016/j.epsl.2004.12.010, 2005.

1950

1951 Sanchez Goñi, M.F., Harrison, S.P.: Millennial-scale climate variability and vegetation

1952 changes during the Last Glacial: concepts and terminology. *Quaternary Science*

1953 *Reviews* 29, 2823–2827, doi: [10.1016/j.quascirev.2009.11.014](https://doi.org/10.1016/j.quascirev.2009.11.014), 2010.

1954

1955 Sanchi, L., Ménot, G. and Bard, E.: Insights into continental temperatures in the northwestern

1956 Black Sea area during the Last Glacial period using branched tetraether lipids, *Quat. Sci.*

1957 *Rev.*, 84, 98–108, doi:10.1016/j.quascirev.2013.11.013, 2014.

1958

1959 Satkūnas, J. and Grigienė, A.: Eemian-Weichselian palaeoenvironmental record from the

1960 Mickūnai glacial depression (Eastern Lithuania), *Geologija*, 54(2), 35–51,

1961 doi:10.6001/geologija.v54i2.2482, 2012.

1962 Schäfer, I. K., Bliedtner, M., Wolf, D., Faust, D. and Zech, R.: Evidence for humid

1963 conditions during the last glacial from leaf wax patterns in the loess-paleosol sequence El

1964 Paraíso, Central Spain, *Quat. Int.*, 407, 64–73, doi:10.1016/j.quaint.2016.01.061, 2016.

1965



- 1966 Scourse, J. D.: Late Pleistocene stratigraphy and palaeobotany of the Isles of Scilly, *Philos.*  
 1967 *Trans. - R. Soc. London, B*, 334(1271), 405–448, doi:10.1098/rstb.1991.0125, 1991.
- 1968
- 1969 Spötl, C., Koltai, G., Jarosch, A. H. and Cheng, H.: Increased autumn and winter  
 1970 precipitation during the Last Glacial Maximum in the European Alps, *Nat. Commun.*, 12(1),  
 1971 doi:10.1038/s41467-021-22090-7, 2021.
- 1972
- 1973 Stewart, J. R. and Lister, A. M.: Cryptic northern refugia and the origins of the modern biota,  
 1974 *Trends Ecol. Evol.*, 16(11), 608–613, doi:10.1016/S0169-5347(01)02338-2, 2001.
- 1975
- 1976 Stivrins, N., Soininen, J., Amon, L., Fontana, S. L., Gryguc, G., Heikkilä, M., Heiri, O.,  
 1977 Kisielienė, D., Reitalu, T., Stančikaitė, M., Veski, S. and Seppä, H.: Biotic turnover rates  
 1978 during the Pleistocene-Holocene transition, *Quat. Sci. Rev.*, 151, 100–110,  
 1979 doi:10.1016/j.quascirev.2016.09.008, 2016.
- 1980
- 1981 Strahl, J.: Zur Pollenstratigraphie des Weichselspätglazials von Berlin-Brandenburg [On the  
 1982 palynostratigraphy of the Late Weichselian in Berlin-Brandenburg], *Brand.*  
 1983 *Geowissenschaftliche Beiträge*, 12, 87–112, 2005.
- 1984
- 1985 Stute, M. and Deak, J.: Environmental isotope study ( $^{14}\text{C}$ ,  $^{13}\text{C}$ ,  $^{18}\text{O}$ , D, noble gases) on  
 1986 deep groundwater circulation systems in Hungary with reference to paleoclimate,  
 1987 *Radiocarbon*, 31(3), 902–918, doi:10.1017/s0033822200012522, 1990.
- 1988
- 1989 Svenning, J., Normand, S. and Kageyama, M.: Glacial refugia of temperate trees in Europe :  
 1990 insights from species distribution modelling, , (Svenning 2003), 1117–1127,  
 1991 doi:10.1111/j.1365-2745.2008.01422.x, 2008.
- 1992
- 1993 Tarasov, P. E., Webb, T., Andreev, A. A., Afanas'eva, N. B., Berezina, N. A., Bezusko, L.  
 1994 G., Blyakharchuk, T. A., Bolikhovskaya, N. S., Cheddadi, R., Chernavskaya, M. M.,  
 1995 Chernova, G. M., Dorofeyuk, N. I., Dirksen, V. G., Elina, G. A., Filimonova, L. V., Glebov,  
 1996 F. Z., Guiot, J., Gunova, V. S., Harrison, S. P., Jolly, D., Khomutova, V. I., Kvavadze, E. V.,  
 1997 Osipova, I. M., Panova, N. K., Prentice, I. C., Saarse, L., Sevastyanov, D. V., Volkova, V. S.  
 1998 and Zernitskaya, V. P.: Present-day and mid-Holocene biomes reconstructed from pollen and  
 1999 plant macrofossil data from the former Soviet Union and Mongolia, *J. Biogeogr.*, 25(6),  
 2000 1029–1053, doi:10.1046/j.1365-2699.1998.00236.x, 1998.
- 2001
- 2002 Tarasov, P. E., Volkova, V. S., Webb, T., Guiot, J., Andreev, A. A., Bezusko, L. G.,  
 2003 Bezusko, T. V., Bykova, G. V., Dorofeyuk, N. I., Kvavadze, E. V., Osipova, I. M., Panova,  
 2004 N. K. and Sevastyanov, D. V.: Last glacial maximum biomes reconstructed from pollen and  
 2005 plant macrofossil data from northern Eurasia, *J. Biogeogr.*, 27(3), 609–620,  
 2006 doi:10.1046/j.1365-2699.2000.00429.x, 2000.
- 2007
- 2008 Tarasov, P.E., Andreev, A.A., Anderson, P.M., Lozhkin, A.V., Haltia-Hovi, E., Nowaczyk,  
 2009 N.R., Wennrich, V., Brigham-Grette, J., Melles, M.: A pollen-based biome reconstruction  
 2010 over the last 3.562 million years in the Far East Russian Arctic e new insights on climate-  
 2011 vegetation relationships at the regional scale. *Clim. Past* 9, 2759-2775, doi: 10.5194/cp-9-  
 2012 2759-2013, 2013.
- 2013

2014 Telford, R. J. and Birks, H. J. B.: Evaluation of transfer functions in spatially structured  
2015 environments, *Quat. Sci. Rev.*, 28(13–14), 1309–1316, doi:10.1016/j.quascirev.2008.12.020,  
2016 2009.

2017

2018 Turner, M. G., Wei, D., Prentice, I. C., & Harrison, S. P. The impact of methodological  
2019 decisions on climate reconstructions using WA-PLS. *Quaternary Research*, 99, 341–356,  
2020 2021.

2022 Valero-Garcés, B. L., González-Sampériz, P., Navas, A., Machin, J., Delgado-Huertas, A.,  
2023 Pena-Monné, J. L., Sancho-Marcén, C., Stevenson, T. and Davis, B.: Paleohydrological  
2024 fluctuations and steppe vegetation during the last glacial maximum in the central Ebro valley  
2025 (NE Spain), *Quat. Int.*, 122(1 SPEC. ISS.), doi:10.1016/j.quaint.2004.01.030, 2004.

2026

2027 Valsecchi, V., Sanchez Goñi, M. F. and Londeix, L.: Vegetation dynamics in the  
2028 Northeastern Mediterranean region during the past 23 000 yr: Insights from a new pollen  
2029 record from the Sea of Marmara, *Clim. Past*, 8(5), 1941–1956, doi:10.5194/cp-8-1941-2012,  
2030 2012.

2031

2032 Vandenberghe, J., French, H. M., Gorbunov, A., Marchenko, S., Velichko, A. A., Jin, H.,  
2033 Cui, Z., Zhang, T. and Wan, X.: The Last Permafrost Maximum (LPM) map of the Northern  
2034 Hemisphere: Permafrost extent and mean annual air temperatures, 25–17ka BP, *Boreas*,  
2035 43(3), 652–666, doi:10.1111/bor.12070, 2014.

2036

2037 Varsányi, I., Palcsu, L. and Kovács, L. Ó.: Groundwater flow system as an archive of  
2038 palaeotemperature: Noble gas, radiocarbon, stable isotope and geochemical study in the  
2039 Pannonian Basin, Hungary, *Appl. Geochemistry*, 26(1), 91–104,  
2040 doi:10.1016/j.apgeochem.2010.11.006, 2011.

2041

2042 Vegas-Vilarrúbia, T., González-Sampériz, P., Morellón, M., Gil-Romera, G., Pérez-Sanz, A.  
2043 and Valero-Garcés, B.: Diatom and vegetation responses to late glacial and early holocene  
2044 climate changes at lake estanya (southern pyrenees, NE Spain), *Palaeogeogr. Palaeoclimatol.*  
2045 *Palaeoecol.*, 392, 335–349, doi:10.1016/j.palaeo.2013.09.011, 2013.

2046

2047 Vegas, J., Ruiz-Zapata, B., Ortiz, J. E., Galán, L., Torres, T., García-Cortés, Á., Gil-García,  
2048 M. J., Pérez-González, A. and Gallardo-Millán, J. L.: Identification of arid phases during the  
2049 last 50 cal. ka BP from the Fuentillejo maar-lacustrine record (Campo de Calatrava Volcanic  
2050 Field, Spain), *J. Quat. Sci.*, 25(7), 1051–1062, doi:10.1002/jqs.1262, 2010.

2051

2052 Velasquez, P., Kaplan, J. O., Messmer, M., Ludwig, P. and Raible, C. C.: The role of land  
2053 cover in the climate of glacial Europe, *Clim. Past*, 17(3), 1161–1180, doi:10.5194/cp-17-  
2054 1161-2021, 2021.

2055

2056 Vicente-Serrano, S. M., Trigo, R. M., López-Moreno, J. I., Liberato, M. L. R., Lorenzo-  
2057 Lacruz, J., Beguería, S., Morán-Tejeda, E. and El Kenawy, A.: Extreme winter precipitation  
2058 in the Iberian Peninsula in 2010: Anomalies, driving mechanisms and future projections,  
2059 *Clim. Res.*, 46(1), 51–65, doi:10.3354/cr00977, 2011.

2060

2061 Williams, J.W., Grimm, E.G., Blois, J., Charles, D.F., Davis, E., Goring, S.J., Graham, R.,  
2062 Smith, A.J., Anderson, M., Arroyo-Cabrales, J., Ashworth, A.C., Betancourt, J.L., Bills,  
2063 B.W., Booth, R.K., Buckland, P., Curry, B., Giesecke, T., Hausmann, S., Jackson, S.T.,

2064 Latorre, C., Nichols, J., Purdum, T., Roth, R.E., Stryker, M., Takahara, H. :The Neotoma  
2065 Paleocology Database: A multi-proxy, international community-curated data resource. *Quat.*  
2066 *Res.* 89, 156-177, doi:10.1017/qua.2017.105, 2018.  
2067  
2068 Williams, J. W. and Jackson, S. T.: Palynological and AVHRR observations of modern  
2069 vegetational gradients in eastern North America, , 4, 485–497, 2003.  
2070  
2071 Williams, J. W., Webb, T., Shurman, B. N. and Bartlein, P. J.: Do Low CO<sub>2</sub> Concentrations  
2072 Affect Pollen-Based Reconstructions of LGM Climates? A Response to “Physiological  
2073 Significance of Low Atmospheric CO<sub>2</sub> for Plant–Climate Interactions” by Cowling and  
2074 Sykes, *Quat. Res.*, 53(3), 402–404, doi:10.1006/qres.2000.2131, 2000.  
2075  
2076 Willis, K. J. and Van Andel, T. H.: Trees or no trees? The environments of central and  
2077 eastern Europe during the Last Glaciation, *Quat. Sci. Rev.*, 23(23–24), 2369–2387,  
2078 doi:10.1016/j.quascirev.2004.06.002, 2004.  
2079  
2080 Wu, H., Guiot, J., Brewer, S. and Guo, Z.: Climatic changes in Eurasia and Africa at the last  
2081 glacial maximum and mid-Holocene: Reconstruction from pollen data using inverse  
2082 vegetation modelling, *Clim. Dyn.*, 29(2–3), 211–229, doi:10.1007/s00382-007-0231-3, 2007.  
2083  
2084 Yu, G. and Harrison, S. P.: Lake status records from Europe: data base documentation,  
2085 NOAA Paleoclimatology Publications Series, Boulder, Colorado., 1995.  
2086  
2087 Zaarur, S., Affek, H. P. and Stein, M.: Last glacial-Holocene temperatures and hydrology of  
2088 the Sea of Galilee and Hula Valley from clumped isotopes in *Melanopsis* shells, *Geochim.*  
2089 *Cosmochim. Acta*, 179, 142–155, doi:10.1016/j.gca.2015.12.034, 2016.  
2090  
2091 Zanon, M., Davis, B. A. S., Marquer, L., Brewer, S. and Kaplan, J. O.: European forest cover  
2092 during the past 12,000 years: A palynological reconstruction based on modern analogs and  
2093 remote sensing, *Front. Plant Sci.*, 9, doi:10.3389/fpls.2018.00253, 2018.  
2094  
2095 Zech, M., Buggle, B., Leiber, K., Marković, S., Glaser, B., Hambach, U., Huwe, B., Stevens,  
2096 T., Sümegi, P., Wiesenberg, G. and Zöller, L.: Reconstructing Quaternary vegetation history  
2097 in the Carpathian Basin, SE-Europe, using n-alkane biomarkers as molecular fossils:  
2098 Problems and possible solutions, potential and limitations, *Quat. Sci. J.*, 58(2), 148–155,  
2099 doi:10.3285/eg.58.2.03, 2010.  
2100  
2101

Tables

Site	Site Name	Country/Ocean	Latitude	Longitude	Elevation	Site Type	Data Type	Samples	Source	Reference
1	MD95-2039 (M)	Atlantic	40.578333	-10.348333	-3381	Marine	Raw Count	21	EPD (E#1472)	Roucoux et al. 2005
2	SU81-18 (M)	Atlantic	37.77	-9.82	-3135	Marine	Raw Count	10	ACER	Turon et al. 2003
3	MD99-2331 (M)	Atlantic	41.15	-9.68	-2110	Marine	Raw Count	41	ACER	Naughton et al. 2006
4	Carn Morval	United Kingdom	49.926111	-6.313889	5	Lake	Digitised	1	Publication	Scourse 1991
5	Gorham Cave	Spain	36.132826	-5.347358	0	Cave	Digitised	1	Publication	Carrion et al. 2008
6	Dozmary Pool	United Kingdom	50.5347222	-4.5358333	265	Lake	Raw Count	32	Author	Kelly et al. 2010
7	Bajondillo	Spain	36.619722	-4.496389	20	Cave	Raw Count	1	EPD (E#1570)	Cortes-Sanchez et al 2011
8	Laguna del maar de Fuentillejo	Spain	38.937996	-4.0539	637	Lake	Digitised	1	Publication	Ruiz-Zapata et al. 2009
9	Padul-1	Spain	37.016338	-3.608503	785	Peat Bog	Digitised	13	Publication	Pons & Reille 1988
10	Padul-2	Spain	37.010833	-3.603889	726	Peat Bog	Digitised	1	Publication	Camuera et al. 2019
11	Cova di Carihuela	Spain	37.4489	-3.4297	1020	Cave	Digitised	1	Publication	Carrion 1992
12	Ifri El Baroud	Morocco	34.75	-3.3	539	Cave	Digitised	1	Publication	Poti et al. 2019
13	MD95-2043 (M)	Mediterranean	36.14	-2.621	-1841	Marine	Raw Count	7	ACER	Fletcher et al. 2008
14	San Rafael	Spain	36.773611	-2.601389	0	Peat Bog	Raw Count	2	EPD (E#574)	Pantalón-Cano 1997
15	Siles	Spain	38.24	-2.3	1320	Lake	Digitised	1	Publication	Carrion 2002
16	Torreçilla de Valmadrid	Spain	41.4469444	-0.895	570	Colluvium	Digitised	1	Publication	Valero-Garcés et al. 2004
17	Navarrés-1	Spain	39.1	-0.683333	225	Peat Bog	Raw Count	1	EPD (E#469)	Carrion & Dupré-Olivier 1996
18	Navarrés-2	Spain	39.1	-0.683333	225	Peat Bog	Raw Count	1	EPD (E#470)	Carrion & Dupré-Olivier 1996
19	Tourbiere de l'Estarres	France	43.0933	-0.3792	356	Lake	Digitised	1	Publication	Jalut et al. 1988
20	Cova de les Malladetes	Spain	39.058	-0.321	20	Cave	Digitised	1	Publication	Dupré-Olivier 1988
21	Lourdes	France	43.033333	-0.075	430	Lake	Digitised	15	Publication	Reille & Andrieu 1995
22	Lake Estanya	Spain	42.0333333	0.53333333	670	Lake	Digitised	1	Publication	Vegas-Villarubia et al. 2013
23	Freychinède	France	42.7833	1.4333	1350	Lake	Digitised	1	Publication	Jalut et al. 1992
24	Banyoles	Spain	42.133333	2.75	173	Lake	Raw Count	13	EPD (E#931)	Pérez-Obiol & Julia 1994
25	Lac du Bouchet B5	France	44.916667	3.783333	1200	Lake	Digitised	14	Publication	Reille & de Beaulieu 1988
26	MD99-2348 (103) (M)	Mediterranean	42.692778	3.841667	-296	Marine	Raw Count	41	EPD (E#1474)	Beaudouin et al. 2007
27	Les Echets G	France	45.9	4.93	267	Peat Bog	Digitised	136	ACER	de Beaulieu & Reille 1984
28	La Grotte Walou	Belgium	50.585278	5.536389	252	Cave	Digitised	1	Publication	Damblon 2011
29	Bergsee	Germany	47.5722222	7.93638889	382	Lake	Digitised	1	Publication	Duprat-Oualid et al. 2017
30	Garaat El-Ouez	Algeria	36.818333	8.33333	45	Peat Bog	Raw Count	6	EPD (E#1501)	Benslama et al 2010
31	Pian del Lago	Italy	44.321561	9.485682	833	Lake	Digitised	1	Publication	Guido et al. 2020
32	Pilsensee	Germany	48.0267	11.1883	534	Lake	Digitised	1	Publication	Küster 1995
33	Orgiano	Italy	45.29	11.43	19	Peat Bog	Digitised	1	Publication	Paganelli 1996
34	Lago della Costa	Italy	45.2702778	11.7430556	7	Lake	Digitised	8	Publication	Kaltenrieder et al. 2009
35	Lagaccione	Italy	42.566667	11.85	355	Lake	Raw Count	7	ACER	Magri 1999
36	Lago Vico	Italy	42.3166667	12.1666667	510	Lake	Digitised	15	Publication	Magri & Sadori 1999
37	Stracciaccia	Italy	42.13	12.32	220	Lake	Raw Count	2	ACER	Giardini 2007
38	Lago di Monterosi	Italy	42.2166667	12.4333333	237	Lake	Raw Count	1	Publication	Bonatti 1970
39	Venice	Italy	45.629523	12.654086	0	Peat Bog	Digitised	1	Publication	Miola et al. 2006
40	Azzano Decimo	Italy	45.8833	12.7165	10	Alluvial Fan	Raw Count	6	ACER	Pini et al. 2009
41	Valle di Castiglione	Italy	41.89	12.75	44	Lake	Raw Count	2	ACER	Follieri et al. 1989
42	Travesio	Italy	46.2	12.87	220	Lake	Digitised	1	Publication	Monegato et al. 2007
43	Orvenco	Italy	46.252088	13.169771	380	Alluvial Fan	Digitised	1	Publication	Monegato et al. 2007
44	Rio Doidis	Italy	46.12	13.19	152	Lake	Digitised	1	Publication	Monegato et al. 2007
45	Billerio	Italy	46.22	13.21	300	Lake	Digitised	1	Publication	Monegato et al. 2007
46	Kersdorf-Briesen	Germany	52.333704	14.269142	44	Lake	Digitised	1	Publication	Strahl 2005
47	Lago Grande di Monticchio	Italy	40.944444	15.6	1326	Lake	Raw Count	6	EPD (E#932)	Watts et al. 1996
48	Nagymohos	Hungary	48.326944	20.436389	297	Peat Bog	Raw Count	14	Publication	Magyari et al 1999
49	Safarka	Slovakia	48.8819444	20.575	600	Peat Bog	Digitised	1	Publication	Jankovska 2008
50	Feher Lake	Hungary	46.45	20.65	86	Lake	Raw Count	10	Publication	Magyari et al. 2014
51	Ioannina	Greece	39.75	20.85	470	Peat Bog	Raw Count	20	ACER	Tzedakis et al. 2004
52	Kokad	Hungary	47.4027778	21.9286111	112	Peat Bog	Raw Count	2	Publication	Magyari et al. 2019
53	Lake Xinias	Greece	39.05	22.27	500	Lake	Raw Count	5	EPD (E#976)	Bottema 1979
54	Mickunai	Lithuania	54.722114	25.532218	143	Lake	Digitised	1	Publication	Satkunas & Grigiene 2012
55	Lake Sfanta Anna	Romania	46.1263889	25.8880556	946	Lake	Digitised	1	Publication	Magyari et al. 2014
56	Megali Limni	Greece	39.1	26.3	323	Lake	Digitised	1	Publication	Margari et al. 2009
57	Straldzha	Bulgaria	42.630278	26.77	138	Peat Bog	Raw Count	3	Publication	Connor et l. 2013
58	MD01-2430 (M)	Turkey	40.796833	27.725166	-580	Marine	Digitised	1	Publication	Valsecchi et al. 2012
59	Lake Iznik	Turkey	40.433889	29.533056	88	Lake	Raw Count	7	EPD (E#714)	Miebach et al 2016
60	M72/5 628-1 (M)	Black Sea	42.1035	36.62383	-418	Marine	Raw Count	6	Pangaea (833387)	Shumilovskikh et al. 2014
61	Dziguta	Georgia	42.99	41.07	35	Peat Bog	Digitised	1	Publication	Arslanov et al. 2007
62	Lake Van LG	Turkey	38.667	42.669	1649	Lake	Raw Count	10	Pangaea (853779)	Pickarski et al. 2015
63	Lake Zeribar	Iran	35.533333	46.116667	1286	Lake	Raw Count	17	EPD (E#714)	van Zeist & Bottema 1977

Table 1. List of selected sites

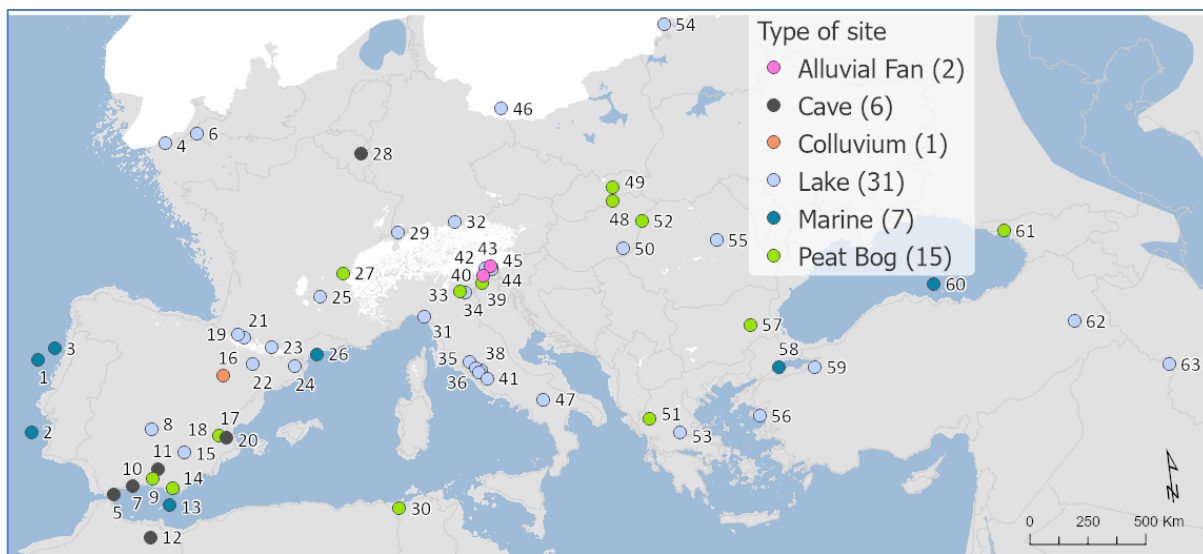
2111  
2112  
2113  
2114  
2115

	<b>RMSE</b>	<b>R2</b>
<b>TANN</b>	2.28	0.9
<b>TDJF</b>	3.35	0.91
<b>TJJA</b>	2.21	0.81
<b>PANN</b>	224.94	0.69
<b>PDJF</b>	78.51	0.69
<b>PJJA</b>	52.49	0.75
<b>Tree Cover</b>	21.03	0.52

2116  
2117  
2118  
2119  
2120  
2121  
2122  
2123  
2124  
2125

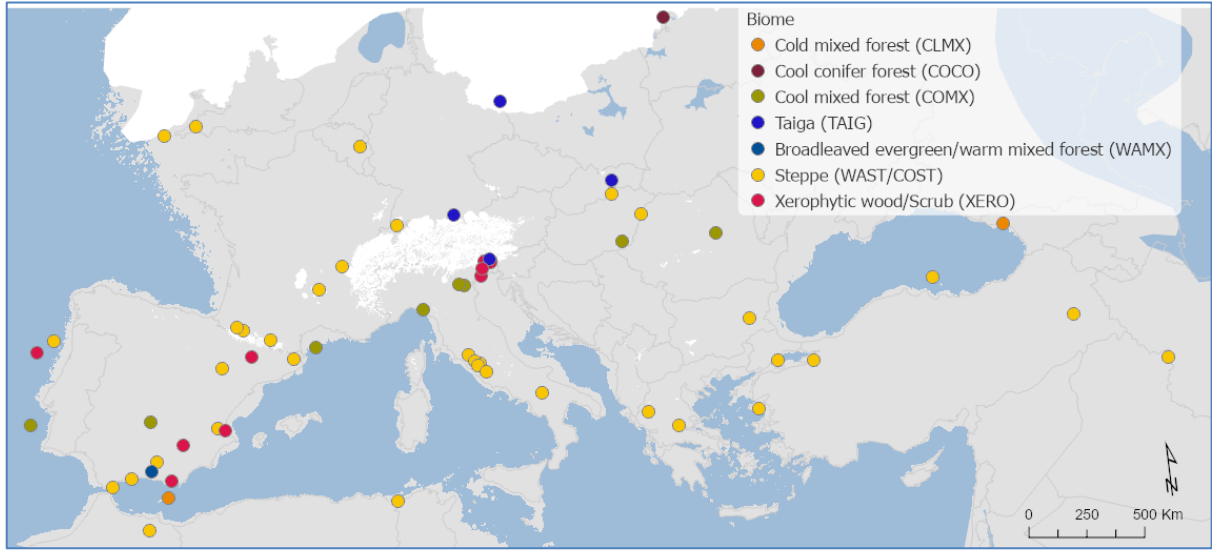
Table 2. MAT performance statistics based on the modern pollen sample training set. This includes Mean Annual Temperature and Precipitation (TANN and PANN), Mean Winter Temperature and Precipitation (TDJF and PDJF) and Mean Summer Temperature and Precipitation (TJJA and PJJA).

2126 **Figures**  
2127  
2128  
2129



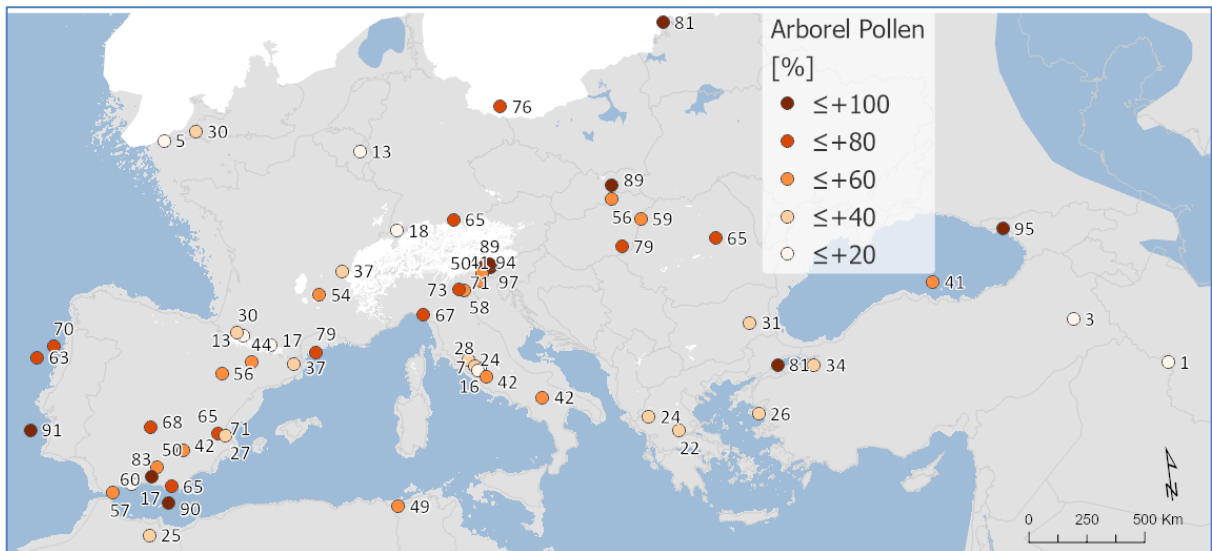
2130  
2131  
2132 **Figure 1. Site locations and archives (Site numbers are as shown in Table 1)**  
2133  
2134  
2135

2136



2137  
2138  
2139  
2140  
2141

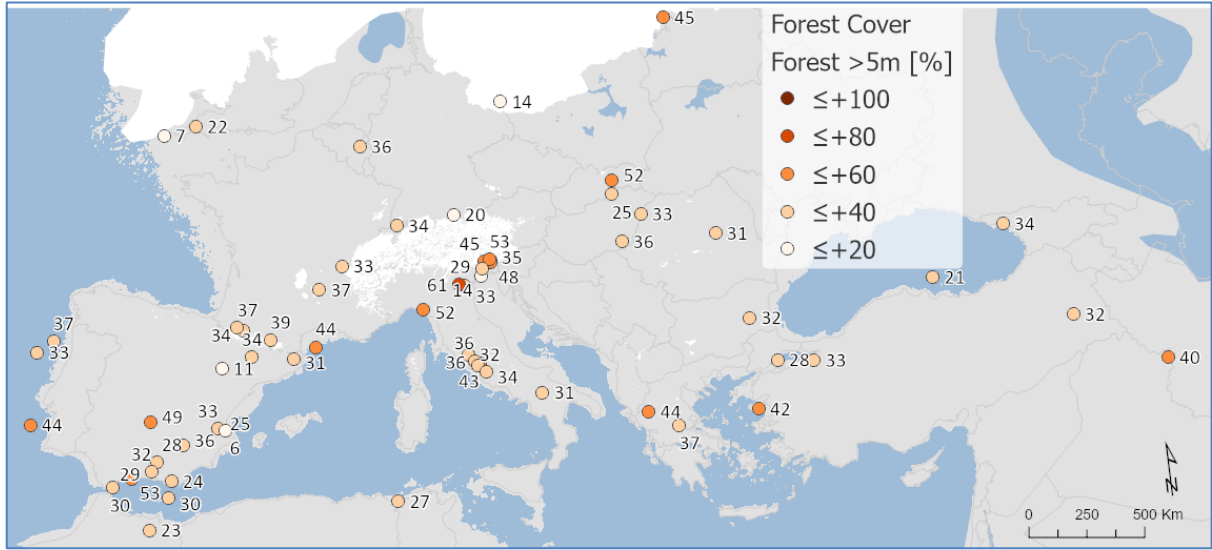
Figure 2. Pollen biomes



2142  
2143  
2144  
2145  
2146

Figure 3. Arboreal Pollen (AP) % forest cover

2147



2148

2149

2150

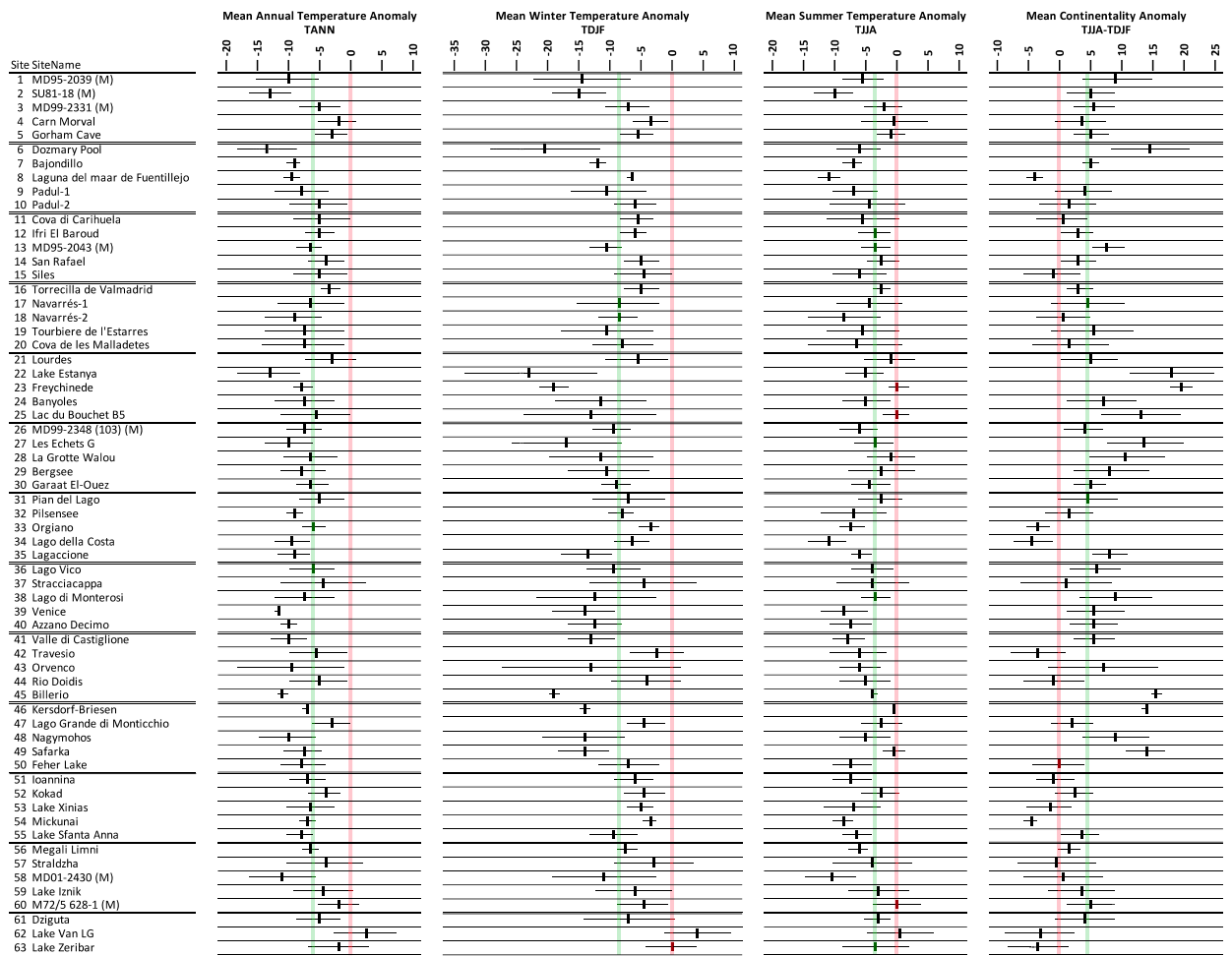
2151

2152

Figure 4. Modern Analogue Technique (MAT) % forest cover



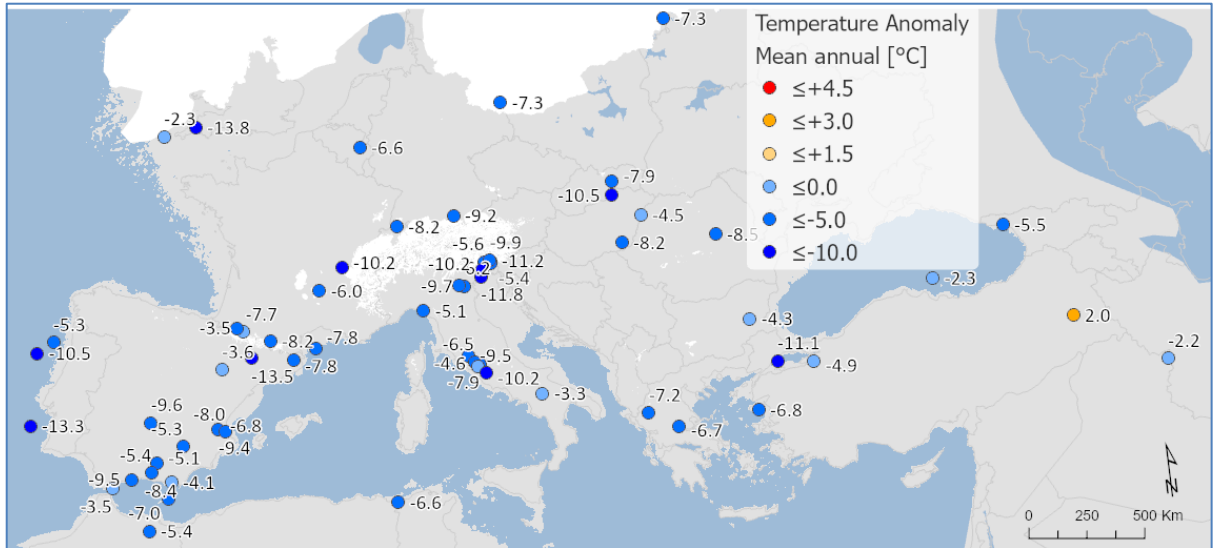
2153  
2154



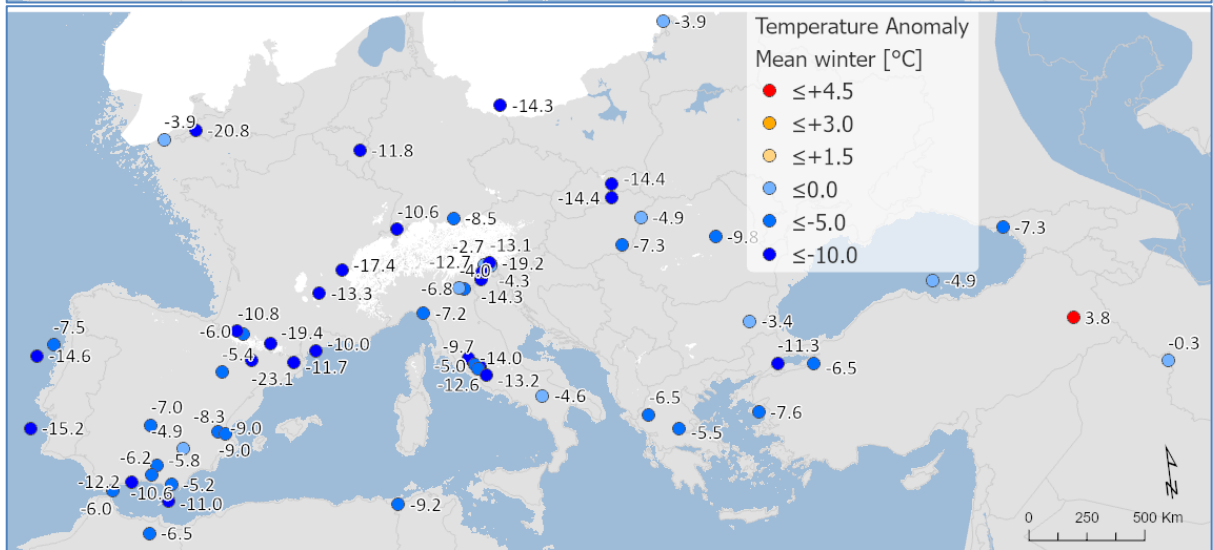
2155  
2156  
2157  
2158  
2159  
2160  
2161  
2162  
2163  
2164

Figure 5. Pollen-based MAT reconstructions for LGM annual, winter and summer temperature anomalies (uncertainties represent one standard deviation). Continentality represents the difference in temperature between summer and winter, with positive anomalies indicating an increase in the temperature difference between summer and winter. All values are expressed as anomalies compared with the present day. The green line indicates the mean for all the sites.

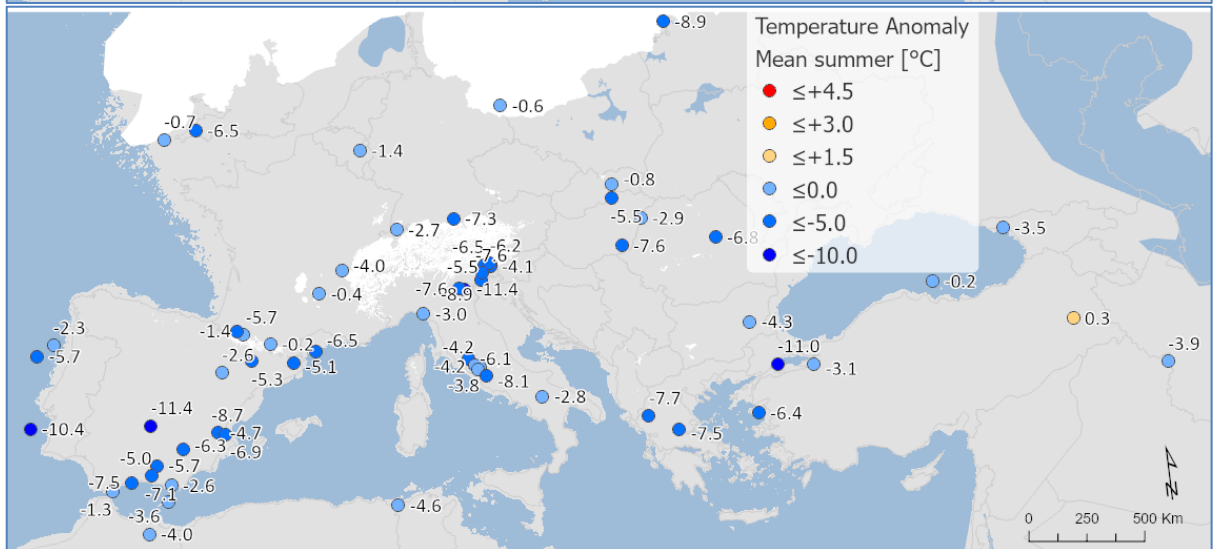
2165

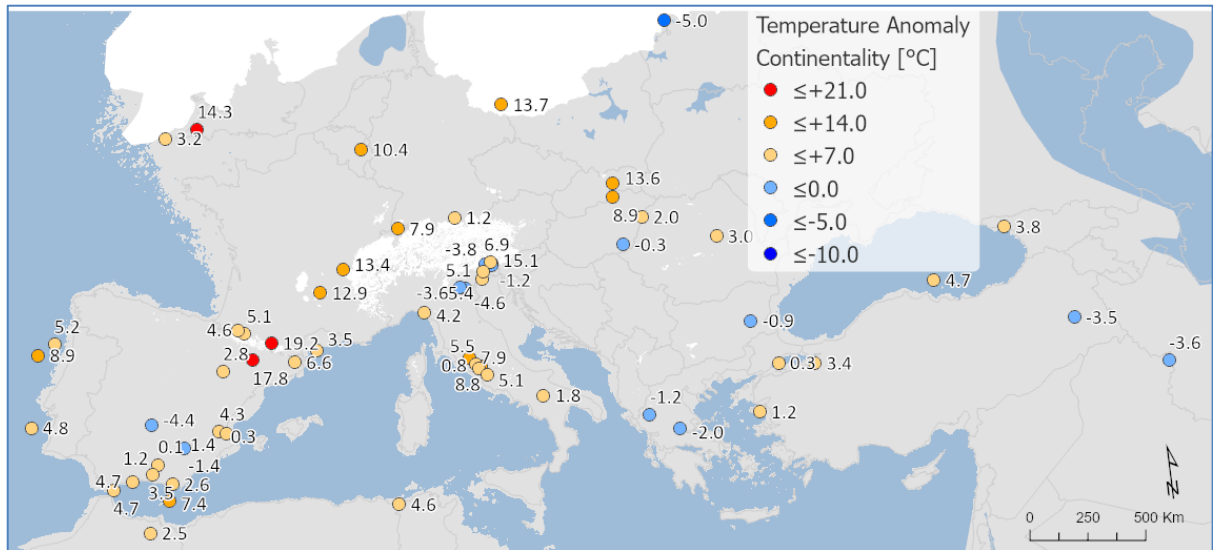


2166



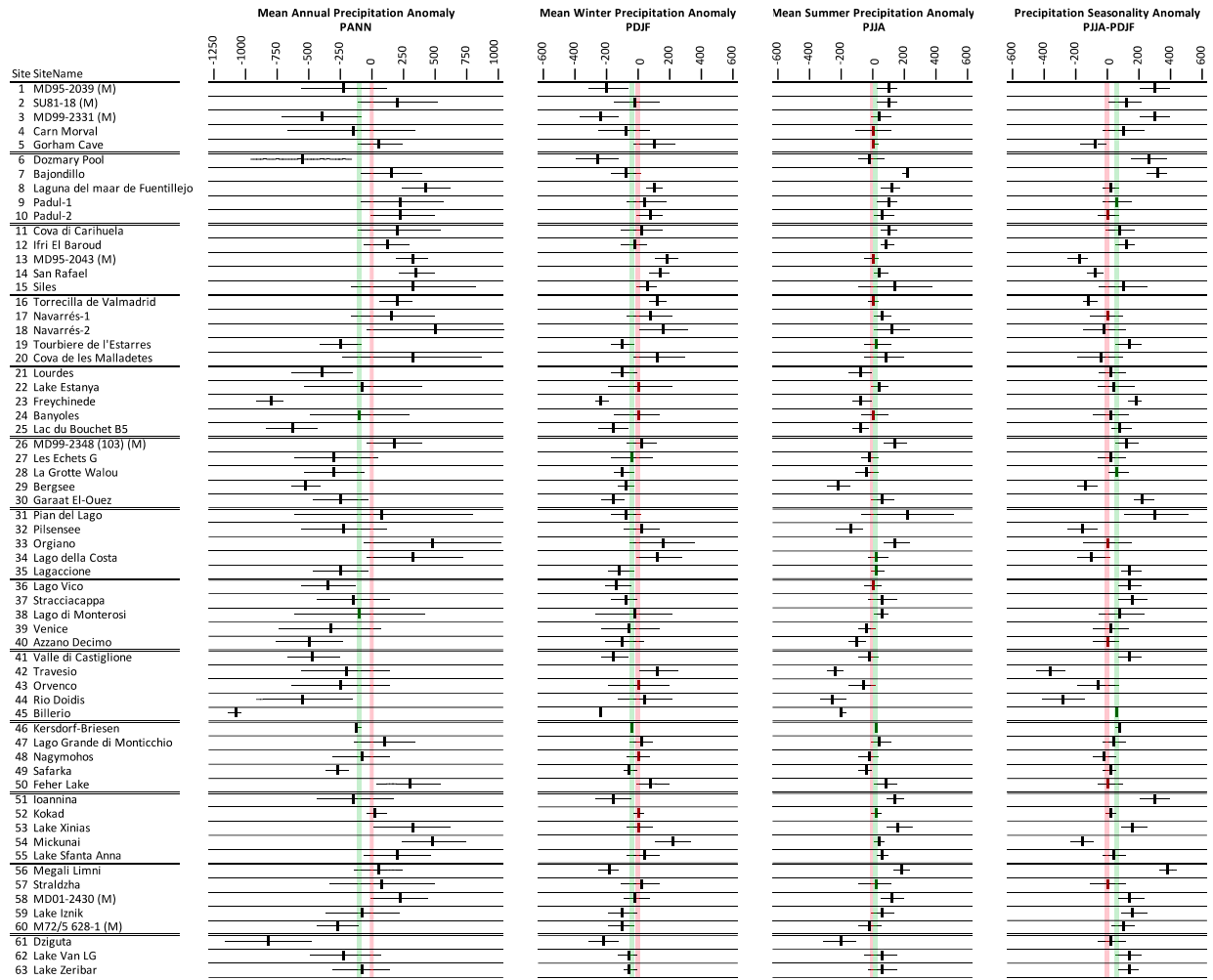
2167





2168  
 2169  
 2170  
 2171  
 2172  
 2173  
 2174  
 2175

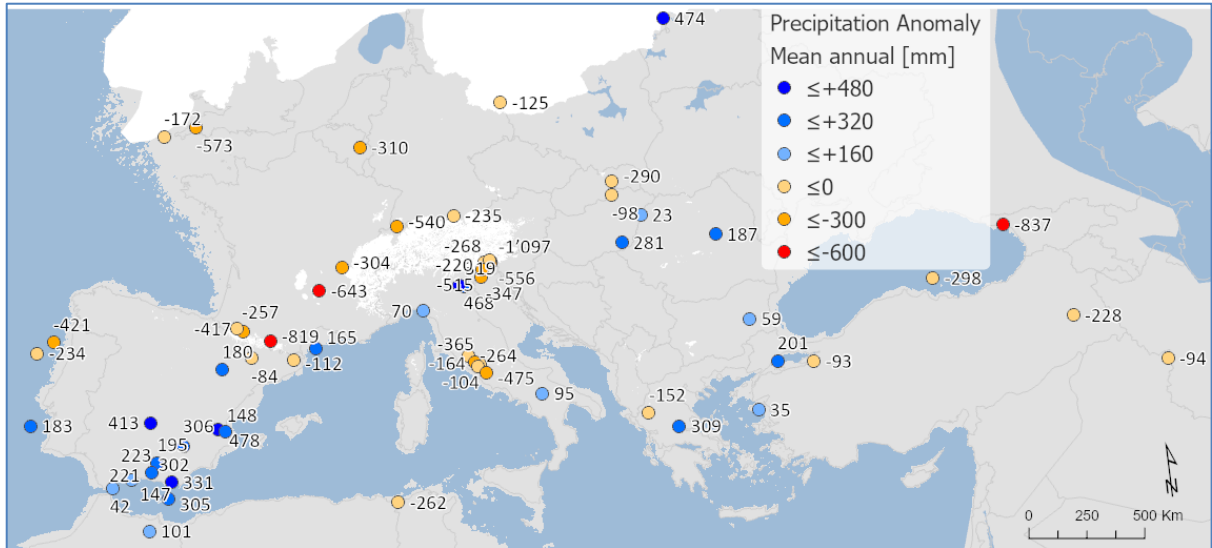
Figure 6. Maps of pollen-based MAT reconstructions for LGM annual, winter and summer temperature anomalies (as shown in figure 9). Continentality represents the difference in temperature between summer and winter, with positive anomalies indicating an increase in the temperature difference between summer and winter. All values are expressed as anomalies compared with the present day.



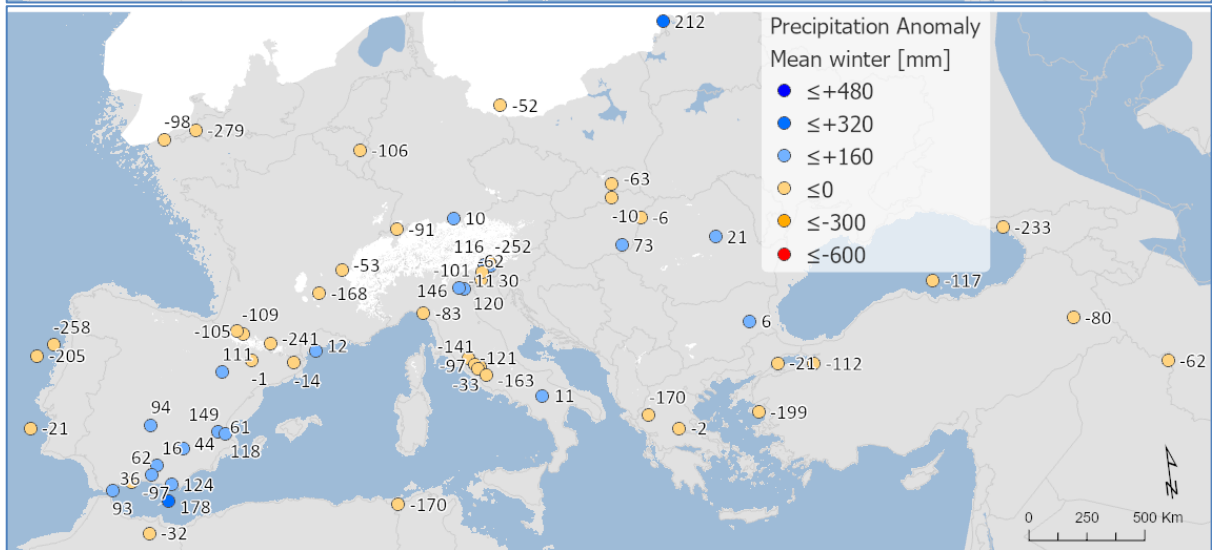
2177  
 2178  
 2179  
 2180  
 2181  
 2182  
 2183  
 2184

Figure 7. Pollen-based MAT reconstructions for LGM annual, winter and summer precipitation anomalies (uncertainties represent one standard deviation). Seasonality represents the difference in precipitation between summer and winter, with positive anomalies indicating an increase in summer precipitation compared to winter. All values are expressed as anomalies compared with the present day. The green line indicates the mean for all the sites.

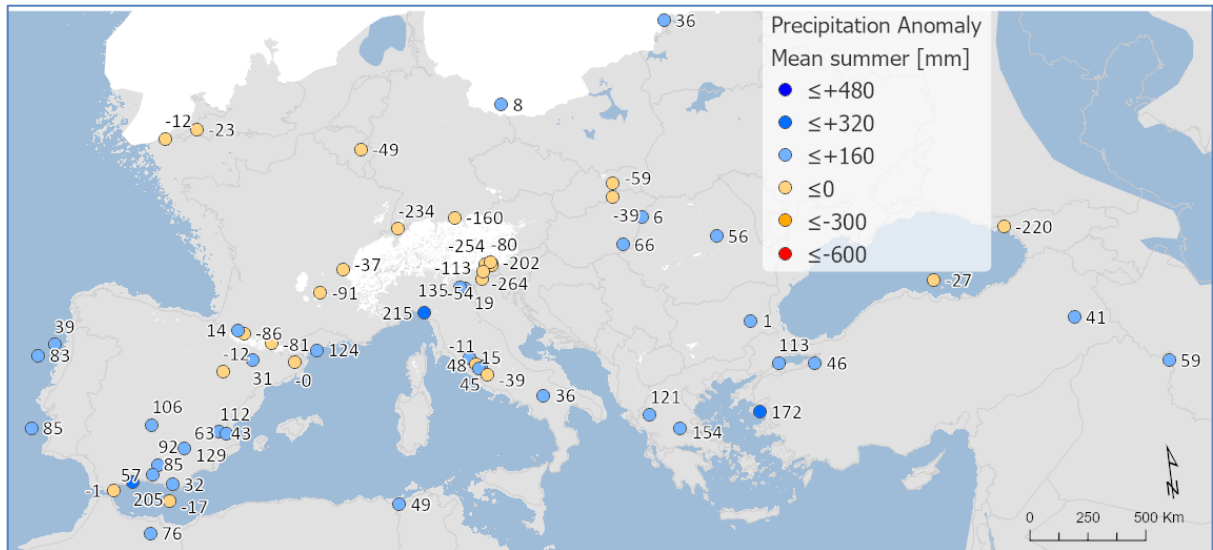
2185



2186

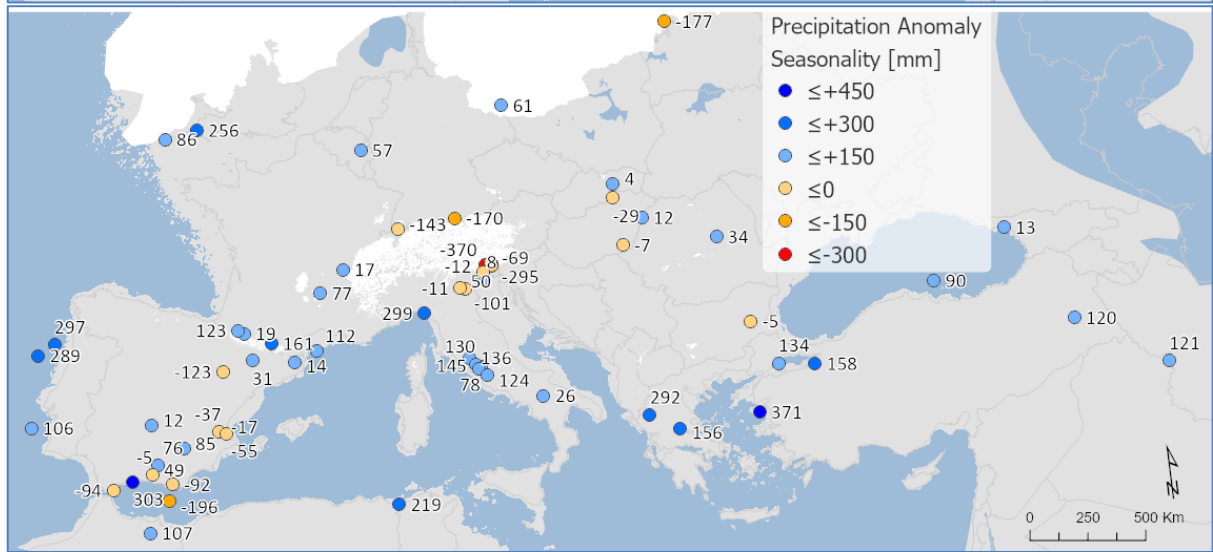


2187



2188

2189



2190

2191

2192

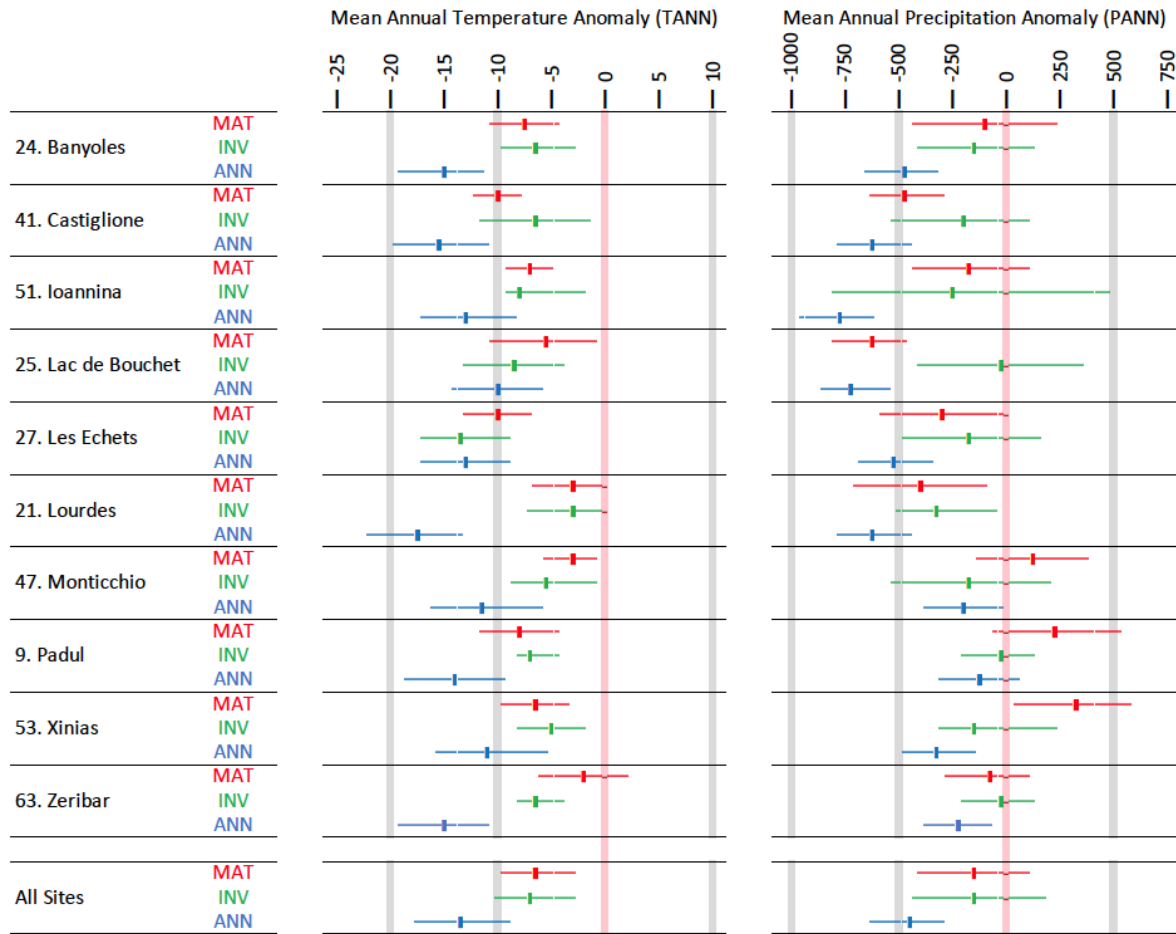
2193

2194

2195

2196

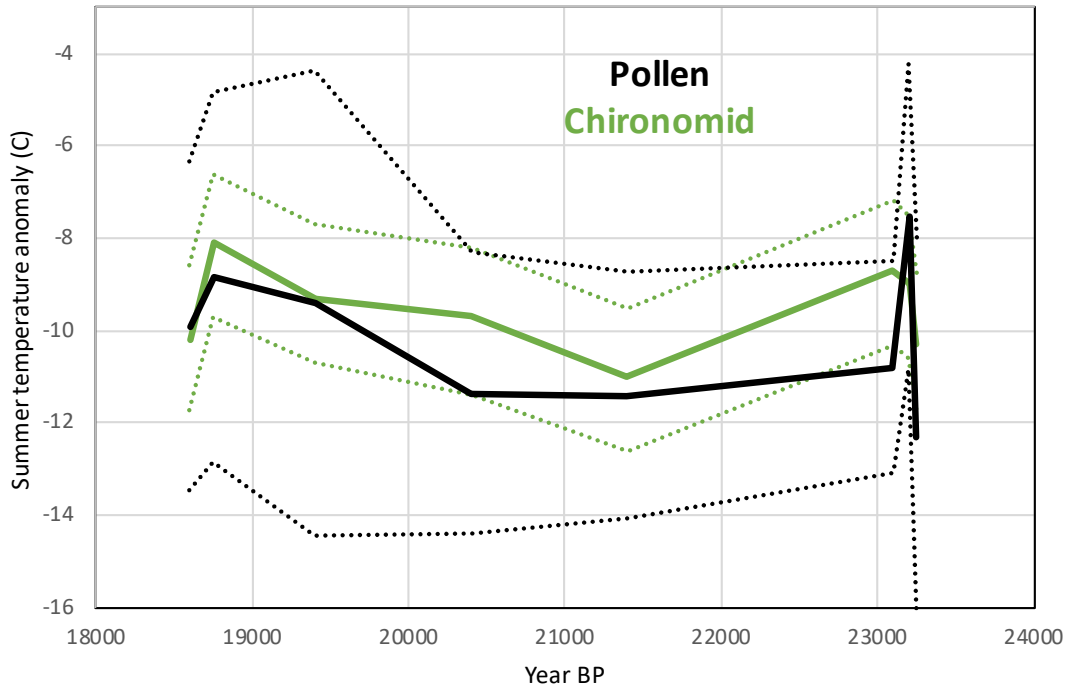
Figure 8. Maps of pollen-based MAT reconstructions for LGM annual, winter and summer precipitation anomalies (as shown in figure 11). Seasonality represents the difference in precipitation between summer and winter, with positive anomalies indicating an increase in summer precipitation compared to winter. All values are expressed as anomalies compared with the present day.



2198  
 2199  
 2200  
 2201  
 2202  
 2203  
 2204  
 2205

Figure 9. A site-by-site comparison between LGM pollen-climate reconstructions based on Modern Analogue Technique MAT (this study), neural-networks ANN (Peyron et al., 1998), and Inverse Modelling INV (Wu et al., 2007). The results show that MAT and INV give similar climate reconstructions, but ANN is significantly cooler/drier.

2206  
2207  
2208



2209  
2210  
2211  
2212  
2213  
2214  
2215

Figure 10. Comparison between LGM pollen-climate MAT and chironomid summer temperature reconstructions at Lago della Costa, Italy (chironomid reconstruction and pollen data from Samartin et al., 2016). Dash lines show uncertainties.



2216  
2217  
2218

Appendix

Site	Site Name	COHMAP Quality	COHMAP										Upper 14C	Upper Cal. BP	Lower 14C	Lower Cal. BP	
			< 17k	18k	19k	20k	21k	22k	23k	24k	25k >						
1	MD95-2039 (M)	3C											14830±80	18166±269	19950±210	23883±374	
2	SU81-18 (M)	2C											17510±270	20952±404	21250±280	25420±441	
3	MD99-2331 (M)	2C											16170±130	19325±303	19770±170	23682±336	
4	Carn Morval	4C												18600±3700	21500±890/800	25867±1127	
5	Gorham Cave	4D													18440±160	22055±341	
6	Dozmary Pool	2C											14568±129	17569±523	18325±216	21769±602	
7	Bajondillo	1C												18701±2154			
8	Laguna del maar de Fuentillejo	5D											16540±90	19847±308			
9	Padul-1	3D											18300±300	21821±412	19100±160	22922±308	
10	Padul-2	1D													17450±539	21082±539	
11	Cova di Carihuela	2C											15700±220	18958±280	21430±130	25659±226	
12	Ifri El Baroud	2D											17296±87	20761±293			
13	MD95-2043 (M)	2C											15440±90	18533±294	18260±120	21951±335	
14	San Rafael	3D											9980±60	11464±133	16860±120	20083±292	
15	Siles	2D											17030±80	20345±351			
16	Torreçilla de Valmadrid	2D											17100±85	20456±366			
17	Navarrés-1	4D											18360±195	22001±353	20700±295	24664±411	
18	Navarrés-2	5D											5150±50	5881±85	16000±	19144±	
19	Tourbiere de l'Estarres	1C											17150±250	20522±470	18970±160	22847±317	
20	Cova de les Malladetes	5D											16300±1500	19686±1723			
21	Lourdes	4D											18510±130	22112±130	20025±175	23952±355	
22	Lake Estanya	5D												9498±50		19184±251	
23	Freychinede	3C											14800±800	17912±856	21300±760	25615±1030	
24	Banyoles	2C												19878±100		27862±3000	
25	Lac du Bouchet B5	4C											15350±350	18513±435	19200±300	23006±384	
26	MD99-2348 (103) (M)	1D											17660±60	21065±310	19350±90	23111±271	
27	Les Echets G	1C											17530±270	20970±407	18030±250	21704±473	
28	La Grotte Walou	1D														21200±700	
29	Bergsee	2D													17780±90	21244±306	
30	Garaat El-Ouez	2C											16010±320	19200±801			
31	Pian del Lago	2D														21260±320	
32	Pilsensee	6D											15860±250	19073±290			
33	Orgiano	2D											17760±160	21221±373	19290±520	23141±621	
34	Lago della Costa	2C											15400±150	18484±330	19285±160	23052±302	
35	Lagaccione	2C											16080±450	19369±527	20615±940	24746±1201	
36	Lago Vico	3C											14385±140	17541±272	20500±230	24430±376	
37	Stracciaccappa	4C											12060±130	14093±281	19745±820	22675±955	
38	Lago di Monterosi	2D											17040±350	20398±544			
39	Venice	5D													18640±100	22277±336	
40	Azzano Decimo	2D											18000±300	21637±529	21025±245	25179±449	
41	Valle di Castiglione	3C											14220±145	17443±270	20300±700	24266±842	
42	Travesio	5D													18780±200	22483±406	
43	Orvenco	2D											17760±160	21221±373	19290±520	23141±621	
44	Rio Doidis	5D													18860±190	22390±373	
45	Billerio	3D													18165±200	21872±382	
46	Kersdorf-Briesen	1D													17622±94	21183±356	
47	Lago Grande di Monticchio	2C												20204±		24014±	
48	Nagymohos	2C											14246±144	17361±425	18159±247	21735±622	
49	Safarka	3D													18287±1512	21912±1781	
50	Feher Lake	1D											17715±250	21190±463	19911±81	23841±313	
51	Ioannina	3C											15330±140	18420±312	20760±230	24748±330	
52	Kokad	5D											14326±63	17433±443	16280±90	19685±538	
53	Lake Xinias	6C											11150±130	13049±160	21390±430	25671±648	
54	Mickunai	1D												21000±2200			
55	Lake Sfanta Anna	1D											17626±96	20955±432			
56	Megali Limni	6D											19072±237	22906±340			
57	Straldzha	6C											14696±65	18022±364	23653±114	28580±390	
58	MD01-2430 (M)	4C											12050±75	14904±324	18310±380	21746±968	
59	Lake Iznik	7D											16910±100	19515±115			
60	M72/5 628-1 (M)	2C											16835±85	18490±	19495±90	21280±	
61	Dziguta	4C											12990±160	15839±483	20560±880	24666±1126	
62	Lake Van LG	2C												18590±62		23290±596	
63	Lake Zeribar	4C											13650±160	16610±399	22000±500	26462±880	

COHMAP chronological quality classification:  
 1C: Bracketing dates within 2000 14C (2360 Cal.) yr interval about the time being assessed  
 2C: Bracketing dates, one within 2000 14C (2360 Cal.) yr and the second within 4000 14C (4682 Cal.) yr of the time being assessed  
 3C: Bracketing dates within 4000 14C (4682 Cal.) yr interval about the time being assessed  
 4C: Bracketing dates, one being within 4000 14C (4682 Cal.) yr and the second being within 6000 14C (7490 Cal.) yr of the time being assessed  
 5C: Bracketing dates within 6000 14C (7490 Cal.) yr interval about the time being assessed  
 6C: Bracketing dates, one within 6000 14C (7490 Cal.) yr and the second within 8000 14C (9681 Cal.) yr of the time being assessed  
 7C: Poorly dated  
 1D: Date within 250 14C (206 Cal.) yr of the time being assessed  
 2D: Date within 500 14C (684 Cal.) yr of the time being assessed  
 3D: Date within 750 14C (975 Cal.) yr of the time being assessed  
 4D: Date within 1000 14C (1123 Cal.) yr of the time being assessed  
 5D: Date within 1500 14C (1881 Cal.) yr of the time being assessed  
 6D: Date within 2000 14C (2360 Cal.) yr of the time being assessed  
 7D: Poorly dated

2219  
2220  
2221  
2222  
2223  
2224  
2225  
2226  
2227  
2228  
2229  
2230  
2231  
2232  
2233  
2234  
2235  
2236  
2237  
2238

Table A1. Chronological control

2239  
2240

Site Number	Site Name	Site Type	TANN	TDJF	TJJA	PANN	PDJF	PJJA
1	MD95-2039 (M)	Marine	15.7	10.7	20.8	1047	427	70
2	SU81-18 (M)	Marine	20.8	15.3	26.5	629	282	25
3	MD99-2331 (M)	Marine	14.6	9.8	19.4	1239	507	88
4	Carn Morval	Lake	12.5	8.7	16.9	1183	392	206
5	Gorham Cave	Cave	18.3	13.4	23.7	740	336	25
6	Dozmary Pool	Lake	10.3	6.0	15.2	1271	422	236
7	Bajondillo	Cave	16.6	10.5	23.4	542	223	27
8	Laguna del maar de Fuentillejo	Lake	16.1	8.1	25.4	474	156	47
9	Padul-1	Peat Bog	16.6	9.6	24.9	417	157	23
10	Padul-2	Peat Bog	16.6	9.6	24.9	417	157	23
11	Cova di Carihuela	Cave	15.7	8.1	25.1	551	187	57
12	Ifri El Baroud	Cave	16.9	10.7	24.0	457	184	22
13	MD95-2043 (M)	Marine	17.9	12.4	24.0	214.2	37	72
14	San Rafael	Peat Bog	18.1	11.9	24.9	243	87	14
15	Siles	Lake	14.4	6.8	23.4	658	195	92
16	Torrecilla de Valmadrid	Colluvium	14.2	6.6	22.5	390	75	82
17	Navarrés-1	Peat Bog	17.0	10.9	23.8	421	96	51
18	Navarrés-2	Peat Bog	17.0	10.9	23.8	421	96	51
19	Tourbiere de l'Estalles	Lake	13.0	6.1	20.4	1045	272	217
20	Cova de les Malladetes	Cave	18.1	12.1	24.8	478	117	60
21	Lourdes	Lake	12.6	5.5	20.1	1002	256	212
22	Lake Estanya	Lake	12.8	5.1	21.0	641	125	152
23	Freychinede	Lake	10.8	3.9	19.0	1128	257	277
24	Banyoles	Lake	14.3	7.7	21.9	698	157	139
25	Lac du Bouchet B5	Lake	8.2	1.3	15.9	1070	251	221
26	MD99-2348 (103) (M)	Marine	14.6	8.0	21.9	618	158	95
27	Les Echets G	Peat Bog	11.4	3.6	19.6	876	175	215
28	La Grotte Walou	Cave	10.3	3.2	17.0	903	215	249
29	Bergsee	Lake	9.6	1.4	17.6	1048	189	387
30	Garaat El-Ouez	Peat Bog	17.3	11.0	24.3	830	360	33
31	Pian del Lago	Lake	12.4	5.1	20.0	995	266	149
32	Pilsensee	Lake	9.3	0.6	17.7	947	151	374
33	Orgiano	Peat Bog	13.0	3.3	22.3	907	200	228
34	Lago della Costa	Lake	12.9	3.3	22.1	888	196	224
35	Lagaccione	Lake	14.2	7.2	21.7	705	203	109
36	Lago Vico	Lake	13.7	6.4	21.5	870	258	132
37	Stracciaccappa	Lake	14.6	7.3	22.4	867	266	115
38	Lago di Monterosi	Lake	15.0	7.7	22.9	837	248	115
39	Venice	Peat Bog	13.4	4.5	22.1	1050	221	277
40	Azzano Decimo	Alluvial Fan	13.3	4.4	22.1	1170	241	311
41	Valle di Castiglione	Lake	16.3	9.1	24.0	988	294	144
42	Travesio	Lake	12.6	3.7	21.3	1415	281	375
43	Orvenco	Alluvial Fan	13.0	3.3	22.3	907	200	228
44	Rio Doidis	Lake	12.8	4.1	21.2	1529	315	392
45	Billerio	Lake	12.8	4.1	21.2	1529	315	392
46	Kersdorf-Briesen	Lake	8.8	-1.0	17.9	538	110	175
47	Lago Grande di Monticchio	Lake	11.5	4.1	19.8	518	154	76
48	Nagymohos	Peat Bog	9.5	-1.5	19.1	616	103	230
49	Safarka	Peat Bog	7.0	-3.2	16.0	755	119	280
50	Feher Lake	Lake	11.0	-0.1	20.7	546	112	185
51	Ioannina	Peat Bog	14.7	6.5	23.3	1000	364	98
52	Kokad	Peat Bog	10.2	-0.9	19.8	601	130	204
53	Lake Xiniás	Lake	15.6	7.5	24.1	563	211	47
54	Mickunai	Lake	6.0	-5.0	16.3	682	131	230
55	Lake Sfanta Anna	Lake	11.6	5.2	18.4	867	253	172
56	Megali Limni	Lake	15.5	8.2	23.4	684	357	28
57	Straldzha	Peat Bog	12.5	2.6	21.8	591	158	135
58	MD01-2430 (M)	Marine	18.0	8.7	27.5	595	219	75
59	Lake Iznik	Lake	13.9	6.1	21.8	677	250	85
60	M72/5 628-1 (M)	Marine	14.5	8.0	21.6	857	251	156
61	Dziguta	Peat Bog	14.1	6.6	21.7	1549	409	373
62	Lake Van LG	Lake	12.0	0.9	23.1	635	201	34
63	Lake Zeribar	Lake	17.1	5.0	29.0	427	167	6

2241  
2242  
2243  
2244  
2245

**Table A2.** Modern climate values for each site used in the calculation of anomalies (taken from WorldClim 2, Fick & Hijmans 2017)

2246  
2247  
2248  
2249

	All surface samples		Steppe only	
	RMSE	R2	RMSE	R2
<b>TANN</b>	2.28	0.9	2.51	0.87
<b>TDJF</b>	3.35	0.91	3.26	0.88
<b>TJJA</b>	2.21	0.81	2.49	0.82
<b>PANN</b>	224.94	0.69	185.7	0.71
<b>PDJF</b>	78.51	0.69	66.5	0.66
<b>PJJA</b>	52.49	0.75	43.8	0.79

2250  
2251  
2252  
2253  
2254  
2255  
2256  
2257  
2258  
2259  
2260

**Table A3.** A comparison of MAT performance statistics based on the modern pollen sample training set using all surface samples from the EMPD2 used in the LGM reconstruction (as shown in Table 3), and a subset of 1588 samples from the EMPD2 that were classified as steppe. The results show little difference between the two different types of samples. The table includes Mean Annual Temperature and Precipitation (TANN and PANN), Mean Winter Temperature and Precipitation (TDJF and PDJF) and Mean Summer Temperature and Precipitation (TJJA and PJJA).

Site Name	Site#	Pollen Biome	Modern Analogue Biome	Modern Analogue Ecoregion
MD95-2039	1	XERO	Mediterranean Forests, woodlands and scrubs	Iberian conifer forests
SU81-18	2	COMX	Mediterranean Forests, woodlands and scrubs	Iberian conifer forests
MD99-2331	3	STEP	Mediterranean Forests, woodlands and scrubs	Alps conifer and mixed forests
Carn Morval	4	STEP	Temperate broadleaf and mixed forests	North Atlantic moist mixed forests
Gorham Cave	5	STEP	Mediterranean Forests, woodlands and scrubs	Cyprus Mediterranean forests
Dozmary Pool	6	STEP	Temperate Coniferous Forest	Alps conifer and mixed forests
Bajondillo	7	STEP	Temperate broadleaf and mixed forests	Central European mixed forests
Laguna del maar de Fuentillejo	8	COMX	Mediterranean Forests, woodlands and scrubs	Northwest Iberian montane forests
Padul	9	STEP	Mediterranean Forests, woodlands and scrubs	Central Anatolian steppe
Padul-15-05	10	WAMX	Mediterranean Forests, woodlands and scrubs	Iberian sclerophyllous and semi-deciduous forests
Cova di Carhuela	11	STEP	Deserts and xeric shrublands	Azerbaijan shrub desert and steppe
Ifri El Baroud	12	STEP	Mediterranean Forests, woodlands and scrubs	Iberian sclerophyllous and semi-deciduous forests
MD95-2043	13	CLMX	Mediterranean Forests, woodlands and scrubs	Southern Anatolian montane conifer and deciduous forests
San Rafael	14	XERO	Mediterranean Forests, woodlands and scrubs	Tyrrhenian-Adriatic Sclerophyllous and mixed forests
Siles	15	XERO	Mediterranean Forests, woodlands and scrubs	Northwest Iberian montane forests
Torreçilla de Valmadrid	16	STEP	Mediterranean Forests, woodlands and scrubs	Southern Anatolian montane conifer and deciduous forests
Navarres	17	XERO	Mediterranean Forests, woodlands and scrubs	Iberian sclerophyllous and semi-deciduous forests
Navarres	18	STEP	Temperate broadleaf and mixed forests	Pyrenees conifer and mixed forests
Tourbiere de IEstarres	19	STEP	Temperate grasslands, savannas and shrublands	Eastern Anatolian montane steppe
Cova de les Malladetes	20	XERO	Mediterranean Forests, woodlands and scrubs	Pyrenees conifer and mixed forests
Lourdes	21	STEP	Temperate broadleaf and mixed forests	Gissaro-Alai open woodlands
Estanya	22	XERO	Temperate broadleaf and mixed forests	Western Siberian hemiboreal forests
Freychinede	23	STEP	Temperate grasslands, savannas and shrublands	Mongolian-Manchurian grassland
Lake Banyoles	24	STEP	Temperate grasslands, savannas and shrublands	Gissaro-Alai open woodlands
Lac du Bouchet B5	25	STEP	Temperate grasslands, savannas and shrublands	Gissaro-Alai open woodlands
MD99-2348-103	26	COMX	Temperate broadleaf and mixed forests	Rodope montane mixed forests
Les Echets G - DIGI	27	STEP	Temperate broadleaf and mixed forests	Western Siberian hemiboreal forests
La Grotte Walou	28	STEP	Temperate broadleaf and mixed forests	Kazakh forest steppe
Bergsee	29	STEP	Temperate broadleaf and mixed forests	Kazakh forest steppe
Garaat El-Ouez	30	STEP	Mediterranean Forests, woodlands and scrubs	Anatolian conifer and deciduous mixed forests
Pian del Lago	31	COMX	Temperate broadleaf and mixed forests	Western European broadleaf forests
Pilsensee	32	TAIG	Tundra	Kola Peninsula tundra
Orgiano	33	COMX	Temperate broadleaf and mixed forests	Western European broadleaf forests
Lago della Costa	34	COMX	Temperate Coniferous Forest	Alps conifer and mixed forests
Lagaccione	35	STEP	Temperate grasslands, savannas and shrublands	Gissaro-Alai open woodlands
Lago Vico	36	STEP	Temperate grasslands, savannas and shrublands	Gissaro-Alai open woodlands
Stracciaccappa	37	STEP	Mediterranean Forests, woodlands and scrubs	Western European broadleaf forests
Lago di Monterosi	38	STEP	Temperate grasslands, savannas and shrublands	Northwest Iberian montane forests
Venice	39	XERO	Tundra	Scandinavian Montane Birch forest and grasslands
Azzano Decimo	40	XERO	Temperate broadleaf and mixed forests	Scandinavian Montane Birch forest and grasslands
Valle di Castiglione	41	STEP	Temperate broadleaf and mixed forests	Tian Shan montane steppe and meadows
Travesio	42	XERO	Mediterranean Forests, woodlands and scrubs	Iberian conifer forests
Orvenco	43	TAIG	Temperate broadleaf and mixed forests	Western Siberian hemiboreal forests
Rio Doidis	44	XERO	Mediterranean Forests, woodlands and scrubs	Cyprus Mediterranean forests
Billerio	45	TAIG	Temperate broadleaf and mixed forests	Western Siberian hemiboreal forests
Kersdorf-Briesen	46	TAIG	Temperate broadleaf and mixed forests	Western Siberian hemiboreal forests
Lago Grande di Monticchio	47	STEP	Temperate broadleaf and mixed forests	Tian Shan montane steppe and meadows
Nagymohos Pleistocene	48	STEP	Tundra	Sarmatic mixed forests
Safarka	49	TAIG	Boreal forests / Taiga	Ural montane forests and tundra
Fehertó	50	COMX	Temperate Coniferous Forest	Alps conifer and mixed forests
Ioannina	51	STEP	Temperate broadleaf and mixed forests	Central European mixed forests
Kokad	52	STEP	Temperate broadleaf and mixed forests	East European forest steppe
Lake Xiniás	53	STEP	Temperate broadleaf and mixed forests	Western European broadleaf forests
Mickunai	54	COCO	Tundra	Scandinavian Montane Birch forest and grasslands
Lake Sfanta Anna	55	COMX	Temperate Coniferous Forest	Alps conifer and mixed forests
Lesvos ML01 Megali Limni	56	STEP	Temperate broadleaf and mixed forests	Rodope montane mixed forests
Straldzha	57	STEP	Temperate broadleaf and mixed forests	Aegean and Western Turkey sclerophyllous and mixed forests
MD01-2430	58	STEP	Temperate broadleaf and mixed forests	Euxine-Colchic broadleaf forests
Lake Iznik	59	STEP	Temperate broadleaf and mixed forests	Tian Shan montane steppe and meadows
M72/5 628-1	60	STEP	Deserts and xeric shrublands	Azerbaijan shrub desert and steppe
Dziguta Core 1	61	CLMX	Temperate broadleaf and mixed forests	Northeastern Spain and Southern France Mediterranean forests
Lake Van LG	62	STEP	Mediterranean Forests, woodlands and scrubs	Aegean and Western Turkey sclerophyllous and mixed forests
Lake Zeribar	63	STEP	Temperate grasslands, savannas and shrublands	Pontic steppe

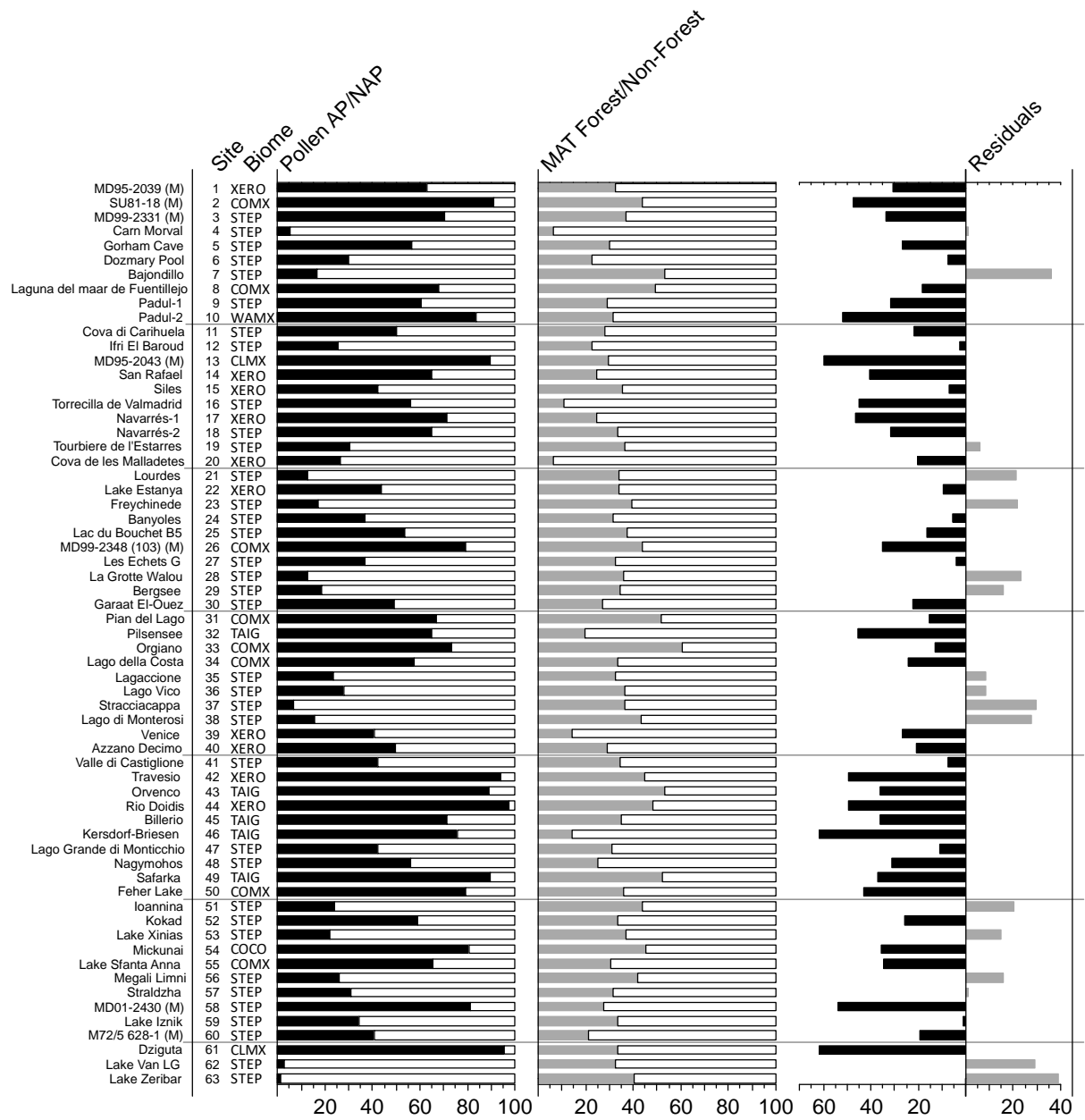
Notes: Modern analogue Biomes and Ecoregions were calculated as the most commonly occurring amongst all 6 best modern analogue pollen samples in all LGM samples for each pollen site/record. These are taken from the EMPD2 (Davis et al 2020), using the classification of Olsen et al 2001.

2261  
2262  
2263  
2264  
2265  
2266  
2267  
2268

**Table A4.** The biome and ecoregion of the modern surface samples used as analogues in the pollen-climate reconstructions.

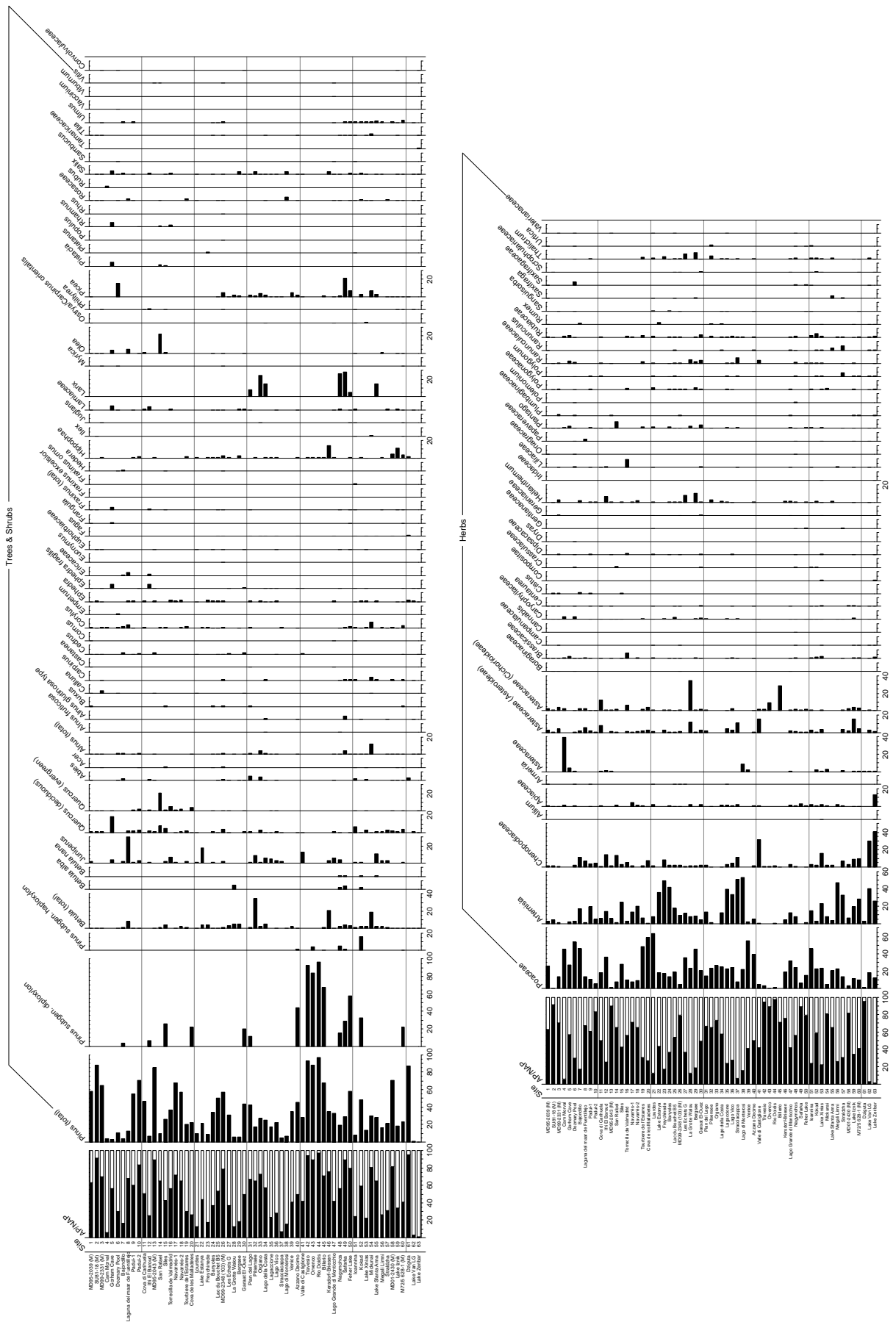
2269  
 2270  
 2271  
 2272  
 2273

**Figures**



2274  
 2275  
 2276  
 2277  
 2278

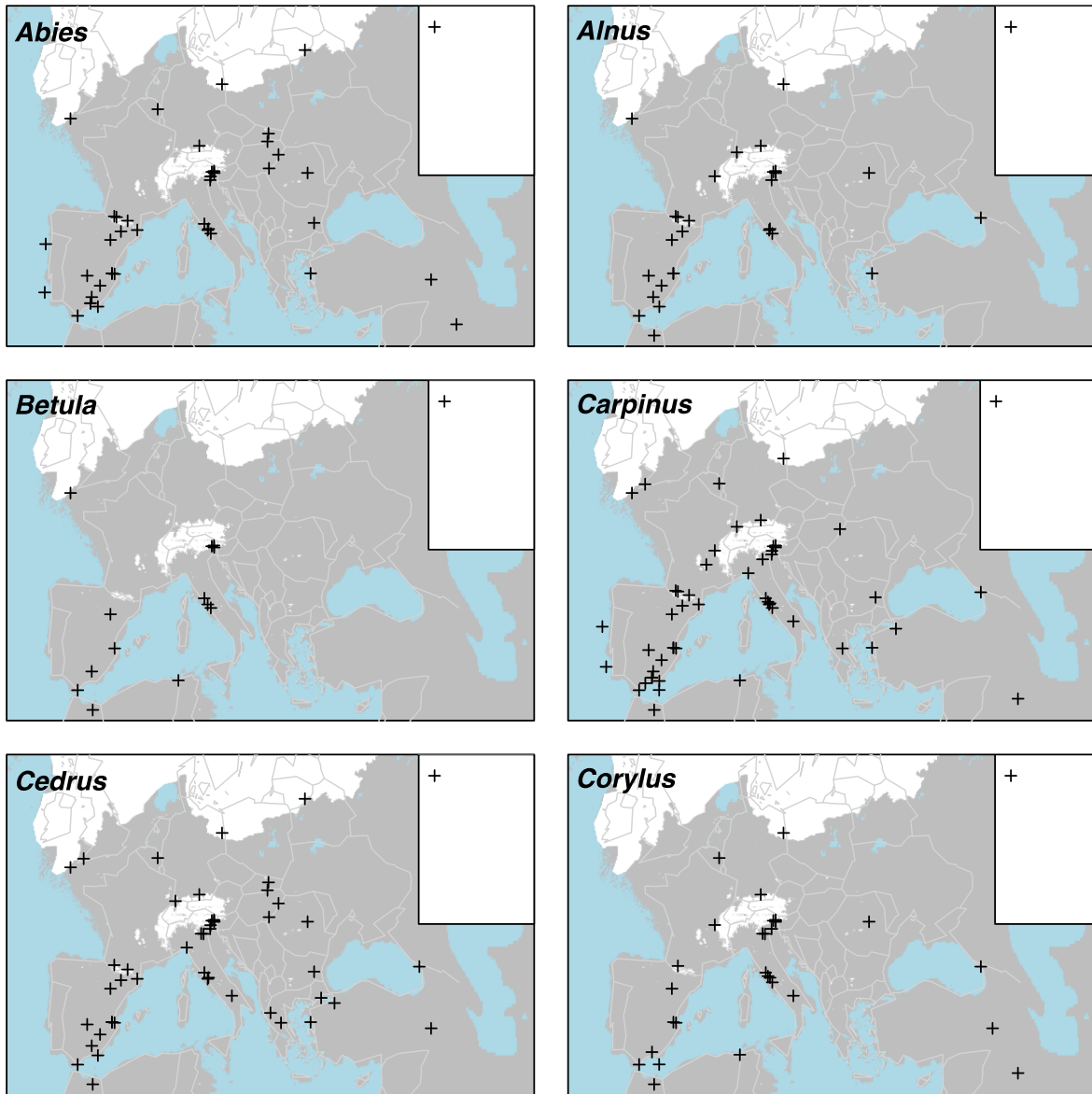
Figure A1. Pollen biomes (see figure 2 for key), Arboreal Pollen (AP) % forest cover, MAT % forest cover and residuals (AP % compared to MAT Forest %)



2279  
2280

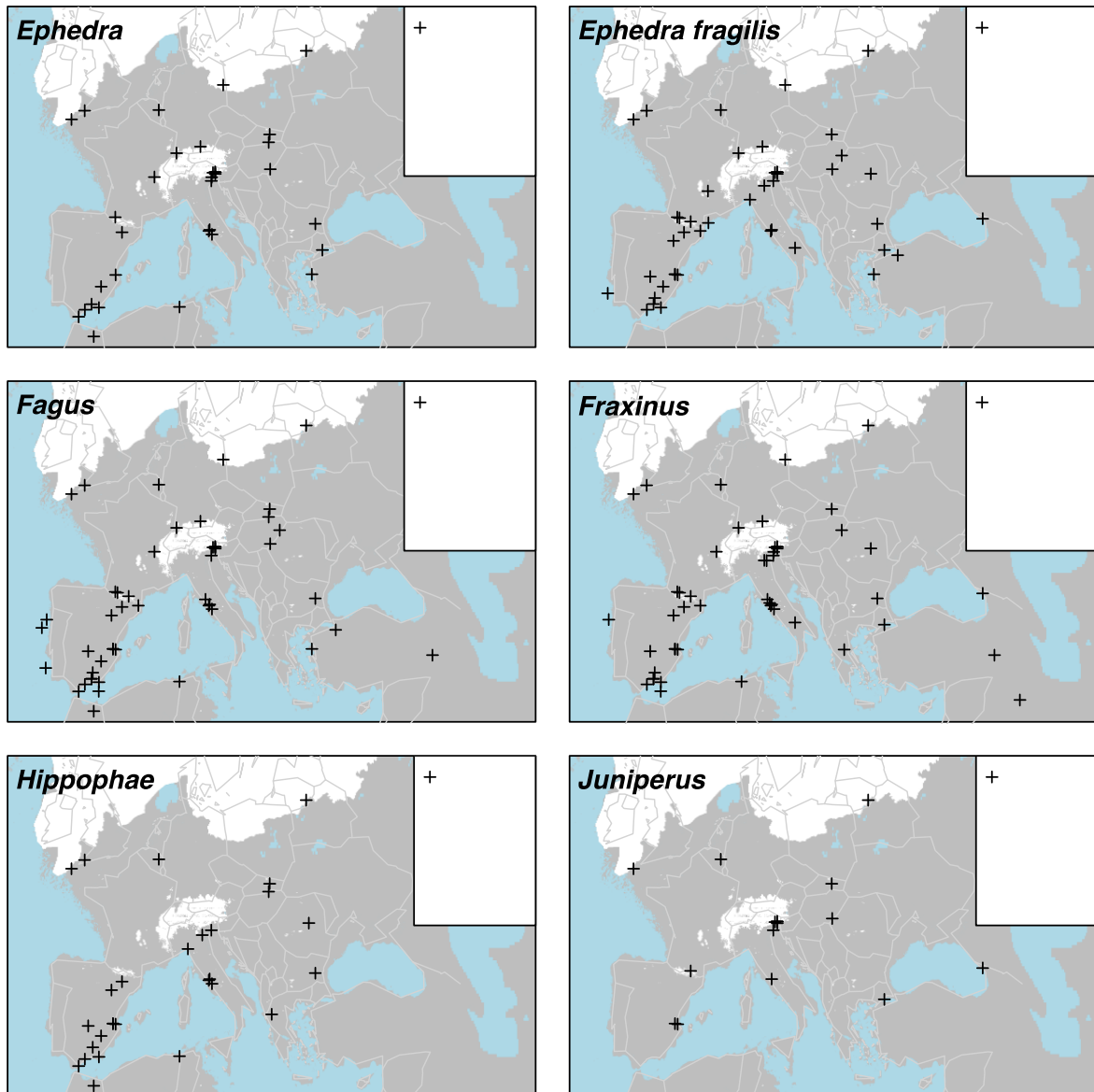
Figure A2. Pollen taxa percentages for all LGM sites/records

2281  
2282  
2283  
2284



2285  
2286  
2287  
2288

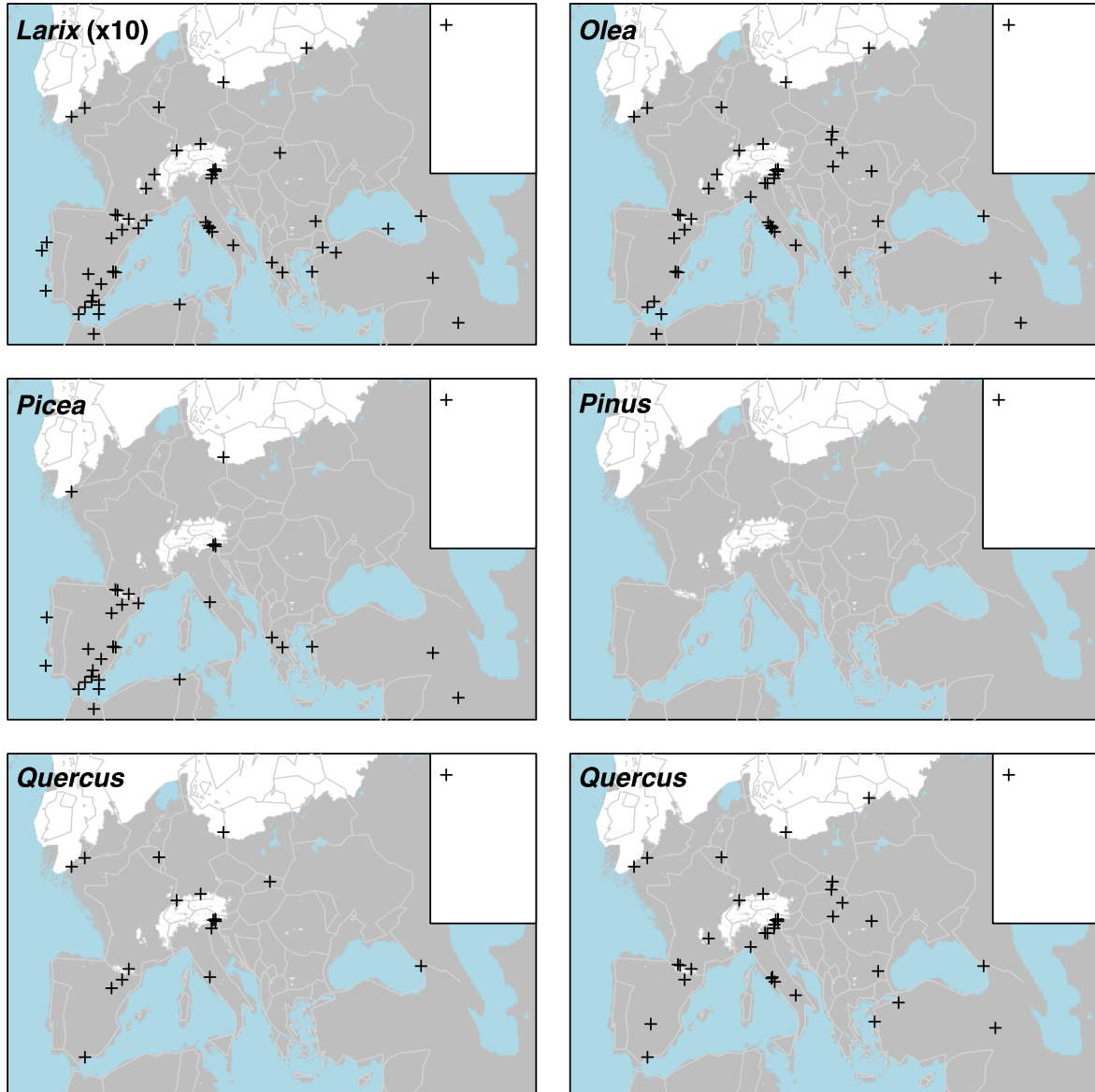
Figure A3a. Percentage maps of *Abies*, *Alnus*, *Betula*, *CarPinus*, *Cedrus* and *Corylus*



2289  
 2290  
 2291  
 2292  
 2293

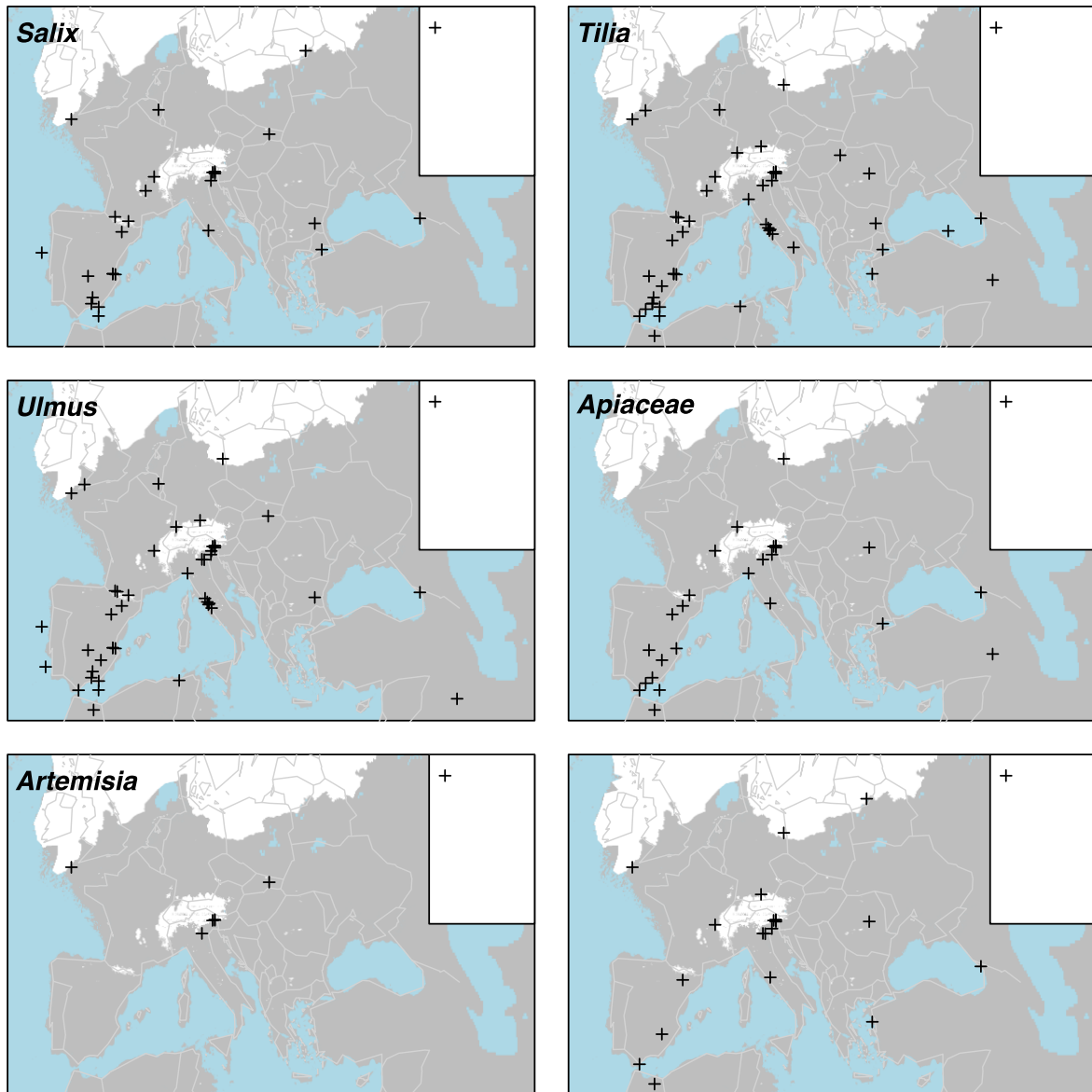
Figure A3b. Percentage maps of *Ephedra*, *Ephedra fragilis*, *Fagus*, *Fraxinus*, *Hippophae* and *Juniperus*





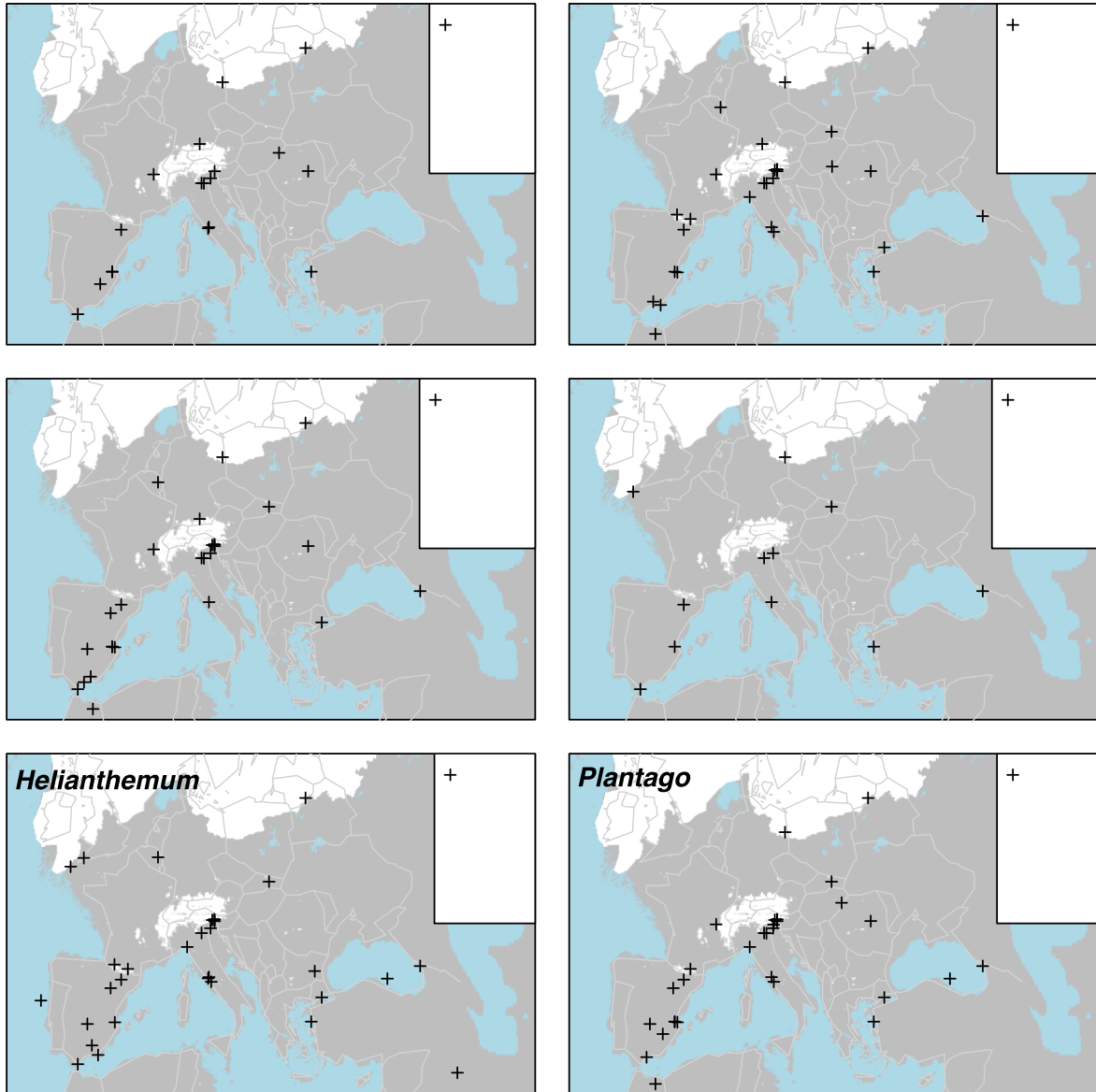
2294  
 2295  
 2296  
 2297  
 2298

Figure A3c. Percentage maps of *Larix* (x10 exaggeration), *Olea*, *Picea*, *Pinus*, *Quercus* (deciduous) and *Quercus* (evergreen)



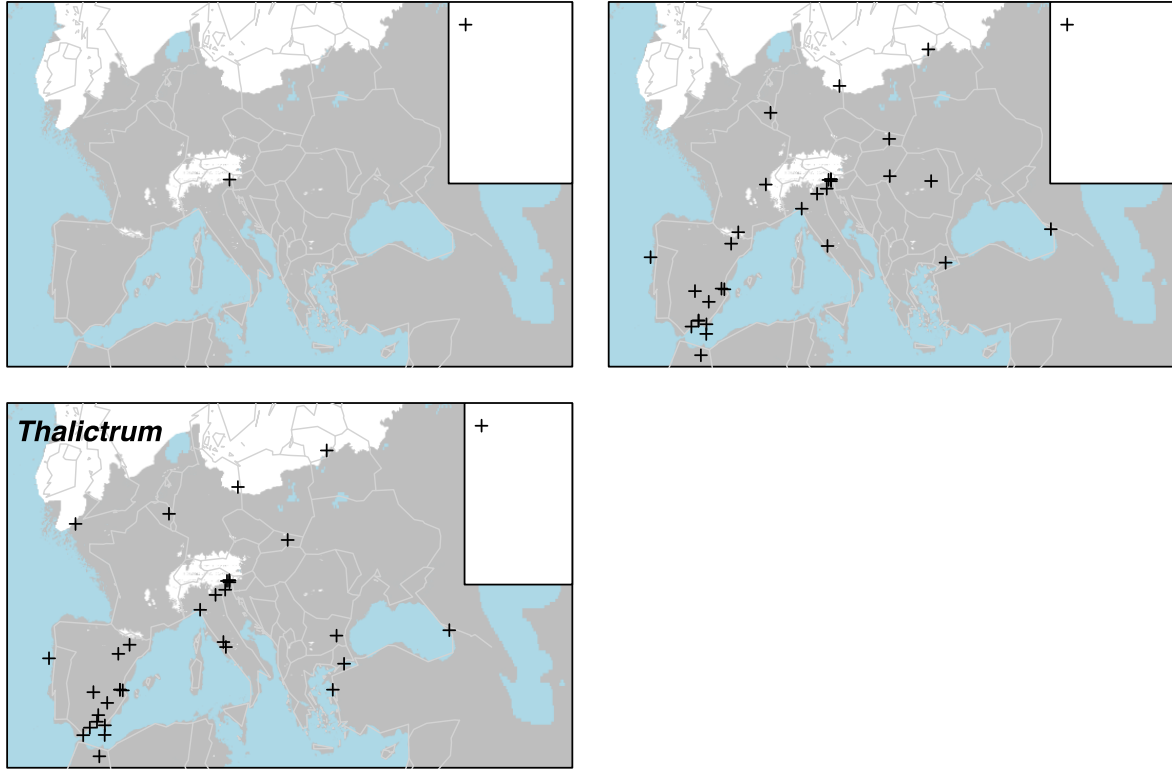
2299  
 2300  
 2301  
 2302

Figure A3d. Percentage maps of *Salix*, *Tilia*, *Ulmus*, *Apiaceae*, *Artemisia* and *Asteraceae* (*Asteroideae*)



2303  
 2304  
 2305  
 2306  
 2307

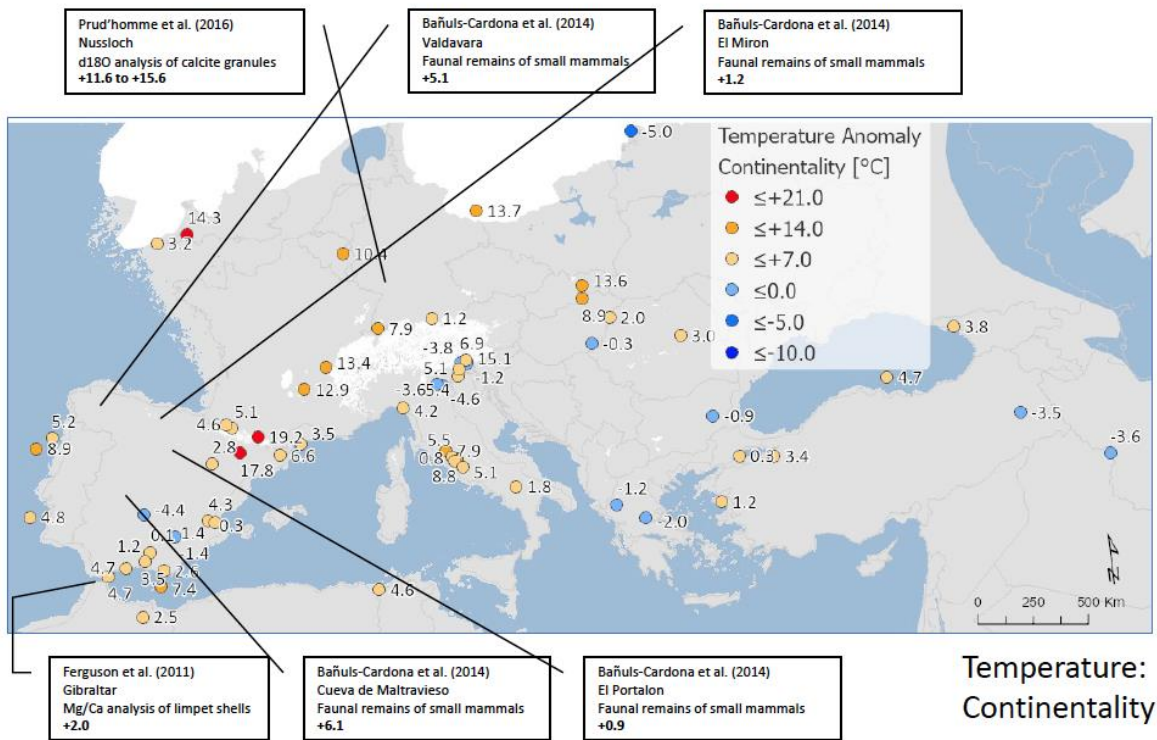
Figure A3e. Percentage maps of Asteraceae (Cichorioideae), Brassicaceae, Caryophyllaceae, Chenopodiaceae, *Helianthemum* and *Plantago*



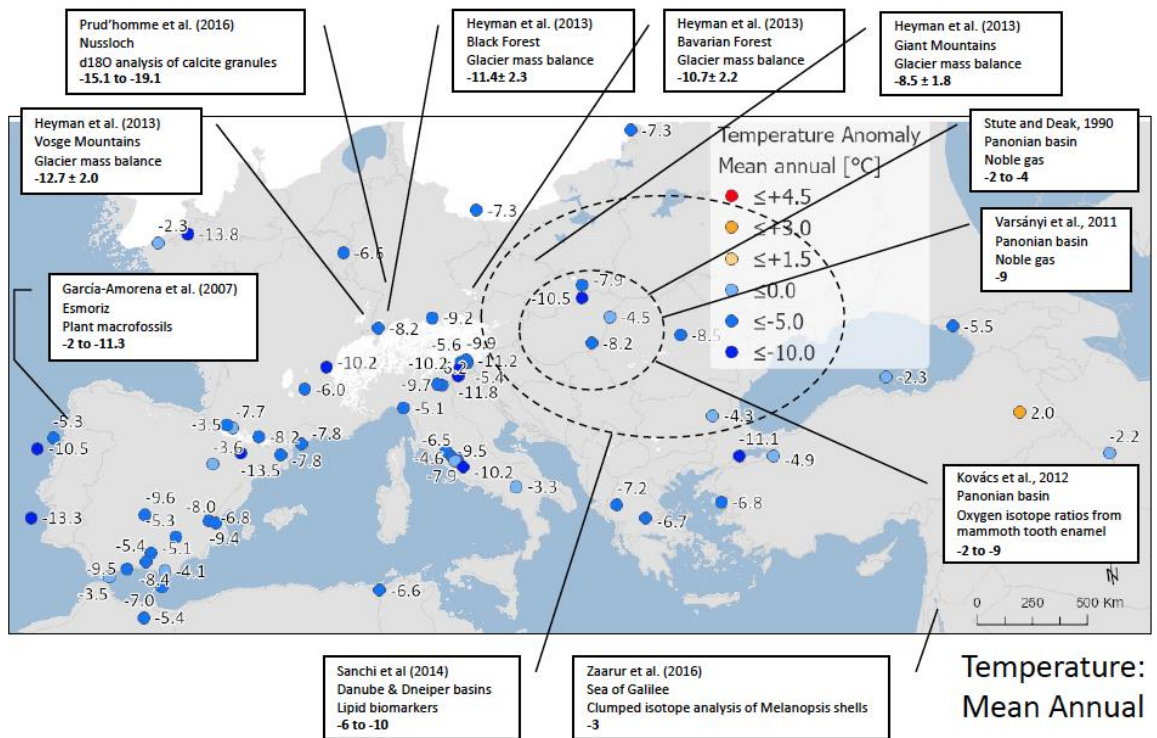
2308  
 2309  
 2310  
 2311  
 2312  
 2313  
 2314  
 2315  
 2316

Figure A3f. Percentage maps of Poaceae, Rubiaceae and *Thalictrum*

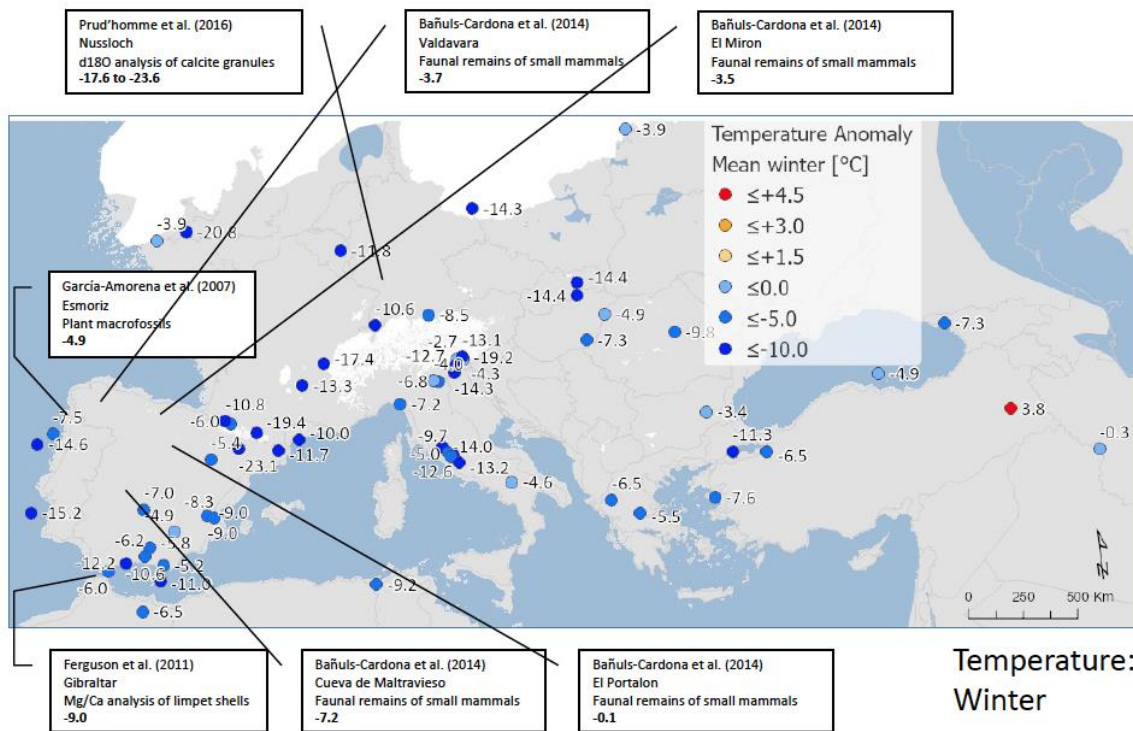
2317



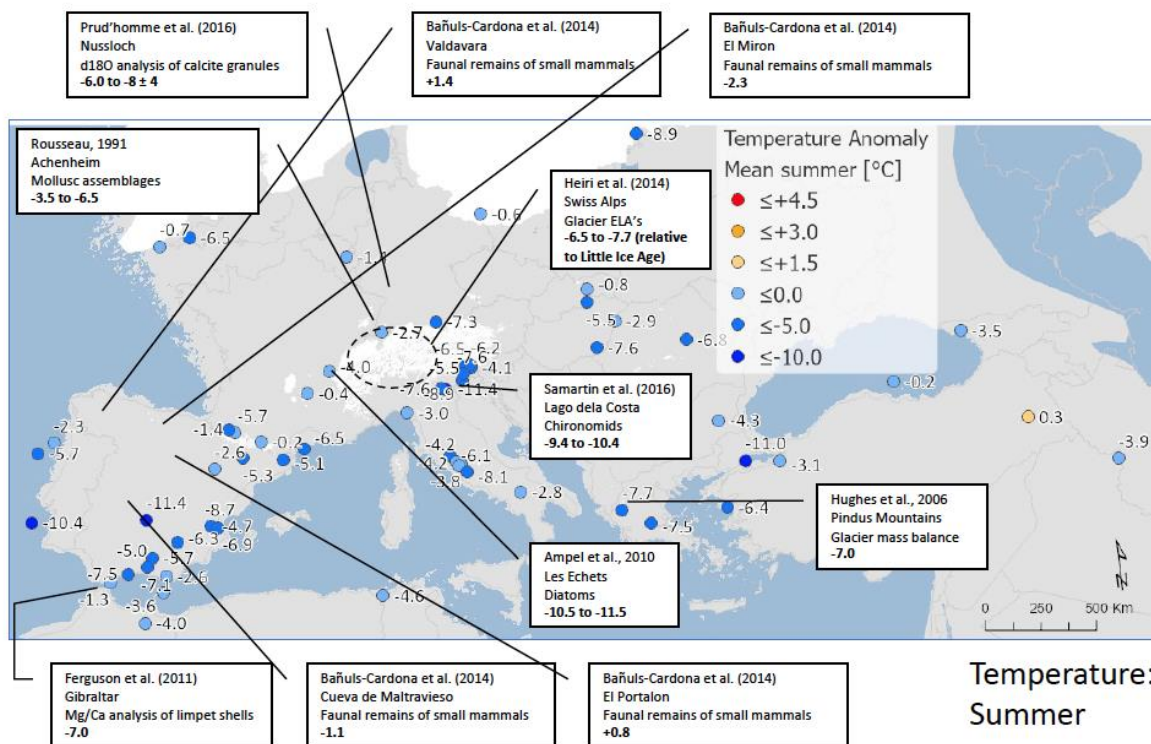
2318  
2319



2320  
2321  
2322



Temperature:  
Winter



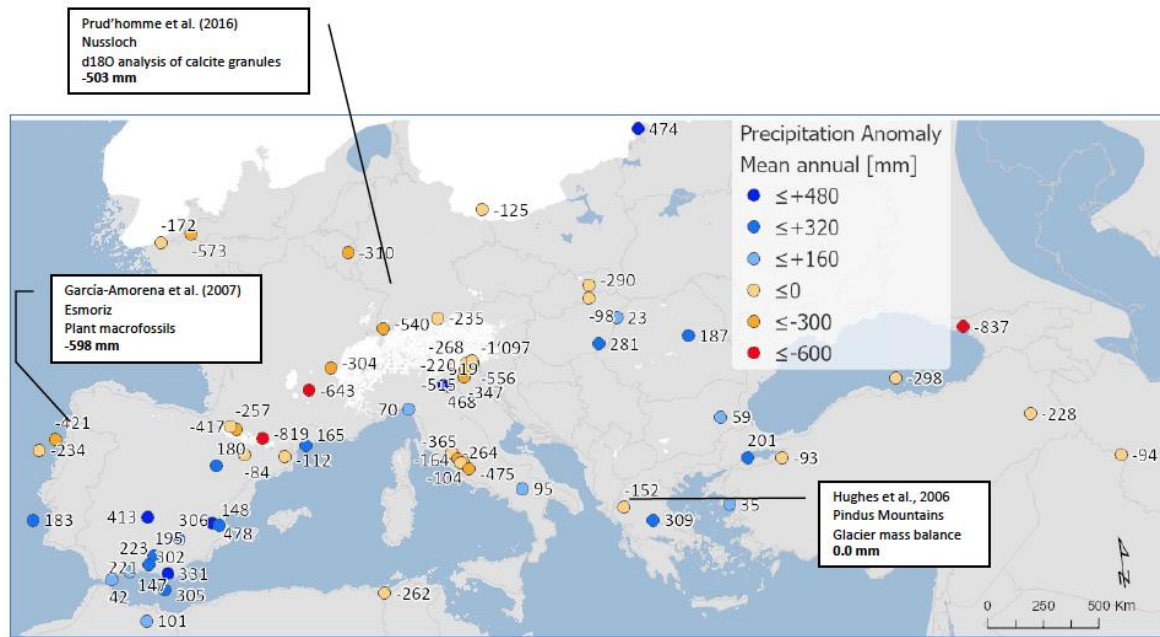
Temperature:  
Summer

2323  
2324

2325  
2326

2327 Figure A4. Maps of pollen-based MAT reconstructions for LGM annual, winter and summer  
2328 temperature anomalies (as shown in figure 10), shown together with the results of other  
2329 published studies. Continentality represents the difference in temperature between summer  
2330 and winter, with positive anomalies indicating an increase in the temperature difference  
2331 between summer and winter. All values are expressed as anomalies compared with the  
2332 present day unless otherwise indicated.

2333



Precipitation:  
Mean Annual

2334  
2335  
2336  
2337  
2338  
2339

Figure A5. Maps of pollen-based MAT reconstructions for LGM annual precipitation anomalies (as shown in figure 12), shown together with the results of other published studies. All values are expressed as anomalies compared with the present day.

2340  
2341